RICE UNIVERSITY

Bioactive Poly(ethylene glycol)-based Hydrogels for Angiogenesis in Tissue Engineering

by

Jennifer Elaine Saik

A THESIS SUBMITTED
IN PARTIAL FULFILLMENT OF THE
REQUIREMENTS FOR THE DEGREE

Doctor of Philosophy

Approved, Thesis Committee:

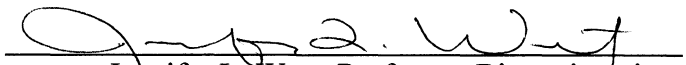

Jennifer L. West, Professor, Bioengineering,
Committee Chair

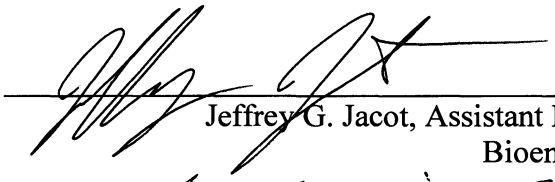

Jeffrey G. Jacot, Assistant Professor,
Bioengineering

Mary E. Dickinson, Associate Professor,
Molecular Physiology and Biophysics

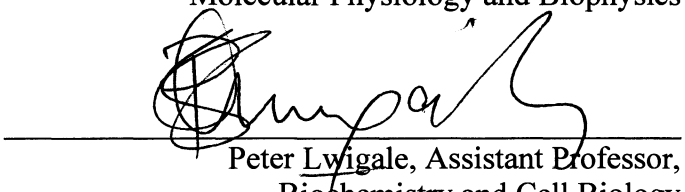

Peter Lwigale, Assistant Professor,
Biochemistry and Cell Biology

Houston, TX
June 2011

ABSTRACT

Bioactive Poly(ethylene glycol)-based Hydrogels for Angiogenesis in Tissue Engineering

by

Jennifer Elaine Saik

Because engineered tissue constructs are inherently limited by their lack of microvascularization, which is essential to provide oxygen for cell survival, this thesis presents rationally designed materials and cell culture techniques capable of supporting functional tubule formation and stabilization. Combining a synthetic scaffold material with cells and their cell-secreted signals instigated tubule formation throughout the scaffold. Poly(ethylene glycol) (PEG) based hydrogels, biocompatible polymers which resist protein adsorption and subsequent nonspecific cellular adhesion, were modified to induce desired cell characteristics. Human umbilical vein endothelial cells were used as a reproducible and readily available cell type. Several tubule-stabilization signals, including platelet derived growth factor-BB (PDGF-BB) and ephrinA1, were covalently immobilized via conjugation to PEG to enable prolonged bioactive signaling and controlled local delivery. All hydrogels were further tested in a mouse cornea micropocket angiogenesis assay, a naturally avascular tissue for easy imaging in a reproducible and quantifiable assay. Hydrogels containing soluble growth factors induced vessel formation in the hydrogel, and the resulting vessel morphology was modulated using different growth factor concentrations. Immobilized PDGF-BB led to tubule

formation in two dimensions, three dimensions, and in the mouse cornea while immobilized ephrinA1 stimulated secretion of extracellular matrix proteins laminin and collagen IV to stabilize the newly formed tubules. Finally, a co-culture of endothelial and pericyte cells encapsulated into hydrogels formed tubules that anastomosed to the host vasculature and contained red blood cells. PEG-based hydrogels represent a promising technique to induce microvascular formation in engineered constructs, leading to stable and functional vessel formation using covalently immobilized growth factors and encapsulated cells. These materials can be used for replacement of damaged or diseased tissues as the current supply of cadaveric donations cannot meet the demand of tissues for the 110,000 people awaiting an organ in the US.

ACKNOWLEDGEMENTS

A sincere thank you to Dr. Jennifer West for providing extensive mentoring and guidance. I appreciate your support in following different career opportunities and research interests. Thank you to Dr. Mary Dickinson in enabling extensive research opportunities to advance the project and providing ample research ideas. For my committee members Drs. Jeff Jacot and Peter Lwigale for offering support and advice throughout the process.

I am extremely grateful to helpful graduate students, post doctoral researchers, and undergraduates who have worked with me in the West and Dickinson labs. Thank you for support, ideas, and focus. Special recognition is give to Drs. Julie Barbick, Stephanie Nemir, Ronke Olabisi, LaShan Simpson, Melissa McHale, and Ross Poche. A sincere thank you to Dan Gould for extensive hours of experiments and analysis. Also, to BJ Gill who took on a new collaborative project with me. To Saniya Ali and Logan Hsu for continuing on with these projects. To my undergraduate students Emily Watkins, Aakash Keswani, and Anindya Samanta. Emily, your ability to devise new solutions to problems and analyze vast amounts of data was immensely helpful. Aakash, your late night data analysis was invaluable.

Finally, my immense gratitude to my parents who moved to Houston for two years to support my education. Thank you for always listening to me and giving so much love.

This research was supported by a National Science Foundation Graduate Research Fellowship, a Howard Hughes Medical Institute Fellowship, and grants from the National Institutes of Health.

Table of Contents

Table of Figures

Tables

Chapter 1: Introduction

A significant portion of this chapter is from JE Saik, MK McHale, and JL West. "Biofunctional Materials for Directing Vascular Repair." *Curr Vas Phama.* Submitted 2011.

1.1 The Need for Therapeutic Angiogenesis

While organ transplantation saves thousands of lives each year, over 110,000 people are currently waiting on the organ transplant list, eighteen patients die every day awaiting an organ, and a person is added to the transplant wait list every thirteen minutes (UNOS, 2011). The increasing demand for donated organs to replace damaged or diseased tissues cannot be met by the current supply from cadaveric and living donors. The field of tissue engineering aims to meet this demand by replacing injured and diseased tissues with functional engineered counterparts (Saik et al., 2011). The first US Food and Drug Administration approved success in tissue engineering was Apligraf® to replace the epidermis in burn patients (Falanga et al., 1999). Despite the success of Apligraf®, successfully engineered tissues have been to date limited to thin or avascular tissues, including skin, cartilage, and bladder (Jain et al., 2005; Atala et al., 2006). In these thin tissues, oxygen, nutrients, and waste can diffuse through the tissue without requiring a functional microvascular system.

Development of more complex tissues, such as lung, liver, or heart, will require a better understanding of how to induce vascularization in tissues, especially capillaries. Therapeutic angiogenesis attempts to induce capillary formation in tissues. This chapter

will first outline the basic biology of blood vessels and neovessel formation. Since tissue engineering mimics the body's natural process by using three basic components to create new tissues: (1) growth factors, (2) biomaterials, and (3) cells, this chapter will review the role of growth factors involved in angiogenesis, the biomaterials used, and *in vivo* assays to demonstrate the material's functionality. Finally, current work involving biomaterials releasing growth factors and encapsulated cells is reviewed. Using the three basic components of cells, growth factors, and biomaterials, this thesis demonstrates the formation of functional and stable tubule networks in tissue engineering scaffolds which can be used for fabrication of more complex engineered tissues.

1.2 Biology of the Microvasculature

Capillaries are composed of endothelial cells, pericytes, and a basement membrane. The thrombo-resistant monolayer of endothelial cells forms a selectively permeable barrier and function to control leukocyte and platelet interactions, blood flow, and vessel tone (Seifalian et al., 2002). The walls of capillaries are lined with a single layer of pericytes, a type of mural cell analogous to the smooth muscle cells found in larger vessels (Edelman et al., 2006). Similar to their mural cell counterpart, pericytes function to contract in order to regulate blood flow and permeability. Unlike smooth muscle cells, pericytes primarily function in the production of basement membrane. Each pericyte covers several endothelial cells in an "umbrella-like" manner as seen in Figure 1-1. With less than 20 nm between pericytes and endothelial cells, pericytes regulate permeability but also support general microvascular integrity (Edelman et al., 2006). Furthermore, vessels lacking pericytes exhibit abnormal features, such as leakage and

impaired perfusion due to abnormal endothelial junctions, endothelial hyperplasia, and hypervariable diameter (Betsholtz et al., 2005). Based on the importance of pericytes, this thesis researched confirmed the presence of pericyte coverage around induced vessels.

The presence of pericytes is not only important to existing capillary networks, but also to neovessel formation. As the body undergoes healing and maintenance of homeostasis, new capillaries must form. These new capillaries arise from either vasculogenesis or angiogenesis (Figure 1-1). Vasculogenesis is *de novo* formation of vessels from bone marrow-derived endothelial progenitor cells. Alternatively, in the angiogenesis pathway, sprouts from pre-existing capillaries extend to form new vessels. Finally, pericytes are recruited to the endothelial cells, derived from either endothelial progenitor cells of pre-existing capillaries, to stabilize vessels. This thesis used both of these natural processes for neovessel formation. Specifically, a co-culture of endothelial cells and pericytes were encapsulated into hydrogels to mimic vascologenesis, and various growth factors were used in soluble and immobilized forms to mimic angiogenesis.

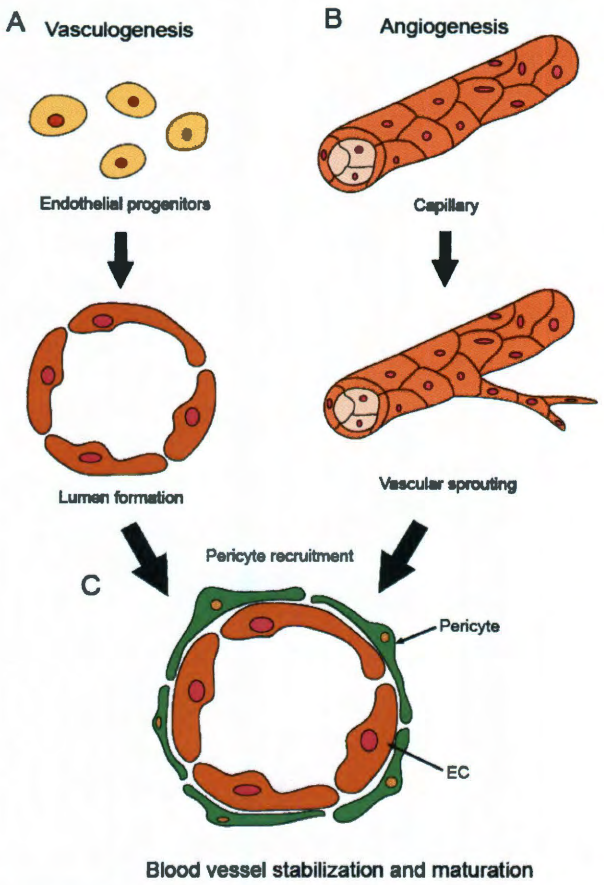

Figure 1-1: Capillary Formation. Capillaries arise from either endothelial progenitor recruitment as in vasculogenesis (A) or new vessel sprouting from pre-existing endothelial cells as in angiogenesis (B). The resultant capillaries are stabilized by pericyte recruitment (C). Figure adapted from (Moon et al., 2008).

1.3 The Process of Angiogenesis

A more detailed understanding of the angiogenic process is necessary in order to mimic the body's natural process. Angiogenesis occurs in four steps as seen in Figure 1-2: (A) plasma proteins (often vascular endothelial growth factor), released during vasodilation and extravasation, signal endothelial cells via a concentration gradient; (B) the connection between endothelial cells and pericytes is interrupted, and endothelial cells detach from the basement membrane; (C) endothelial cells migrate and extend filapodia in response to the released proteins; vacuoles form and fuse to create tubule lumen; and (D) stabilizing pericytes are recruited to lay basement membrane proteins (Madeddu, 2005). The resulting vessels are stabilized and remodeled as necessary, and endothelial cells return to their normal quiescent state. Based on the natural process of angiogenesis, this

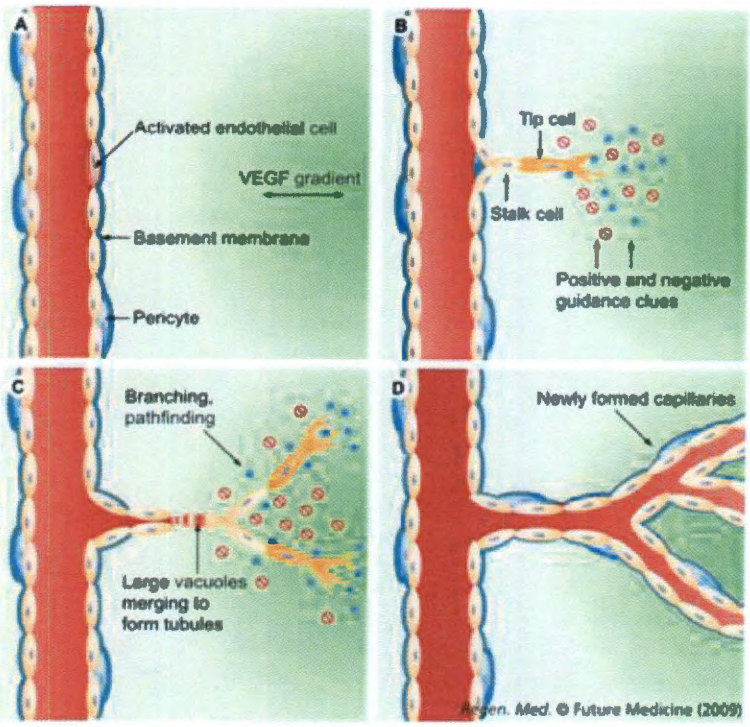

Figure 1-2: The process of angiogenesis. (A) A growth factor gradient is detected by an endothelial cell, and the endothelial cell becomes activated. (B) The activated tip endothelial cell degrades the basement membrane in order to migrate down the growth factor gradient. (C) Large vacuoles form and merge to make tubule lumen. (D) Pericytes are recruited and stabilize newly formed vessels with deposition of basement membrane. Figure from (Phelps et al., 2009).

thesis research used growth factors, such as VEGF, to establish a concentration gradient. Furthermore, the presence of vacuoles and pericytes was confirmed using staining as an indicator of remodeling and stable capillary formation.

1.4 The Role of Growth Factors in Angiogenesis

In the process of angiogenesis, growth factors play an important role in the development of neovessels. Vascular endothelial growth factor (VEGF), considered the key angiogenic factor, stimulates endothelial cells to migrate, proliferate, and differentiate (Nomi et al., 2006). VEGF-A, the most characterized VEGF molecule, is composed of five isoforms as a result of alternative splicing: $VEGF_{121}$ is completely soluble; $VEGF_{165}$ is mostly soluble but also has affinity for heparin sulfate proteoglycans on cell surfaces; and $VEGF_{145}$, $VEGF_{189}$, and $VEGF_{206}$ all remain sequestered on the cell surface due to their high affinity for heparin (Park et al., 1993). Gene knockout mice confirm the importance of VEGF in that a mouse lacking even one VEGF gene fails to develop past early embryonic stages (Carmeliet et al., 1996). Several VEGF receptors have also been identified, with all VEGF isoforms binding VEGFR-1 and VEGFR-2. Hypoxia is the most important inducer of VEGF expression, mediated by HIF-1 and HIF-2 along with an increase in mRNA stability (Marti, 2005). However, VEGF-induced vessel formation is often leaky and tumor-like (Jain et al., 2005). In this thesis, VEGF was initially used as an established method to induce angiogenesis.

In addition to VEGF, fibroblast growth factor (FGF) is also known for its ability to initiate angiogenesis. FGF was the first angiogenic growth factor to be discovered and represents a family consisting of over 20 molecules, of which FGF-2 or basic FGF is

involved in angiogenesis. FGF-2 stimulates endothelial cell proliferation and migration, and FGF-2 regulates expression of key angiogenic molecules, such as collagenases, β1 integrins, and urokinase type plasminogen activator (Bikfalvi et al., 1997). FGF-2 also induces migration and proliferation of smooth muscle cells (Jackson et al., 1993). Hypoxia induces macrophages to release FGF-2 to stimulate growth of endothelial cells. This thesis used FGF as an alternative to VEGF to initiate angiogenesis, especially in combination with stabilizing factors such as platelet derived growth factor.

As compared to early stage growth factors like FGF and VEGF known to initiate angiogenesis, platelet-derived growth factor (PDGF) is involved in the later stages of angiogenesis involving stabilization and remodeling. PDGF was identified as a key protein secreted from platelets in the 1970s. PDGF forms homo- and heterodimers of A- and B-polypeptide chains. The three-dimensional structure and amino acid sequence show great similarity to VEGF, as well as to nerve growth factor and transforming growth factor β (Heldin et al., 1999). Two PDGF receptors exist, and ligand-induced receptor dimerization initiates receptor autophosphorylation.

PDGF receptor autophosphorylation induces widespread activities throughout the body, especially in the development of the kidneys, lungs, CNS, and blood vessels. Specific to the vascular system, endothelial cells not only produce PDGF but also display PDGF receptors (Bar et al., 1989). Although PDGF is not involved in initial vessel formation, PDGF-BB is involved in neovessel stabilization and functionalization by inducing functional anastomoses and recruiting pericytes. Mice lacking the PDGF-B chain exhibited defective blood vessel development and microaneurysms, likely as a result of the inability of neovessels to attract stabilizing pericytes (Lindahl et al., 1997).

PDGF also induces pericyte production of extracellular matrix (ECM) proteins, including fibronectin, collagen, and proteoglycans, necessary for the basement membrane of capillaries. Furthermore, PDGF stimulates fibroblasts to produce and secrete collagenases. This thesis research presents PDGF in an immobilized form for its involvement in anastomosis formation and collagenase secretion.

Similar to PDGF, ephrins are involved in the later remodeling and stabilization stages of capillary network formation. Eph receptors and their ephrin ligands are a family of receptor tyrosine kinases involved in growth, differentiation, and patterning of tissues. Ephrin ligands are categorized as type A for having a glycophosphatidylinositol-anchor or type B for having a transmembrane domain. Signaling can occur in a forward manner by ephrin ligands activating eph receptors or in reverse by eph receptors activating ephrin ligands (Heroult et al., 2006). Unlike other receptor tyrosine kinases, ephrins mediate cell adhesion, repulsion, and migration rather than proliferation. Expression of ephrinA1 is induced by tumor necrosis factor-α, interleukin-1 beta, and VEGF (Cheng, Brantley, and Chen, 2002). These factors lead to activation of ephrinA1 and its EphA2 receptor, which has been shown to be involved in angiogenesis by initiating endothelial cell migration and capillary invasion (Brantley et al., 2002). An immobilized form of ephrinA1 was used in this thesis research for its ability to modulate angiogenesis from the role of cell adhesion.

Angiogenesis requires coordinated expression of several key growth factors. A single factor such as VEGF is not sufficient to form functional vasculature, and in fact, presentation of VEGF alone can lead to induction of tortuous and leaky vessels (Marti, 2005). In addition, spatial and temporal regulation of growth factor expression ensures

accurate vessel growth and remodeling. For example, when combined with FGF, PDGF receptors are upregulated, causing proliferation of smooth muscle cells and stabilization of neovessels (Hollinger et al., 2008). Growth factors, such as VEGF, FGF, and PDGF, can be incorporated both individually and in combination in natural and synthetic biomaterials.

1.5 *In vivo* Angiogenic Assays

Three *in vivo* angiogenesis assays, including the chorioallantoic membrane (CAM) assay, dorsal skinfold assay, and cornea micropocket, are commonly used to evaluate the response of vessels to externally applied stimuli. The chorioallantoic membrane, or CAM, is an extra-embryonic membrane used as a gas exchange surface during the 21 days prior to chick hatching (Figure 1-3). The CAM assay was originally developed to study embryonic tissue grafts and involves breaking open an egg and applying the experimental substance to the membrane surface. Advantages of the CAM assay include low cost, ease of access to chick embryos, and low immunogenicity due to the lack of a complete immune system. However, angiogenic efficacy in the CAM assay is limited to ten days due to the developing chick, background

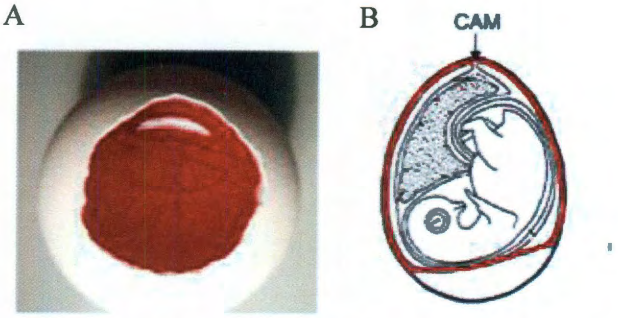

Figure 1-3: The CAM assay for testing angiogenic activity of biomaterials. (A) Image of the egg with vessels at day 10 and (B) location of the CAM (in red) around the chick embryo. Adapted from (Vargas et al., 2007).

vessels must be distinguished from new angiogenesis in response to treatment, and genetic modifications to chicks is limited (Vargas et al., 2007).

In order to study angiogenesis in rodents, which are amenable to genetic modification, the dorsal skinfold chamber can be used. In this technique, the experiment is carried out within a transparent backpack chamber that is placed over the skinfold, providing ease of visualization for the duration of study (Figure 1-4) (Laschke et al., 2006). On the other hand, experimental protocols are limited in that any implants are restricted in size to 5 mm in diameter and 1 mm in height, and background vessels must be subtracted from induced vessels.

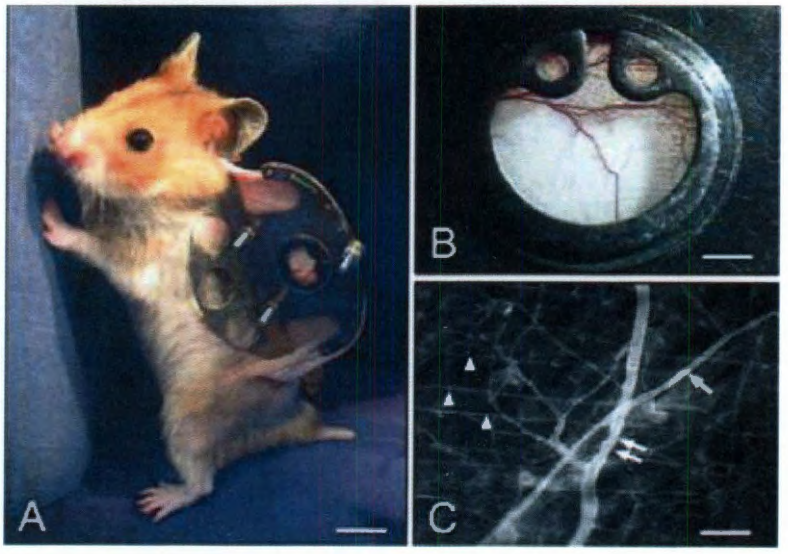

Figure 1-4: The dorsal skinfold chamber for studying *in vivo* angiogenesis. (A) skinfold chamber seen on a hamster. (B) The observation window allows imaging of large microvessels. (C) Intravital microscopy can be used to image arterioldes (arrows), capillaries (arrowheads), and venules (double arrows). Figure from (Laschke et al., 2006).

A third *in vivo* angiogenesis assay is conducted in the mouse cornea, which is a reproducible and quantifiable assay in an otherwise avascular tissue and will be used for all *in vivo* work in this thesis. The cornea consists of three cell layers: the outer

epithelium, the thick stroma, and the inner endothelium. The thick stromal layer is composed of type I collagen fibers and keratinocytes. The endothelium is a monolayer of mitrochondria-rich endothelial cells lined with Descemet's membrane, a modified basement membrane. The cornea is a continuous layer with the connective tissue sclera, and therefore limbic vessels surround the edge of the cornea. The cornea functions, along with the lens, to refract light and focus the eye. In fact, the cornea represents greater than 60% of the eye's focusing power (Beebe, 2008). As a result of the cornea's functional role, the cornea is a transparent tissue. To maintain transparency, the cornea is both an angiogenic and immune privileged site, in which transport of nutrients and oxygen occurs through diffusion.

Avascularity of the cornea is maintained by three key molecules: (1) a soluble VEGF receptor, (2) pigment epithelium-derived factor (PEDF), and (3) thrombospondins. The soluble VEGF receptor Flt-1 binds and sequesters any VEGF present in the cornea (Ambati et al., 2007). The importance of sFlt1 was established when reduction of sFlt1 expression in genetically modified mice led to corneal neovascularization, and Florida manatees with vascularized corneas exhibited decreased sFlt1 expression (Beebe, 2008). Pigment ephithelium derived factor was identified in avascular cartilage, and inhibition of PEDF activity induces corneal neovascularization (Beebe, 2008). The third molecule that maintains avascularity is thrombospondins (TSP), a family of four secreted molecules. Thrombospondin 1 and 3 were also identified in asvacular cartilage, and TSP-1 and -2 are expressed in the cornea. Genetically modified mice lacking TSP-1 showed reduction of corneal neovascularization in response to inflammation, and mice lacking TSP-2 developed vascularized irises (Cursiefen et al., 2004). Even though the cornea normally

remains avascular, neovascularization can be induced in response to injury or implantation (Muthukkaruppan et al., 1979). The cornea micropocket angiogenesis assay takes advantage of the potential to induce neovascularization in the cornea by stimulating limbic vessels to branch and invade the cornea stroma in response to implantation of a biomaterial (Figure 1-5) (Rogers et al., 2007).

Similar to the angiogenic privilege nature of the cornea, the cornea is also an "immune privileged" tissue in order to maintain transparency. The immune privileged state is actively maintained by the reduced expression of major histocompatibility complex (MHC) class I expression and reduced numbers of immune cells expressing MHC class II. Furthermore, an immunosuppressive environment is maintained by the presence of soluble factors such as α-melanocyte-stimulating hormone and vasoactive intestinal polypeptide (Cursiefen, 2007). Due to the cornea's avascular nature, nutrient and oxygen transport occur by diffusion. Nutrient transport is from the aqueous humor, interstitial fluid, and tear film of the eye. Oxygen diffusion occurs from the air through the epithelium and stroma. Normal tissues are considered hypoxic when the oxygen concentration is below 5%, but the cornea normally has 2% oxygen (Helbig et al., 1993).

Due to the cornea's unique features of visibility, accessibility, and avascularity (Kenyon et al., 1996), the mouse cornea has been used as an optimal *in vivo* site to study angiogenesis since the 1970s and was used for the work in this thesis (Muthukkaruppan et al., 1979). In an otherwise avascular tissue, all vessels induced to invade the cornea stroma are in response to the bioactive hydrogel. The cornea enables visualization of the developing vasculature over time by allowing imaging of live animals. Although the cornea restricts implant size, this assay provides a well established, quantitative, and

reproducible technique (Rogers et al., 2007). Based on the ease of imaging over time and lack of background vessels, the mouse cornea micropocket was used for the presented thesis research.

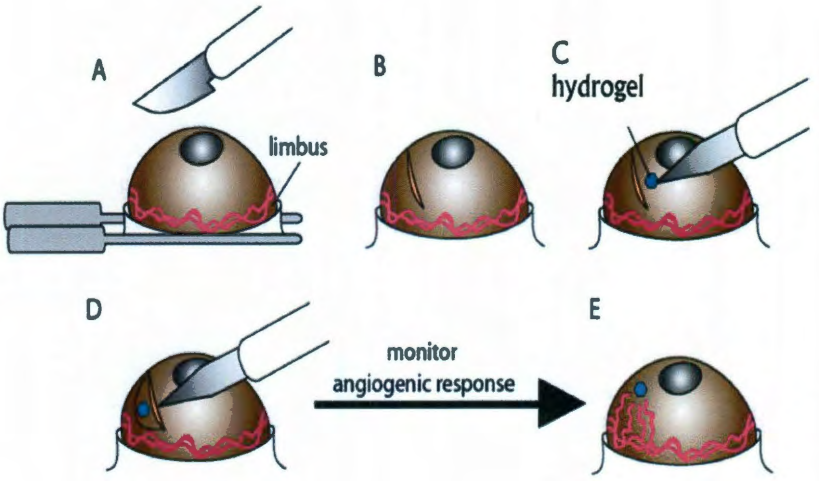

Figure 1-5: The mouse cornea micropocket. The eye is anesthetized (A) and a partial-thickness incision is made (B). A micropocket is created (C) and the hydrogel is placed in the micropocket (D). Bioactive hydrogels promote natural limbic vessels surrounding the cornea to invade the cornea stroma in response to angiogenic stimulation (E). Figure adapted from (Rogers et al., 2007).

1.6 Biomaterials for Guiding Vessel Growth

Many biomaterials have been investigated to induce and guide vessel growth because biomaterials provide a scaffold for delivery of growth factors and cell seeding. Natural materials are commonly used, including collagen and its gelatin derivatives, fibrin, and alginate, because they are either components of or similar to components of the natural ECM. Collagen is the most abundant ECM consitutent, representing about

25% of the total protein mass in the body. Collagen is naturally degraded by cell-secreted matrix metalloproteinases (MMPs), specifically collagenases and serine proteases, allowing cellular infiltration via host degradation. Furthermore, mechanical properties of collagen matrices can be enhanced with the addition of chemical crosslinkers (Drury et al., 2003). Similar to collagen, fibrin is a natural component of the body, found in clots formed during the wound healing cascade. Fibrin provides both structural and biochemical cues (Patel et al., 2004). Furthermore, fibrin is capable of providing a reservoir for growth factors, which induce endothelial cell tubulogenesis *in vitro*. Alginate and chitosan are hydrophilic, linear polysaccharides commonly used *in vivo*. Alginate, commonly isolated from brown seaweed and bacteria, is readily available and forms gels under gentle conditions to allow optimal bioactivity (Drury et al., 2003).

While natural materials incorporate ECM components, synthetic polymers are often used as scaffolds because they allow precise modification of various parameters, such as mechanical properties, degradation rates, and drug delivery rates based on alteration of molecular weights, chemical structures, and crosslinking modes. Three commonly used synthetic biomaterials include poly(lactide-co-glycolide), polyurethane, and poly(ethylene glycol). The most highly researched synthetic polymer is poly(lactide-co-glycolide) (PLGA) because it combines glycolic acid and lactic acid in various ratios to design specific degradation and drug release rates. Additionally, PLGA degrades by hydrolysis into two biocompatible components (Patel et al., 2004). Polyurethanes are another type of synthetic biomaterial used for their biocompatibility and versatility. Although polyurethanes are commonly used as biomaterials for heart valves and dialysis

membranes, they have only recently been used in angiogenesis applications due to issues surrounding their biodegradation (Patel et al., 2004).

This thesis used poly(ethylene glycol) diacrylate (PEGDA), an FDA approved biocompatible polymer. PEGDA resists protein absorption and subsequent nonspecific cell adhesion, thus providing a "blank slate" which can be modified with bioactive ligands to create desired characteristics, such as cell adhesion and possibly differentiation (DeLong et al., 2005). PEGDA hydrogels are biocompatible, hydrophilic materials with tunable mechanical properties (Figure 1-6) (Hahn et al., 2007). Fully hydrated polymers mimic the mechanical properties of soft tissues (West et al., 1999). The polymer can be photopolymerized via light by incorporating a photosensitive chemical into the polymer solution. Mild crosslinking conditions enable cellular encapsulation into the material

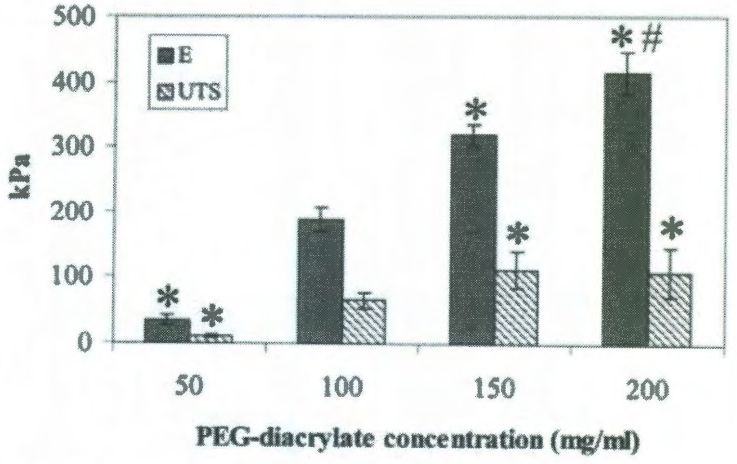

Figure 1-6: Tunable mechanical properties of PEGDA hydrogels. Increased PEGDA concentration allows increasing Young's modulus (E) and ultimate tensile stress (UTS) to mimic various tissues in the body (Gunn et al., 2005).

while maintaining cell viability. Bioactivity is commonly incorporated into PEG materials by attaching the free amine or carboxyl group of a peptide or protein to a

bifunctional PEG molecule, leaving the other end to crosslink into the hydrogel. For example, several bioactive oligopeptides known to interact with cell surface receptors have been incorporated into the hydrogel, including RGDS, showing the concentration of RGDS conjugated to the surface of the gel affected cell adhesion (Gunn et al., 2005; Hern et al., 1997). Based on these ideal characteristics, PEG-based hydrogels were used for the presented research.

1.7 Growth Factor Release from Biomaterials

Biomaterials have provided a delivery vehicle for growth factors involved in angiogenesis, including VEGF, FGF, and PDGF. These materials can be designed to provide various release profiles of growth factors, enabling controlled response. VEGF released increased viability of ischemic flats in rat dorsal skin (Mittermayr et al., 2008) and increased human umbilical vein endothelial cell (HUVEC) proliferation (King et al., 2000). Similarly, FGF-2 release has been used to enhance angiogenesis (Miyoshi et al., 2005; Fujita et al., 2007; Chinen et al., 2003) and induced more smooth muscle cell mitogenicity (Guan et al., 2007; Gou et al., 2008). Similar to FGF, PDGF-BB has been released from PLGA microspheres on a nanofibrous scaffold, which resulted in increased blood vessel number in an *in vivo* soft tissue wound repair model (Jin et al., 2008).

In order to better mimic the natural angiogenic process, combinations of growth factors have been released from biomaterials (Wong et al., 2003) (Nillesen et al., 2006) (Lee et al., 2003). For example, an *in vivo* Matrigel plug assay was used to elicit the effects of a combination of FGF-2 and VEGF, finding that VEGF enhances endothelial PDGF-B expression, and that FGF-2 enhances mural PDGF receptor β (PDGFR-β)

expression. The combinations of the factors induce significant mural cell recruitment, necessary for a functional vessel (Kano et al., 2005). The combination of VEGF and PDGF is not used based on evidence that VEGF-mediated activation of VEGFR-2 suppresses PDGFR-β expression in mural cells, thereby limiting the vascular response (Greenberg et al., 2008). This interaction is confirmed when VEGF-R2 is inhibited.

Seminal work in the mouse cornea and ischemic hindlimb models investigated three combinations of growth factors including VEGF and FGF-2, VEGF and PDGF-BB, and FGF-2 and PDGF-BB (Cao et al., 2003). Cao's study found a synergistic effect of FGF-2 and PDGF-BB (Figure 1-7), which was further investigated on a molecular level, suggesting that vascular endothelial cells are unresponsive to PDGF until FGF activation. The synergistic response results because FGF transcriptionally turns on PDGF receptor expression in endothelial cells, and PDGF-BB then induces a positive feedback signal by amplifying FGF-2 expression in vascular mural cells (Cao et al., 2008). Based on the work of Cao et al. illustrating this synergistic angiogenic response, this thesis research used a combination of FGF-2 and PDGF-BB.

1.8 Controlled Delivery of Growth Factors Using Biomaterials

Since growth factors have such substantial effects in the body, many growth factors have been examined in clinical trials which showed varied results. However, the same desirable biological effects also have the potential to create significant

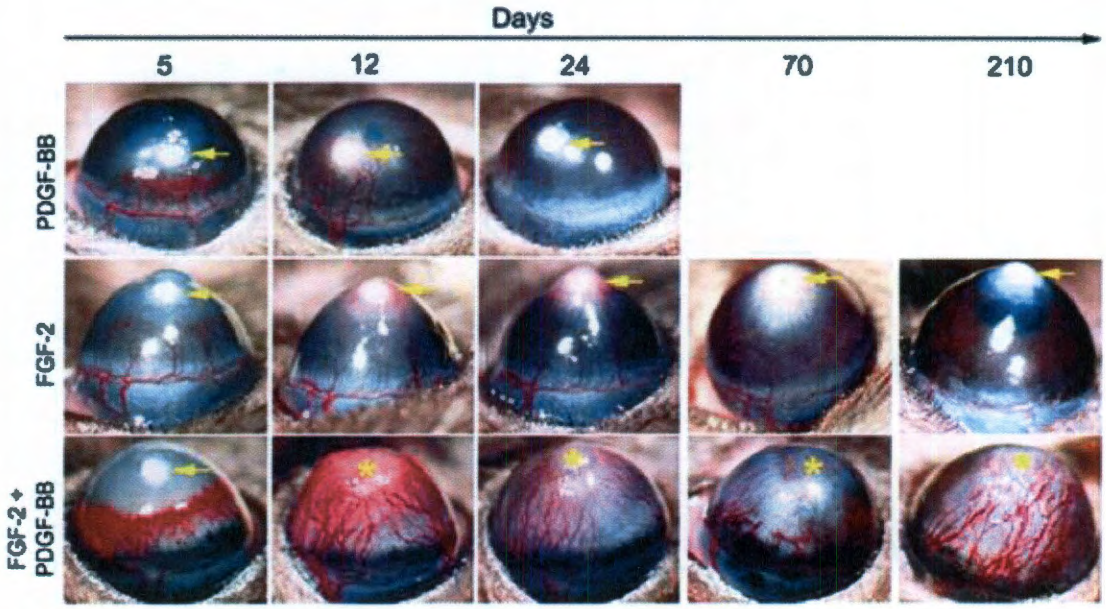

Figure1-7: Synergistic effects of FGF-2 and PDGF-BB as seen in the mouse cornea micropocket model. Notice the synergistic vessel formation in response to the combination of PDGF-BB and FGF-2. Also, vessels are stable for at least 210 days. Adapted from (Cao et al., 2003).

complications. Even in slow-release applications, high levels of growth factors circulate in the body, potentially inducing harmful side effects. Release of growth factors can lead to unintended angiogenesis, as seen in pathologies including retinopathy, rheumatoid arthritis, and tumor growth (Patel et al., 2004). Since VEGF induces vascular permeability, circulating VEGF has been associated with transient edema in 34% of patients (Baumgartner et al., 2000) and multi-organ edema leading to death in a high percentage of animals (Epstein et al., 2001). Systemic VEGF was also found to promote

atherosclerotic lesion growth and instability of atherosclerotic plaques. The combination of VEGF and FGF has been shown to produce vasodilation and hypotension through the nitric-oxide-mediated pathway, resulting in death of 50% of pigs tested (Epstein et al., 2001). In clinical trials, delivery of growth factors showed initial promise, but subsequent phase II trials failed to show efficacy (Semenza, 2006). Therefore, biomaterials have been used to provide a more controlled delivery system of potent growth factors and covalent linkage of growth factors to biomaterial matrices offers the promise of local bioactivity without the unintended systemic effects.

To improve the cellular response to releasable factors, biomaterials can be designed to control both spatial and temporal characteristics of angiogenic factor release. Control over spatial release is critical because undirected growth factor release leads to many pathological side effects. Many growth factors including FGF-2 and VEGF have a half life of less than one hour when released into the body due to cellular degradation (Lee et al., 2000). Control over temporal release can thus better mimic the natural process of angiogenesis, leading to more stable and functional vessel formation. Ennet et al. examined temporal VEGF release kinetics by combining PLGA scaffolds with PLG microspheres. In order to obtain sustained, local VEGF release for 21 days, VEGF release was tailored based on alterations in polymer composition, matrix composition, and scaffold size (Ennett et al., 2006). This system was improved upon by temporally controlling the release of both VEGF and PDGF-BB from PLGA (Figure 1-8) (Richardson et al., 2001). Both spatial and temporal release kinetics of VEGF and PDGF-BB were controlled using a similar porous PLGA scaffold to first deliver VEGF in one spatial region with subsequent release of PDGF-BB in an adjacent spatial region,

thereby leading to more mature vessels *in vivo* (Chen et al., 2007). VEGF was also released from biomaterials based on mechanical signals. Since blood vessels and many other tissues operate under a mechanically dynamic environment, alginate hydrogels were used as a matrix to mechanically control growth factor release by reversibly binding the growth factor to the hydrogel carrier (Lee et al., 2000). While biomaterials have enabled controlled growth factor delivery, many challenges still face growth factor delivery in the body. To overcome these challenges, growth factors can be covalently bound to the hydrogel, and this technique is used for this thesis research.

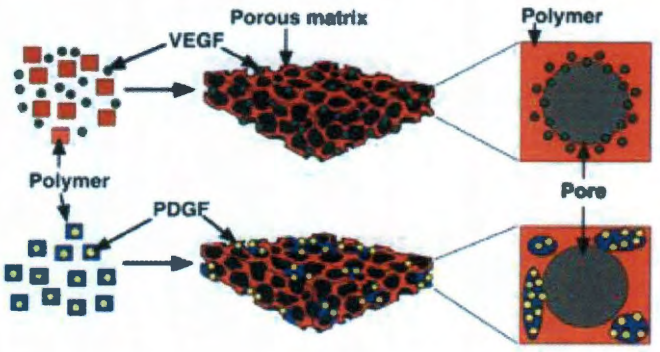

Figure 1-8: Spatial and Temporal Control of VEGF and PDGF Release. Temporal release of VEGF followed by PDGF was achieved by mixing VEGF with the polymer solution and pre-encapsulating PDGF into polymer microspheres. VEGF was subject to rapid release due to association with the surface of the polymer in contrast to PDGF release, which was regulated by the degradation of the polymer used to form the microspheres. Adapted from (Richardson et al., 2001).

1.9 Immobilized Growth Factors

Growth factors covalently attached to matrices enable prolonged delivery and bioactivity in a local, controlled manner. Heparan sulfate proteoglycans and fibrin naturally bind certain growth factors in order to deliver them during wound healing. For example, heparan sulfate proteoglycans regulate the biological activities of certain growth factors including VEGF and FGF-2. Heparan sulfate stabilizes these growth

factors by protecting them from proteolytic degradation thereby creating long-term reservoirs. VEGF has been the most highly studied, with covalent incorporation via both fibrin attachment (Ehrbar et al., 2008) and heparan attachment (Steffens et al., 2004) leading to significantly more vessel growth *in vivo*. Similar to the effects of VEGF, neovascularization was enhanced when sustained delivery of FGF-2 was achieved by allowing FGF-2 to bind to covalently incorporated heparan sulfate in collagen matrices (Pieper et al., 2002). Maynard et al. created a synthetic sulfated tetrapeptide which mimics heparin binding to VEGF in order to improve upon natural heparin, which is often heterogeneous and difficult to modify (Maynard et al., 2005). Covalent attachment can also be achieved via synthetic means, such as VEGF attachment to collagen matrices via a disuccinimidyldisuccinatepolyethyleneglycol (SS-PEG-SS) linker (Koch et al., 2006).

Another synthetic method to covalently attach proteins is poly(ethylene glycol), which represents an optimal method to covalently incorporate growth factors due to improved solubility, decreased immunogenicity, and increased stability. Due to PEG's hydrophilicity, proteins

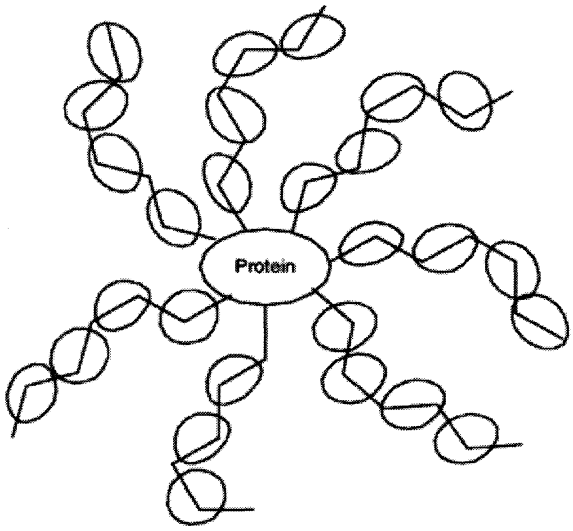

Figure 1-9: Schematic representation of a PEGylated protein. The protein is surrounded by long hydrophilic PEG chains with circles representing the cloud of water around the ether-oxygen groups of the polymer. Adapted from (Veronese et al., 2008).

conjugated to PEG are surrounded by a water cloud which decreases degradation by proteolytic enzymes and cells (Figure 1-9) (Veronese, 2001; Veronese et al., 2008). Furthermore, the water cloud causes an increase in protein size, leading to slower kidney filtration and longer blood circulation (Roberts et al., 2002). Based on these desirable characteristics, many drugs have been PEGylated and used in clinical therapy. Since the development of the first PEGylated drug in the 1970s, PEGylated pharmaceuticals are now used in the treatment of many chronic diseases including leukemia, rheumatoid arthritis, and hepatitis C. A summary of FDA-approved PEGylated pharmaceuticals is listed in Table 2.

Table 1-1: FDA approved PEGylated proteins. Table from (Veronese et al., 2008).

Trade name	Generic name	Parent drug	Size of PEG moiety (kDa)	Indication	Year of approval
Adagen®	Pegademase	Adenosine deaminase	5	SCID	1990
Oncaspar®	Pegaspargase	Asparaginase	5	Leukemia	1994
Neulasta®	Pegfilgrastim	G-CSF	20	Neutropenia	2002
PegIntron®	Peginterferon-α-2b	Interferon-α-2b	12	Hepatitis C	2000
Pegasys®	Peginterferon-α-2a	Interferon-α-2a	40	Hepatitis C	2001
Somavert®	Pegvisomant	hGH	5	Acromegaly	2003
Macugen®	Pegaptanib	Anti-VEGF aptamer	40	AMD	2004
Mircera®	PEG-EPO	Erythropoietin	40	Anemia	2007
Cimzia®	Certolizumab pegol	Anti-TNFα Fab'	40	Rheumatoid arthritis and Crohn disease	2008

AMD = age-related macular degeneration; **EPO** = erythropoietin; **G-CSF** = granulocyte colony-stimulating factor; **hGH** = human growth hormone; **SCID** = severe combined immunodeficiency disease; **TNF** = tumor necrosis factor; **VEGF** = vascular endothelial growth factor.

The first example of an immobilized protein via PEG conjugation was epidermal growth factor (EGF) in 1996. Prolonged EGF delivery is particularly important because a constant dose of EGF signaling is required over several hours to affect DNA synthesis. While use of slow-release polymers would prolong EGF delivery, maintaining constant levels of EGF is challenging. Ideal delivery systems account for cellular uptake and proteolytic degradation to ensure adequate levels of EGF are present while continuing to

allow cell surface events including signal transduction to occur. By PEGylating EGF, the growth factor maintained bioactivity in a nonendocytosible and nondiffusable form which maintained efficacy in eliciting DNA synthesis (Kuhl et al., 1996). Other growth factors have since been PEGylated, including bone morphogenic protein-2 (BMP-2) (Liu et al., 2007), TGF-β1 (Mann et al., 2001), TGF-β2 (Bentz et al., 1998), and FGF-2 (DeLong et al., 2005). Two PEGylated factors, VEGF and ephrinA1, have been specifically studied for their angiogenic effects. PEG-ephrinA1 induced endothelial tubulogenesis with luminal diameters in the range of 5-30 μm (Moon et al., 2007). PEGylated VEGF not only increased endothelial cell tubulogenesis, but also increased endothelial cell motility 14-fold and cell-cell connections 3-fold in a 3D biodegradable gel (Leslie-Barbick et al., 2009). Based on these significant results, PEGylated growth factors were used during the thesis work to induce neovessel formation.

1.10 Cellular Encapsulation for Angiogenesis in Biomaterials

Another approach to creating vascularized tissues is the use of cells, which naturally secrete angiogenic growth factors. Cells can be seeded on the surface of biomaterials or encapsulated in biomaterials. Cell-based approaches eliminate the time-delay inherent in releasing growth factors to stimulate host angiogenesis and also eliminate the need to optimize dose and release of growth factors. For example, Chen et al. allowed a co-culture of human umbilical vein endothelial cells (HUVECs) and fibroblasts to form tubes *in vitro* for seven days before *in vivo* implantation. Scaffolds containing pre-formed tubes led to anastamosis with the host vasculature within 5 days as compared to 14 days for scaffolds without pre-formed tubes. Additionally, the number

and area of perfused lumens was significantly higher in prevascularized scaffolds (Chen et al., 2008).

A wide variety of cell sources has been investigated from mesenchymal stem cells, adipose stem cells, endothelial progenitor cells, and human embryonic stem cells. Nor et al. showed the feasibility of this approach when human dermal microvascular endothelial cells (HDMEC) seeded on poly L-lactic acid (PLLA) scaffolds formed functional vessels, which anastomosed with the host vasculature (Nor et al., 2001). The response was enhanced when HDMECs were cocultured with human osteoblasts on a 3D bone biomaterial composed of hydroxyapatite, calcium phosphate, and nickel titanium (Unger et al., 2007). A co-culture using three cell types, keratinocytes, fibroblasts, and endothelial cells, decreased the response time to form capillary-like structures in a skin-substitute from fourteen days to four days (Tremblay et al., 2005). Koike et al. formed long-term stable vessels when HUVECs were used alone and in combination with pericyte precursor cells (10T1/2) on a fibronectin-type I collagen matrix (Koike et al., 2004). HUVECs alone formed vessels with minimal perfusion, but HUVECs and 10T1/2 cells formed a functional vascular network capable of anatosmosing with host circulatory system up to one year later as seen in Figure 1-10 (Au et al., 2007). When HUVECs were cocultured with 10T1/2 cells, 10T1/2 cells displayed a smooth muscle cell morphology and began expressing pericyte markers, such as α-smooth muscle actin, smooth muscle myosin, and calponin (Hirschi et al., 1998).

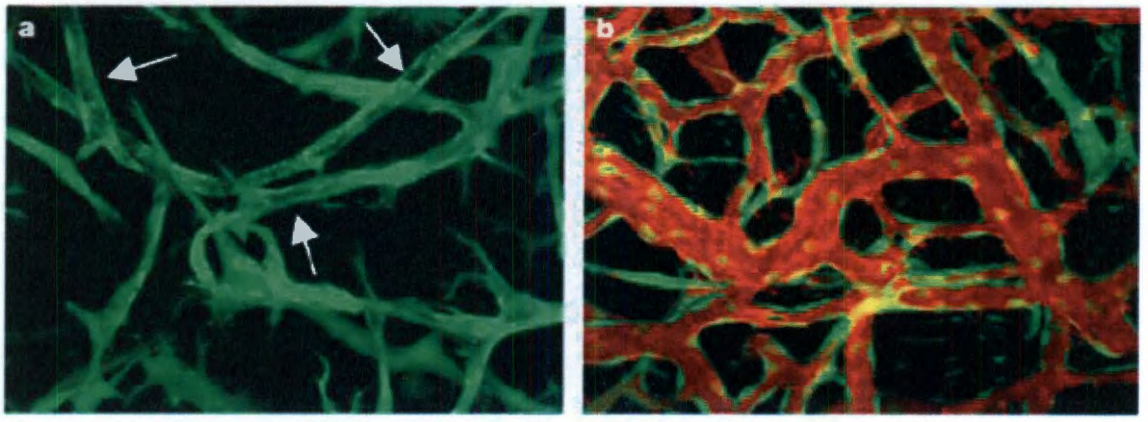

Figure 1-10: Engineered blood vessels using HUVECs and 10T1/2 cells. (A) Vacuoles (arrows) resembling the lumen of capillaries were seen four days after implantation, but were not perfused (indicated by the absence of red). (B) Engineered vessels were functional and stable four months after implantation. Figure adapted from (Koike et al., 2004).

Endothelial progenitor cells, identified in 1997 in human peripheral blood as a key player in adult neovascularization, have also been used in therapeutic angiogenesis. Endothelial progenitor cells begin as mononuclear hematopoietic progenitor cells capable of differentiating into endothelial cells as part of vasculogenesis when released from the bone marrow into peripheral circulation upon a physiological stimulus. Human embryonic stem cells, differentiated into platelet/endothelial cell adhesion molecule-1 (PECAM-1) expressing endothelial-like cells, showed an angiogenic response in SCID mice and an ischemic hindlimb (Levenberg et al., 2002; Cho et al., 2007). When the differentiated endothelial-like cells were combined with 10T1/2 cells, the tubule structures were observed after only two days *in vivo* (Wang et al., 2007). Other stem cells sources, including hematopoietic stem cells and mesenchymal stem cell in the bone marrow have also shown a vascular response (Moioli et al., 2008).

Cellular response has been enhanced with the addition of growth factors. Lower doses of growth factors than currently used in clinical trials can be used to act upon the

transplanted vessel-forming cells, promoting survival, proliferation, and differentiation. Peters et al. showed that functional vessels were formed after seven days when human microvascular endothelial cells were seeded with VEGF in PLG (Peters et al., 2002). The combination of dermal fibroblasts and HUVECs showed significantly more capillary formation in response to FGF-2 and VEGF (Hudon et al., 2003). Frerich et al. enhanced capillary formation by combining two cell types, HUVECs and stromal cells from adipose tissue, along with two growth factors, VEGF to stimulate angiogenesis and insulin-like growth factor (IGF)-1, to stabilize the capillary structures (Frerich et al., 2001). Others have even transfected cells to overexpress angiogenic growth factors in order to ensure prolonged, local growth factor delivery (Ikeda et al., 2004; De Coppi et al., 2005; Rinsch et al., 2001). A co-culture of endothelial cells and pericytes was encapsulated into PEG hydrogels along with soluble factors in order to induce anastomosis formation between cell-formed tubules and host vasculature. This thesis research is further discussed in Chapter 5.

1.11 Innovative Biomaterial Design

Alternative methods to induce neovascularization involve using patterning techniques such as microchannel designs to mimic capillary networks and allow biomaterials to guide neovascularization (Hoffmann et al., 2010). Endothelial cells can then be seeded along the microchannels, providing a vasculature in the scaffold capable of connecting with the host vasculature. This method eliminates time delays involved in inducing angiogenesis. For example, a fibrin gel containing a polyurethane mesh releasing VEGF was grown in a CAM angiogenic assay to enable prevascularization.

Once the polyurethane mesh contained capillary networks through the scaffold, it underwent a freeze-thaw cycle and was implanted *in vivo*. Revascularization of the networks occurred within three days of implantation, possibly due to enhanced adhesion from ECM proteins such as collagen IV and laminin from prevascularization or a chemotactic effect from cell remnants attracting host macrophages, which secrete endothelial signals (Sanders et al., 2003). Using a similar technique, polyvinyl alcohol matrices releasing FGF-2 were implanted into the rat mesentery and allowed to prevascularize for one week before seeding hepatocytes onto the scaffolds. Prevascularization increased the mean number of vessels and survival of hepatocytes, probably due to improved oxygen transport (Ogawa et al., 2001). Stosich et al. created cylindrical channels within hydrogel networks and examined the effects of patterned networks when combined with FGF-2 release. Hydrogels with channels but without FGF-2 showed host infiltration only in the microchannels, and hydrogels with FGF-2 but without microchannels showed random and isolated areas of vessel infiltration. Hydrogels containing both FGF-2 and microchannels showed significant infiltration in channels (Stosich et al., 2007). While the thesis work presented does not use a prevascularization technique, future research could combine a prevascularization technique with immobilized growth factors and encapsulated cells as presented in this thesis.

1.12 Summary

Although much research has been performed to induce angiogenesis, significant work remains before a tissue engineering scaffold containing a functional

microvasculature system can be utilized in a clinical setting. Poly(ethylene glycol) based hydrogels act as a biocompatible scaffold to deliver growth factors in both soluble and immobilized forms. The hydrogels were rendered biodegradable by incorporating an MMP-degradable sequence into the polymer backbone (West et al., 1999). Finally, mild crosslinking conditions enable cellular encapsulation into the matrix. This thesis includes several novel techniques and combinations of growth factors and cells to improve upon the existing work to promote neovessel formation in poly(ethylene glycol) hydrogels. Specifically, PDGF-BB and ephrinA1 were covalently immobilized to the hydrogels and shown to promote angiogenesis. Furthermore, for the first time PEG hydrogels were tested in an *in vivo* model of the mouse cornea micropocket. Bioactive hydrogels with releasable growth factors were shown to induce angiogenesis. The response was then tailored using rational design of hydrogels. Finally, encapsulated cells forming tubule networks throughout the hydrogels were implanted and shown to anastomse to host vasculature. These fundamental contributions bring ever closer the reality of using biomaterials containing a microvascular system in a clinical setting.

Chapter 2: Biomimetic Poly(ethylene glycol) Hydrogels Promote Angiogenesis in a Mouse Model

Portions of this chapter were obtained from:

RA Poche, **JE Saik,** JL West, ME Dickinson. "The mouse cornea as a transplantation site for live imaging of engineered tissue constructs." *Cold Spring Harbor Protocols.* doi:10.1101/pdb.prot5416. (cover)

JJ Moon, **JE Saik**, RA Poche, JE Barbick, SH Lee, AA Smith, ME Dickinson, JL West. "Biomimetic hydrogels with pro-angiogenic properties" *Biomaterials.* 14:3840-7, 2010.

RA Poche, IV Larina, ML Scott, **JE Saik,** JL West, ME Dickinson. "*Flk1-myr::mCherry* mouse as a useful reporter to characterize multiple aspects of ocular blood vessel development and disease." *Developmental Dynamics.* 238:2318–2326, 2009. (cover)

2.1 Introduction

Biomaterials can provide a local, controlled delivery system for release of angiogenic growth factors as potential treatments for ischemic disease or to improve blood supply to engineered tissues. Precise control over delivery of growth factor concentrations is necessary to induce the desired cellular responses (Tayalia et al., 2009). Current methods to deliver growth factors to induce angiogenesis *in vivo* rely on bolus injections. However, clinical trials examining bolus injections of these agents highlight the concern of harmful side effects resulting from systemic injection, including hypotension, edema, and vasodilation (Epstein et al., 2001). Many of these side effects may be mitigated by achieving precise control of local growth factor delivery over the time scale necessary to produce the desired biological response. For instance, growth factors can be incorporated into the precursor solution, thus entangling the signals into the scaffold following polymer crosslinking. Growth factors are then released from the

scaffold via diffusion, establishing a concentration gradient. Growth factor delivery for angiogenesis has been achieved using natural scaffolds (Mittermayr et al., 2008; Miyoshi et al., 2005; Fujita et al., 2007; Chinen et al., 2003; Nillesen et al., 2006) as well as synthetic polymers (Lee et al., 2000; Guan et al., 2007; Ennett et al., 2006; Richardson et al., 2001). Scaffolds delivering vascular endothelial growth factor (VEGF) have been used to induce dose dependant, pro-angiogenic responses including increased vascularization, pericyte coverage, and vessel perfusion (Davies et al., 2008). VEGF dose and temporal distribution was also found to govern endothelial cell phenotype in an in vitro model and optimal angiogenic sprouting *in vivo* (Silva et al.).

Although many growth factors have been shown to have angiogenic properties, the majority of work has focused on three growth factors as discussed in chapter 1: vascular endothelial growth factor (VEGF), platelet derived growth factor (PDGF-BB), and fibroblast growth factor (FGF-2). VEGF, released in response to hypoxia, stimulates endothelial cells to migrate, proliferate, and differentiate (Nomi et al., 2006). Hypoxia also induces macrophages to release FGF-2, which stimulates endothelial cell proliferation and migration, and regulates the expression of key angiogenic molecules, such as collagenases and β1 integrins (Bikfalvi et al., 1997). PDGF-BB is involved in the stabilization of developing capillaries by recruiting pericytes and inducing them to produce the extracellular matrix proteins that constitute the basement membranes of functional blood vessels. In addition, PDGF-BB has been implicated as a key factor in anastamosis formation (Betsholtz et al., 2005; Khachigian et al., 1995).

VEGF has been widely used to induce angiogenesis, but VEGF-induced vessels have been shown to be unstable, leaky and hemorrhagic (Jain, 2005; Jain et al., 2005).

Cao et al. used Hydron pellets to deliver VEGF, PDGF-BB, or FGF-2 alone and in combinations to the mouse cornea. Analysis of resulting vessel formation in response to either PDGF-BB or VEGF alone indicated total vessel regression by 24 days and by 70 days for FGF-2-induced vessels (Cao et al., 2003). Notably, vessels formed in response to the combination of FGF-2 and PDGF-BB was stable for over 210 days. Hydron pellets containing growth factors were also removed from the eye 6 days after implantation, causing total vessel regression within one week of all samples but those containing PDGF-BB and FGF-2. As compared to VEGF-induced vessels which were highly leaky, vessels formed in response to PDGF-BB and FGF-2 remodeled into well-defined branching and organized structures that were not leaky when perfused with fluorescent dextran (Cao et al., 2003). As an indicator of vessel maturity 25 days after implantation, 70% of vessels formed in response to PDGF-BB and FGF-2 were desmin positive as compared to only 40% for FGF-2 induced vessels (at this point all PDGF-BB induced vessels had regressed). The addition of VEGF antagonists confirmed the VEGF-independent vessel formation using PDGF-BB and FGF-2 (Cao et al., 2003). Findings were corroborated in the hind limb ischemia model, which shows that PDGF-BB and FGF-2 increased collateral vessel growth and paw blood perfusion, and vessels were well organized and stable for over 60 days. The synergistic response was later found to result because FGF-2 transcriptionally turns on PDGF-BB receptor expression in endothelial cells and PDGF-BB then induces a positive feedback signal by amplifying FGF-2 expression in vascular mural cells (Cao et al., 2008).

In light of the data showing that the combination of FGF-2 and PDGF-BB promote the formation of more stable vessel structures than VEGF, there is a tremendous

interest in using these factors to promote tissue repair and to induce angiogenesis and perfusion of biomaterial scaffolds for tissue engineering. The combination of these factors is a powerful tool for controlling the angiogenic response, and in this study a range of responses to concentrations of these factors was determined in order to tune the angiogenic response to these factors and to control angiogenesis *in vivo*.

This thesis research used poly(ethylene glycol) (PEG) diacrylate, a photocrosslinkable and biocompatible polymer, to deliver angiogenic growth factors in a local, controlled manner. Hydrogels were further modified with an immobilized RGD peptide (a sequence commonly found in fibronectin and other cell-adhesive proteins) (Gunn et al., 2005; DeLong et al., 2005) and rendered them proteolytically degradable by incorporating matrix metalloproteinase (MMP) sensitive cleavable peptide sequences into the polymer backbone (Moon, 2008; West et al., 1999) to allow for invading cells to degrade the material (Moon, Saik, Poché et al., 2010). The photocrosslinking process enables inclusion of releasable growth factors prior to crosslinking for local, controlled delivery to induce host vessel invasion (Leslie-Barbick et al., 2009). In this manner, releasable factors and covalently bound adhesive factors can work in concert to induce rapid and stable vascularization of these constructs. This research demonstrates a slow-release profile of growth factors from these materials enabling prolonged, local delivery of the encapsulated agents. This release was modulated by adjusting the polymer molecular weight and solution concentration and by incorporating the proteins either before or after hydrogel crosslinking.

Through the adjustment of growth factor concentrations, this thesis research has induced a microvasculature which is morphologically similar to target tissues, including

skin and skeletal muscle. Normal tissues require a precise and unique vessel pattern to maintain an equilibrium between growth and cellular demands (Jain et al., 2005; Jain, 2003). Each tissue possess a unique microvascular morphology (Humphrey et al., 2001) related to initial development, metabolic need, physiological function and ultrastructural shape and dynamics (Caplan, 1985). For example, skeletal muscle contains uniquely shaped vessels for delivery of nutrients while allowing for the linear application of forces (Carlson, 1973; Tong et al., 2004). In fact, Jain postulated that skeletal muscle is incredibly difficult to recapitulate due to its dense perfusion and high metabolic rate (Jain et al., 2005). This system combines tailored, local delivery of growth factors in angiogenic scaffolds along with quantification of induced vessel morphological and space filling parameters.

The mouse cornea serves as the *in vivo* implantation site because induced vessels can be quantitatively examined microscopically (Gaudric et al., 1992; Auerbach et al., 2003), enabling high resolution imaging over time, and the external nature of the cornea allows for facile surgical implantation and analysis. The cornea is a transparent tissue covering the outer surface of the eye which, together with the lens, functions to transmit and refract light. The mature cornea consists of an outer stratified epithelial cell layer, an inner collagenous stroma with a sparse population of keratocytes, and an inner endothelial cell monolayer (for descriptions of eye anatomy and histology, see (Zieske, 2004)). For efficient transmittance of light, the cornea has evolved as an avascular tissue. Nevertheless, the cornea is still capable of experiencing substantial neovascularization in response to severe physical, chemical, and thermal injury, implantation of tumors and other physiological insults (Muthukkaruppan et al., 1979; Gimbrone et al., 1973;

Langham, 1953). The mouse corneal micropocket angiogenesis assay has capitalized upon this property and is often considered the gold standard to determine whether signaling peptides, drugs, etc. function as proangiogenic or anti-angiogenic factors in vivo (Kenyon et al., 1996; Rogers et al., 2007). This assay has several advantages. For example, because the cornea is normally avascular, there are no background vessels present. Thus, the researcher does not have to make any assumptions as to whether the observed changes in vascular structure are the result of remodeling of preexisting vessels or neovascularization (Kenyon et al., 1996; Rogers et al., 2007). Another major advantage of this system is that the cornea is a relatively immune privileged site and is externally located (Streilein, 2003, 2003). These properties lend themselves to minimally invasive and high-throughput transplantation of experimental tissue constructs and also allow live imaging of construct vascularization in vivo (Poche et al., 2010). The mouse cornea also provides a well established and reproducible assay (Kenyon et al., 1996).

By correlating the resulting vessel formation to the growth factor dose delivered, this thesis research induced a vascular structure with a desired fractal dimension. Importantly, in only tuning for the appropriate fractal dimension, the desired diameters and branch points as well as density and lacunarity of target vessel networks were also recreated. This robust system is capable of characterization of vessel morphology and the study of angiogenesis, for applications in tissue engineering, ischemic disease and tumor vessel biology.

2.2 Materials and Methods

2.2.1 Synthesis and Purification of Poly (ethylene glycol) Diacrylate (PEGDA)

Poly (ethylene glycol) (PEG) (MW = 6000 Da; Fluka, Milwaukee, WI) was acrylated by reacting dry PEG with acryloyl chloride (Sigma, St. Louis, MO) and triethyl amine (TEA; Sigma, St. Louis, MO) in anhydrous dichloromethane (DCM; Sigma, St. Louis, MO) under argon gas overnight at 1:4 PEG:acryloyl chloride and 1:2 PEG:TEA molar ratios. The resulting solution was purified using 2 M K_2CO_3 to separate the solution into aqueous and organic phases. After allowing the solution to separate overnight, PEGDA, in the organic phase, was further purified using anhydrous $MgSO_4$ to remove residual aqueous solution. $MgSO_4$ was removed via filtration before precipitating PEGDA, using diethyl ether. PEGDA was separated via filtration and dried overnight under vacuum. PEGDA powder was stored at -20°C under argon gas.

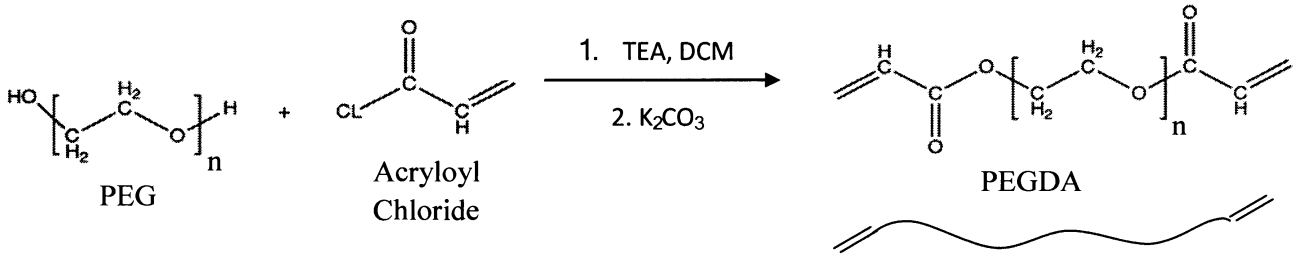

Figure 2-1: Synthesis of PEGDA.

2.2.2 Synthesis and Purification of PEG-succinimidyl carbonate (PEG-SMC)

PEG (Fluka/Sigma, MW = 3400 Da) was reacted with Ag_2O (Sigma, St. Louis, MO), acryloyl chloride (Sigma, St. Louis, MO), and KI (Sigma, St. Louis, MO) in anhydrous dichloromethane (DCM; Sigma, St. Louis, MO) at 4°C overnight, at molar excess ratios of 1.5, 1.1, and 0.3 respectively. Silver was removed by filtering the

solution through Celite 521 (Spectrum Chemical Mfg Corp, Gardena, CA). A Rotovap was used to dry the solution prior to dissolution in di H_20. Using HCl, pH was adjusted to 3, and the solution was heated to 35°C for one hour. Iodine was removed by adding activated charcoal (Fisher, Pittsburg, PA), and the solution was filtered through Celite 521. NaCl and DCM were added, followed by DCM extraction. Phase separation with 2 M K_2CO_3 was used to remove any acid and chloride ions. Sodium sulfate (Fisher) was used to dry the monoacrylated PEG, and a Rotovap was used to concentrate the solution. Ethyl ether was used to precipitate monoacrylated PEG followed by vacuum filtration. A four molar excess of disuccinimidyl carbonate (Sigma) was reacted with the monoacrylated PEG in anhydrous acetonitrile (Sigma) and pyridine (Sigma) under argon gas overnight. A Rotovap was used to dry the resulting product prior to dissolving in anhydrous DCM. The solution was filtered and PEG-SMC was purified in acetate buffer (0.1 M, pH 4.5, 15% NaCl) via phase separation. The purified PEG-SMC was dried using anhydrous $MgSO_4$. Ethyl ether was used to precipitate out PEG-SMC which was filtered and dried overnight under vacuum. Proton nuclear magnetic resonance spectroscopy (^{1}H-NMR, Avance 400 Hz; Bruker, Billerica, MA, USA) and matrix-assisted laser desorption/ionisation-time of flight mass spectrometry (MALDI-TOF; Bruker Daltonics, Dillerica, MA, USA) were used to characterize synthesized PEG-SMC. The final PEG-SMC product was stored at -80°C under argon gas.

2.2.3 Synthesis and Purification of PEG-RGDS

Sodium bicarbonate buffer (50mM, pH of 8.5) was used to dissolve both synthesized PEG-SMC and the cell-adhesive peptide Arg-Gly-Asp-Ser (RGDS, Figure,

American Peptide, Sunnyvale, CA) separately. PEG-SMC solution was added to the RGDS solution in a 1.1:1 PEG-SMC: RGDS molar ratio. Under gentle rocking, the mixture was allowed to react at 4°C for four days, followed by a final four hours at 25°C. The reacted solution was dialyzed against four liters di H_2O via a 1000 Da molecular weight cutoff dialysis membrane (Spectrum Laboratories, Rancho Dominguez, CA) for 24 hours with repeated di H_20 changes. The resulting PEG-RGDS solution was lyophilized and stored at -80°C under argon gas. Coupling efficiency of PEG-RGDS was analyzed by a gel permeation chromatography (GPC) system equipped with a PLgel column (5μm, 500Å, Polymer Laboratories, Amherst, MA) and an evaporative light scattering (ELS) detector (Polymer Laboratories). The PEG-RGDS was dissolved in 0.1% ammonium acetate in dimethylformamide (DMF) solvent and tested against a PEG-SMC standard.

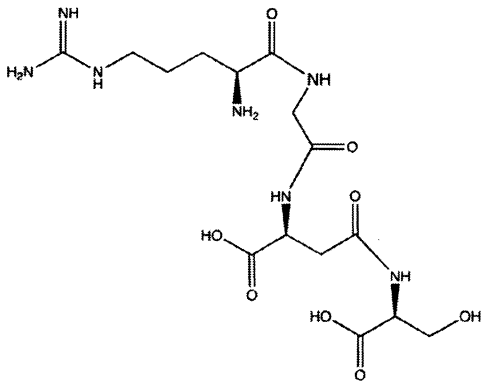

Figure 2-2: Chemical Structure of RGDS

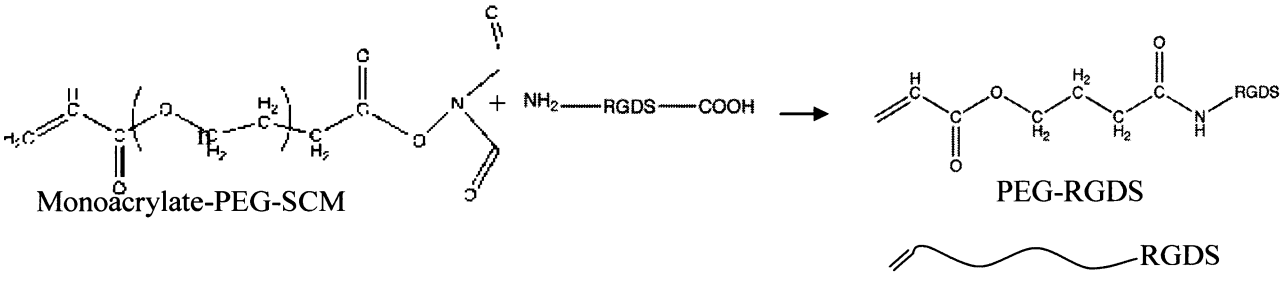

Figure 2-3: Peptide coupling to PEG monoacrylate.

Fluorescent PEG-RGDS was synthesized by reacting PEG-RGDS with alexa fluor 488 carboxylic acid (Invitrogen) with 10-fold dye molar excess in DMF. The solution was reacted on a rocker for two hours, lyophilized, and stored under argon in a -80°C freezer until use.

2.2.4 Synthesis of hydrogels to vary FGF release

An ELISA was also used to quantify the release of FGF from hydrogel formulations that differed in polymer molecular weight and percent composition. 3.4 kDa and 35 kDa PEGDA hydrogels (10% w/v) with 27 ng/gel FGF were synthesized in a manner similar to that described above (n=3). Additional 3.4 kDa hydrogels were formulated with the same concentration of FGF, but with PEGDA solution concentrations of 5% and 20% (n=3).

To quantify the influence of protein loading procedures on the release of growth factors, FGF was first fluorescently labeled by reaction with Alexa Fluor® 350 carboxylic acid, succinimidyl ester (Invitrogen, Carlsbad, CA) at a 1:10 molar ratio in HBS. Fluorescently-labeled FGF was incorporated into hydrogels before crosslinking by mixing into the prepolymer solution at a concentration of 58 ng/gel (n=6) or after crosslinking by soaking hydrogels for 4 h in a growth factor-rich solution at a concentration of 0.4 μg/ μl (n=5). The hydrogel soak solution was read on a Fluorolog (Horiba, Edison, NJ) plate reader at designated time points and compared to a standard curve.

2.2.5 Synthesis of Degradable Hydrogels

Hydrogels were rendered degradable based on a collagenase-sensitive sequence GGGPQGIWGQGK (abbreviated PQ). The PQ peptide was synthesized using Fmoc chemistry on an APEX 396 solid phase peptide synthesizer (Aapptec) and characterized using MALDI-TOF. The PQ peptide was used to link two PEG chains, in order to create PEG-PQ-PEG. PEG-PQ-PEG was synthesized by dissolving the PQ peptide into anhydrous dimethyl sulfoxide (DMSO) and adding diisopropylethylamine (DIPEA). Similarly, acrylol-PEG-SCM (Laysan) was dissolved into DMSO. The PEG-SCM solution was dripped into the PQ-peptide solution with a 2.1 molar excess of PEG-SCM. This mixture was placed on a rocker overnight before being dialyzed in a regenerated cellulose membrane to remove unwanted products. After dialysis, the solution was lyophilized and characterized with gel permeation chromatography.

2.2.6 Incorporation and quantification of VEGF, PDGF, and FGF in hydrogels

Hydrogels were prepared to a final concentration of 10% PEG-PQ-PEG and 3.5 μmol/ml PEG-RGDS. The photoinitiator 2-dimethoxy-2-phenylacetophenone (acetophenone, Sigma) was prepared as a stock solution by dissolving 300 mg acetophenone in 1 ml N-vinylpyrrolidone (NVP) and used at a concentration of 10 μl/ml polymer solution. Growth factors were added to the liquid prepolymer solution at concentrations of 320 ng/gel for VEGF and PDGF and 80 ng/gel for FGF. These concentrations correspond to doses necessary to induce *in vivo* vascular responses. Hydrogels were polymerized between two glass slides separated by a 0.005 inch thick poly(tetra fluoroethylene) spacer. 0.12 μl polymer solution was injected between slides

using a Hamilton syringe and exposed to UV light (B-200SP UV lamp, UVP, 365 nm, 10 mW/cm^2) for two min. Hydrogels were immediately placed in HEPES buffered saline (HBS) with 0.1% bovine serum albumin and kept in a 37 °C incubator. Buffer was collected and replenished at desired time points. Three hydrogels were analyzed for FGF, 4 for VEGF, and 5 for PDGF. Growth factor release was quantified using ELISAs (R&D Systems, Minneapolis, MN for VEGF and PDGF and Ray Biotech, Norcross, GA for FGF).

2.2.7 Degradation of PEG-PQ-PEG

Degradation of PEG-PQ-PEG hydrogels was monitored using the tryptophan absorbance peak (280 nm). Since the PQ-peptide contains a tryptophan, its degradation was examined by quantifying tryptophan in the surrounding solution over time. A collagenase buffer was created by mixing 0.2 mg/ml collagenase IV, 0.2 mg/ml sodium azide, and 10mM calcium chloride in HEPES-buffered saline (HBS). A proteinase K buffer was used as a positive control and made by mixing 0.2 mg/ml proteinase K with 0.2 mg/ml sodium azide in HBS. The polymer solution was created by dissolving 10% (weight/volume) PEG-PQ-PEG and 10 µl/ml 2,2-dimethoxy-2-phenylacetophenone in HBS. The polymer solution was sterile filtered. Five µL droplets were formed at the bottom of 200 µL sterile cuvettes by exposing to UV light (B-200SP UV lamp, UVP, 365 nm, 10 mW/cm^2) for two minutes. Hydrogels were covered in sterile PBS overnight to enable swelling. PBS was then exchanged with either collagenase or proteinase K buffer. Absorbance measurements at 280 nm were taken for all samples at multiple timepoints using a UV spectrophotometer (Varian).

2.2.8 Synthesis of Hydrogels

Six kDa PEGDA or degradable PEG-PQ-PEG was dissolved in HBS. Polymer solution varied from 5% to 15% polymer weight percentage solutions. The photoinitiator acetophenone was dissolved with N-vinylpyrrolidone (NVP) (300 mg/mL) and added to the polymer solution at a concentration of 10 μL/mL. The solution was vortexed and sterile filtered. Hydrogels were polymerized between two glass sides separated by a 0.005 inch thick poly(tetra fluoroethylene) (PTFE) spacer. The glass slides and spacer were secured using clips. Growth factors were mixed into the polymer solution to create desired concentrations of VEGF, PDGF-BB, and FGF-2 per gel. Growth factor concentrations were used based on previously established optimal concentrations in the mouse cornea (Rogers et al., 2007). 0.12 μL polymer solution was inserted in between glass slides using a Hamilton syringe. Hydrogels made with acetophenone were exposed to UV light (B-200SP UV lamp, UVP, 365 nm, 10 mW/cm^2) for two minutes while hydrogels formed with Irgacure 2959 were exposed to the same light for 7 minutes. Hydrogels synthesized with eosin Y were exposed to white light for 40 seconds. After exposure, crosslinked hydrogels were immediately inserted into the cornea micropocket.

2.2.9 FLK1-myr::mCherry Mice

Mice expressing the mCherry fluorophore via the Flk1 promoter have previously been characterized (Larina, 2009). Mice used in this study were from the colony established in the Dickinson lab at Baylor College of Medicine containing fluorescently labeled endothelial cells, and all experiments were in accordance with an IACUC and

AALAS approved animal protocol at Baylor College of Medicine. These mice allowed for facile visualization and imaging of blood vessels for this study.

2.2.10 Hydrogel Implantation into the Mouse Cornea Micropocket Angiogenesis Assay

Using a modified version of the previously described corneal micropocket angiogenesis assay (Rogers et al., 2007), hydrogels were implanted into a mouse cornea, and corneal angiogenesis was imaged 7 days post-implantation. The novel *Flk1-myr::mCherry* transgenic mouse line was used to enable *in vivo* imaging of angiogenesis via fluorescently labeled endothelial cells (Larina et al., 2009). Mice were anesthetized by intraperitoneal injection of Avertin (0.2 ml/10g body weight of a 1.25% solution) and maintained on a pad heated to 37 °C. As a local anesthetic, one drop of proparacaine (0.5%, Bausche and Lomb) was applied to the eye immediately before the surgery. Next, a partial thickness incision was made into the mouse cornea, and the micropocket was created using a von Graef knife. Using a number 5 forceps, hydrogels were implanted into the micropocket immediately after cross-linking. Subsequently, a bacitracin zinc/polymyxin B sulfate antibiotic ointment (Bausch and Lomb) was applied to the corneal surface upon which the mouse was returned to the heated cage for recovery.

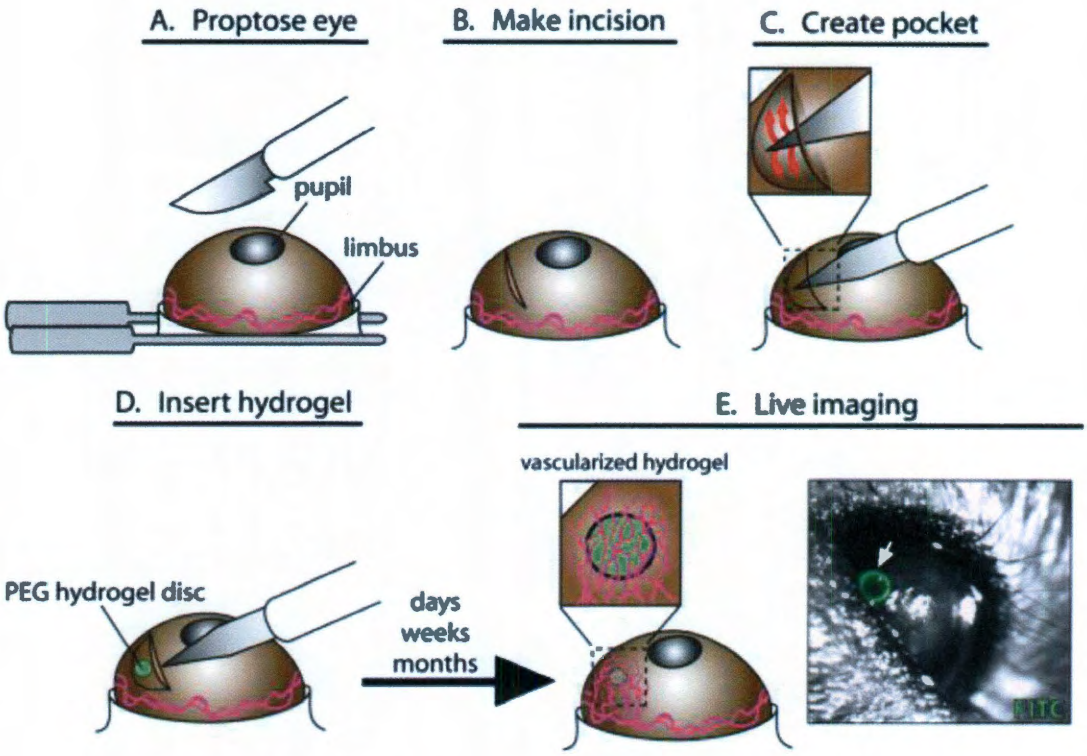

Figure 2-4: Modified corneal micropocket assay. *(A-E)* Shown here is an illustration detailing the steps involved in surgical implantation of fluorescently labeled hydrogel discs into the mouse cornea. By incorporating a fluorescent dye such as fluorescein isothiocyanate (FITC), the hydrogel is easily observed within the corneas of live mice (*E*, arrowhead) (Poche et al., 2010).

Seven days post-implantation, the mice were sacrificed using CO_2 inhalation. The eyes were enucleated and fixed in 4% paraformaldehyde for one hour at 4°C. Fixed eyes were washed with phosphate buffered saline (PBS, pH 7.3) and corneal flat-mount preparations were made (Figure 2-5). Imaging was performed using a Zeiss LSM 510 META inverted microscope system (Carl Zeiss Inc) equipped with a Zeiss Plan-Apochromat 20×/0.75 NA objective. 543-nm and 488-nm lasers were used to excite the *Flk1-myr::mCherry* and fluorescent PEG-RGDS, respectively.

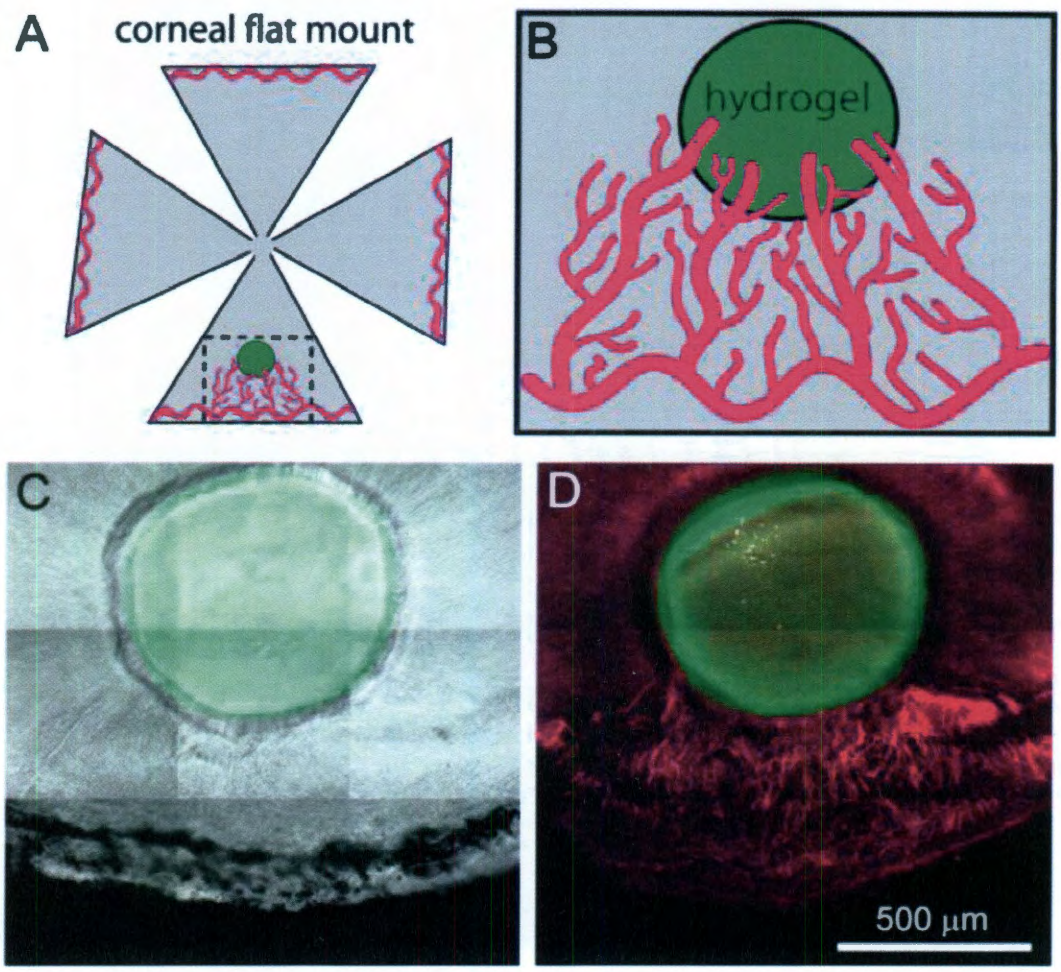

Figure 2-5: Corneal flat mounts from implanted Flk1-myr::mCherry transgenic mice. (*A*) Schematic depiction of a corneal flat mount showing how the tissue is separated into quadrants, with one quadrant containing the implanted hydrogel and induced host vessels. (*B*) Blown-up view of the boxed region in panel *A*. (*C,D*) Tiled, confocal images of an actual corneal flat mount show a green fluorescently labeled hydrogel (containing VEGF) sitting adjacent to the limbic region (*C*) and Flk1-myr::mCherry+ (magenta) neovessels extending toward the hydrogel (*D*) (Poche et al., 2010).

2.2.11 Analysis of Angiogenic Response

At designated timepoints, eyes were excised from euthanized mice, and the cornea was dissected and flatmounted by cutting the cornea in four locations 90 degrees

apart, creating a relatively flat corneal surface. Confocal images of Flk1-myr::mCherry labeled vessels were acquired from flatmounted corneas containing the tissue constructs using an LSM 510 META (Carl Zeiss) confocal microscope and a C-Apochromat 40x/1.2NA water immersion lens. A 543 nm laser was used to excite the mCherry fluorophore, and 22 micron thick z-stacks of vessels labeled by mCherry directly on the scaffolds were collected such that the step size between two successive images in z-stacks was 1.1 microns. This thickness was chosen because previous studies of vasculature were similar parameters were measured used these dimensions for tissue imaging (Gould et al., 2011). Each 8-bit image in the z-stacks consists of 512 x 512 pixels.

2.2.12 Vessel Branch Points and Diameters

The branching was quantified, using the LSM image browser to count the total number of branch points per three dimensional image field in each image of vessels. Diameters were likewise quantified, and the results were compared using ANOVA with post hoc Tukey test.

2.2.13 Image processing

Images of the vascular beds were processed in similar fashion to what was reported previously (Gould et al., 2011). Briefly, stacks of the vessels were projected then thresholded in order to create binary images for processing. Thresholds were kept constant between images of vessel beds to ensure comparison methods. Images of

vessels were first converted to projections using Image J and then converted to 8-bit grayscale. These projections were opened in adobe and had an unsharp mask applied to them, which serves as a high-pass filter to remove haziness from around the vessels while preserving vessel diameters. The finished grayscale image was opened in MATLAB and a threshold of 90 in all cases was applied and determined to be the most useful at recreating the appearance of the original vessels.

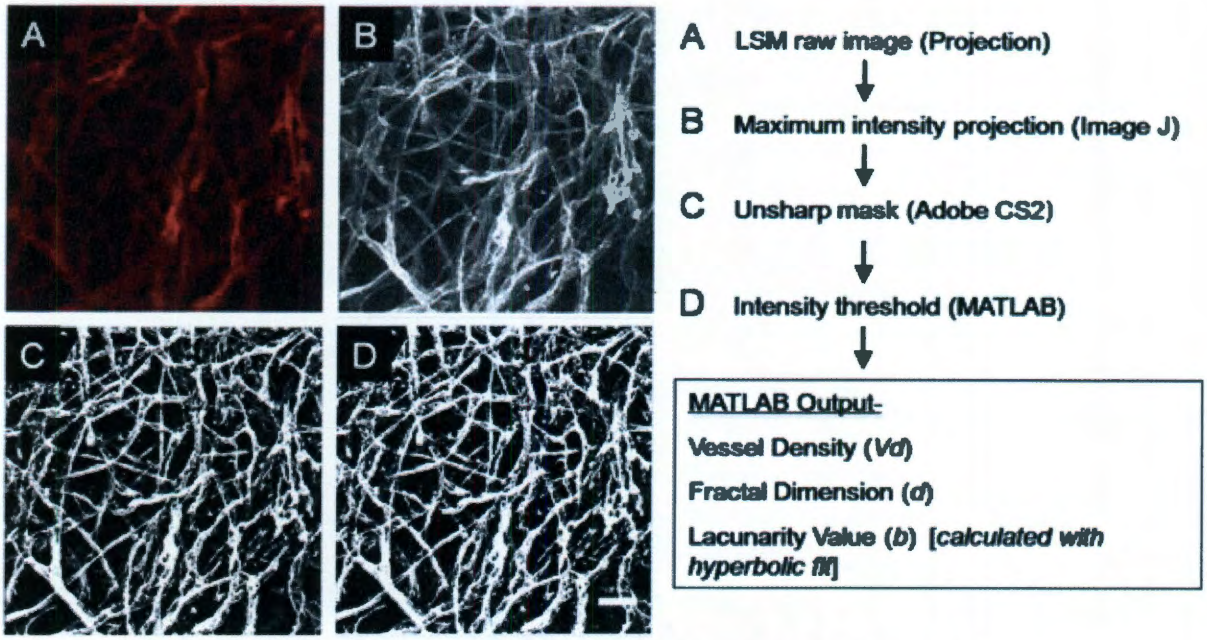

Figure 2-6: Image Processing. Raw LSM images z-stacks of 22 microns are formulated into a 3D projection. Next, ImageJ is used to form a maximum intensity project. An unsharp mask is applied in Adobe Photoshop, followed by thresholding in MATLAB. The final images are used for quantification of vessel parameters.

2.2.14 Fractal Dimension, Lacunarity, and Multifractal Spectra

Induced vessel morphology was assessed by imaging vessels and applying algorithms developed and described in Gould et al. (Gould et al., 2011) to determine

vessel density, diameter, fractal dimension, and lacunarity (Figure 2-7). Also, the programs used to extract these parameters are available online through the MATLAB central file exchange (Vadakkan, 2009, 2009).

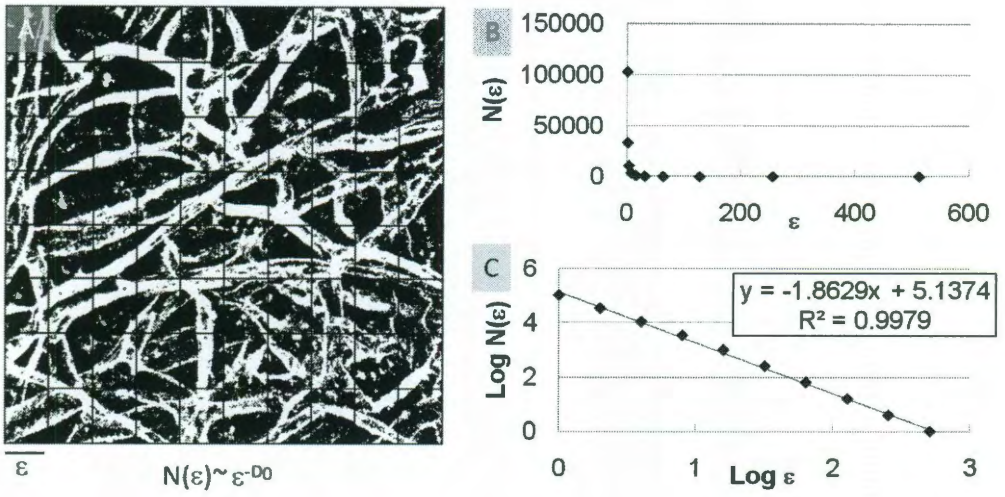

Figure 2-7: Measurement of the Fractal Dimension Using a Box-counting Algorithm. Here, A demonstrates the application of a grid to the image of engineered vessels. After applying a grid, positive boxes (containing at least one white pixel) are counted. B shows the plot of positive box number versus box size. C shows the log (positive boxes) versus log (box size) plot. The slope of this line is the fractal dimension.

2.2.15 Statistical Analysis

A one-way ANOVA was used to quantify differences in VEGF, PDGF, and FGF release at 7 days. A student's t-test was used to quantify differences in FGF release at final time points. P-values less than 0.05 were considered significant.

2.3 Results and Discussion

2.3.1 Characterization of PEG-materials

Gel permeation chromatography was used to confirm attachment of PEG-SMC to the cell adhesive peptide RGDS and MMP-sensitive peptide PQ. Figure 2-8 shows a GPC analysis of PEG-RGDS with peak 1 representing PEG-RGDS and peak 2 representing unreacted PEG-SMC. Figure 2-9 shows GPC analysis of PEG-PQ-PEG with the blue line representing PEG-SMC, the black line representing PEG-PQ-PEG, and the red line as the UV absorbance from the PEG-PQ-PEG sample. UV absorbance was seen due to inclusion of tryptophan into the degradable PQ sequence and confirmed the presence of the PQ sequence. Decrease in the PEG-SMC peak on the PEG-PQ-PEG sample confirmed the presence of mostly reacted PEG-SMC.

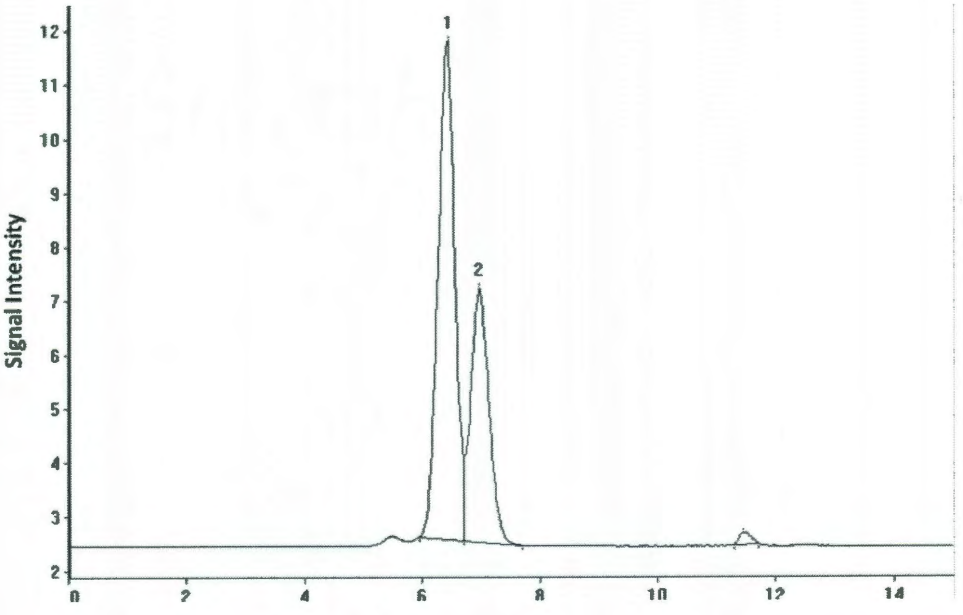

Figure 2-8: GPC data confirming conjugation of PEG-RGDS. Peak 1 represents the PEG-RGDS peak and peak 2 represents unreacted PEG-SMC.

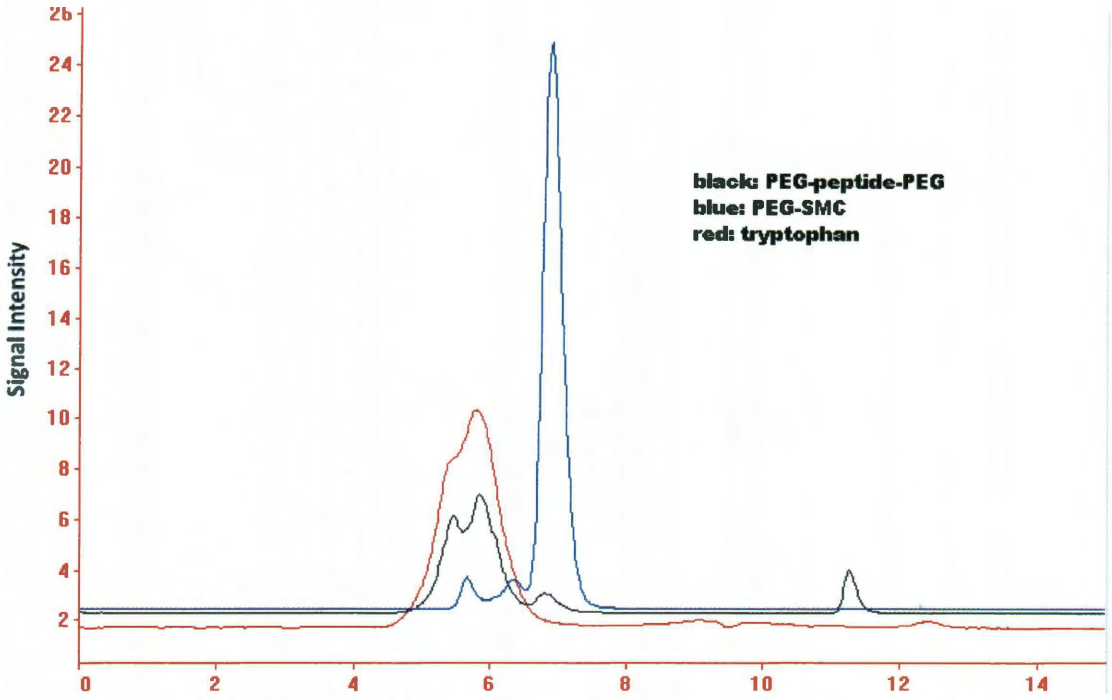

Figure 2-9: Conjugation of PEG-PQ-PEG. The blue line shows PEG-SMC; the black line shows the PEG-PQ-PEG; and the red line shows the tryptophan peak from the PQ sequence in the PEG-PQ-PEG.

Degradation of PEG-PQ-PEG was evaluated because the rate of degradation of implants is critical to the implant's success. A scaffold that degrades too slowly will impede cell motility and proliferation. On the other hand, a scaffold that degrades too quickly may lack structural integrity necessary at the site of implantation. The ideal rate of degradation is based on native cell ingrowth via cell-secreted proteases. Cell migration is critical to inflammation, wound healing, and tumorigenesis and is controlled by degradation of the extracellular matrix. The collagenase sensitive sequence GGGPQGIWGQGK (abbreviated PQ) was incorporated into the polymer backbone to render the hydrogels sensitive to cell-secreted MMPs. The collagenase sensitive

sequence was synthesized and its molecular weight was confirmed at 1141 grams/mol via MALDI-TOF in Figure 2-10.

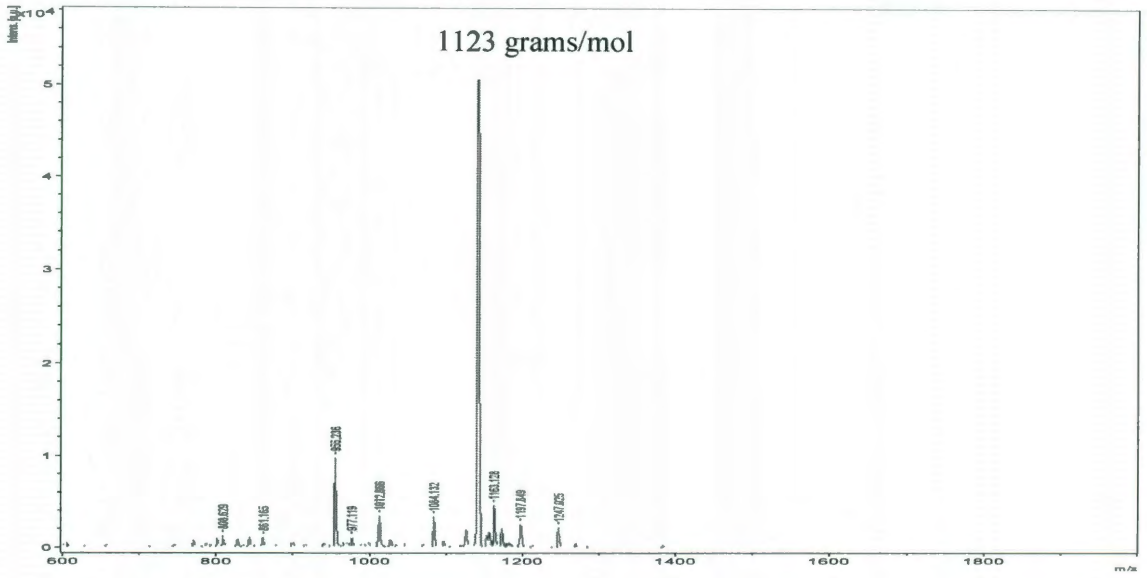

Figure 2-10: MALDI-TOF conformation of PQ molecular weight at 1141 grams/mol.

Degradation of hydrogels was measured via spectrophotometer measurements at 280 nm into the hydrogel. Absorbance at 280 nm remained relatively unchanged for control gels in buffer while absorbance in both the collagenase and proteinase K buffers increased, indicating degradation in response to specific cellular enzymes, such as collagenases as seen in Figure 2-11. Proteinase K was used as a positive control, therefore the reading at 48 hours was considered 100% degraded and all other readings were compared to the 48 hour proteinase K value. Control gels showed a slight increase, probably from unconjugated PEG-PQ-PEG chains being released from the hydrogel.

Control gels were used to indicate that hydrogels do not undergo nonspecific degradation in normal buffer conditions.

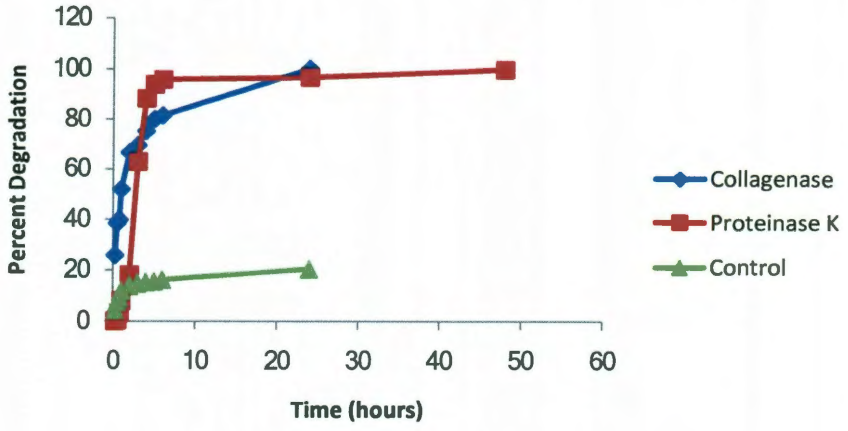

Figure 2-11: Degradation of PEG-PQ-PEG. Absorbance readings of PEG-PQ-PEG hydrogels in collagenase (blue) and proteinase K (red) solutions showing degradation via release of tryptophan into the solution over time. Control gels (green) confirm gels do not undergo nonspecific degradation.

2.3.2 Growth Factor Release from Hydrogels

PEG-based hydrogels were evaluated for the release of the angiogenic growth factors VEGF, PDGF, and FGF. All factors follow the same profile with an initial burst release, similar to that needed to initiate an angiogenic response *in vivo*, followed by slow release for over seven days (Figure 2-12). The subsequent slow diffusion from hydrogels is advantageous for maintaining prolonged local growth factor action at the site of delivery. VEGF-loaded hydrogels demonstrated the highest total protein delivery with a release of 92% of the theoretically loaded amount. This is statistically higher than the

releases of both PDGF and FGF, which were measured at 66% and 52%, respectively ($p<0.05$). Since the diffusion of growth factors within a hydrogel matrix depends on specific protein characteristics including molecular weight, folding structure, dimerization, and charge distribution, any of these characteristics may have contributed to the release profiles seen here. For example, the similarity between the release curves of PDGF and FGF could be attributed to the fact that these proteins have similar molecular weights and dimerizations.

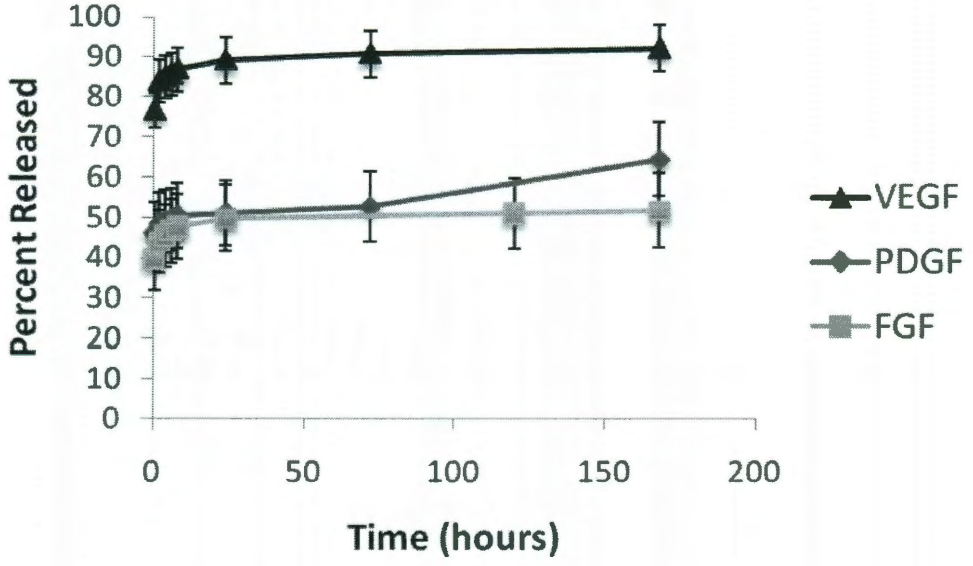

Figure 2-12: Growth factor release from degradable PEG-PQ-PEG hydrogels. An initial burst release during the first 30 min is followed by consistent delivery over the next 7 days. This growth factor release profile is well suited to the establishment of an angiogenic response where an initial response can be stimulated followed by prolonged signaling.

To adjust the amount of FGF released from PEG hydrogels, polymer molecular weight, polymer weight percentage, and protein incorporation methods were varied. The

amount of FGF released form 35 kDa PEG hydrogels was statistically greater than that released from 3.4 kDa hydrogels (Figure 2-13A). 35 kDa PEGDA has longer polymer chains in between crosslinkable acrylate groups, leaving more space for diffusion of growth factors than the smaller 3.4 kDa polymer. Similarly, the loose hydrogel mesh formed from less densely packed 5% PEGDA gels also led to a statistically significant increase in amount of FGF released at 8 hours when compared to 20% hydrogels (Figure 2-13B).

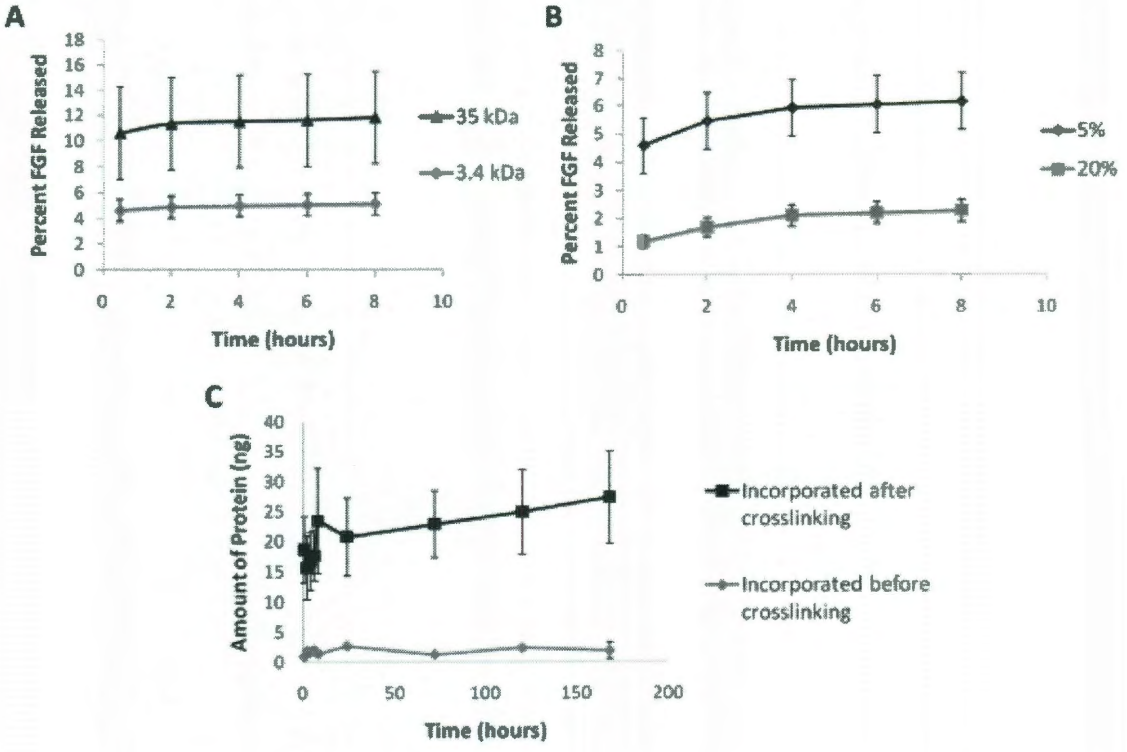

Figure 2-13: Methods to vary FGF release. (A) More FGF is released from 35 kDa PEGDA hydrogels than 3.4 kDa hydrogels ($p=0.02$). (B) 5% (w/v) polymer gels release more FGF than 20% hydrogels ($p=0.003$). (C) Incorporating FGF after crosslinking hydrogels results in more FGF release than incorporating FGF before crosslinking ($p<<0.01$).

The method of soluble factor loading was also shown to influence the protein release. Hydrogels for which the growth factors were soaked in after crosslinking exhibited higher release than those formed with the signaling molecules present during polymerization (Figure 2-13C). This effect may be due to the fact that incorporation after crosslinking relies solely on diffusion of growth factors into the matrix, and as such any molecule that is able to migrate in, should also be free to release from the hydrogel at later time points. On the other hand, incorporation before crosslinking may physically entangle some growth factors making them unavailable for subsequent release. These data indicate that the protein loading method is an important consideration when designing the appropriate hydrogel formulation for *in vivo* use.

2.3.3 Confirmation of Hydrogel Placement

In order to verify proper placement of hydrogels in between layers of cornea stromal tissue, hydrogels were labeled with fluoroscein-o-acrylate and imaged. Proper placement was confirmed based on images of the eye (A) and histology of the cornea as seen in both white light (B) and fluorescence (C).

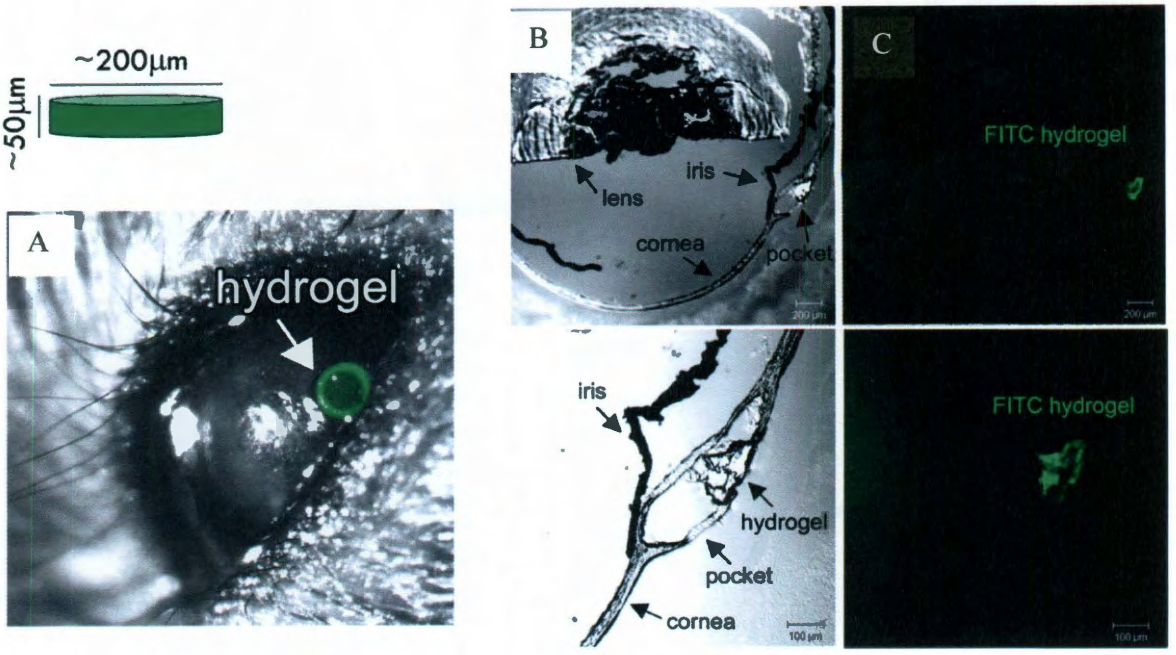

Figure 2-14: Proper placement of the hydrogel in a cornea micropocket is confirmed with fluorescein-o-acrylate labeled hydrogels. (A) Histology further confirms creation of a micropocket containing a hydrogel under white light (B) and fluorescence (C).

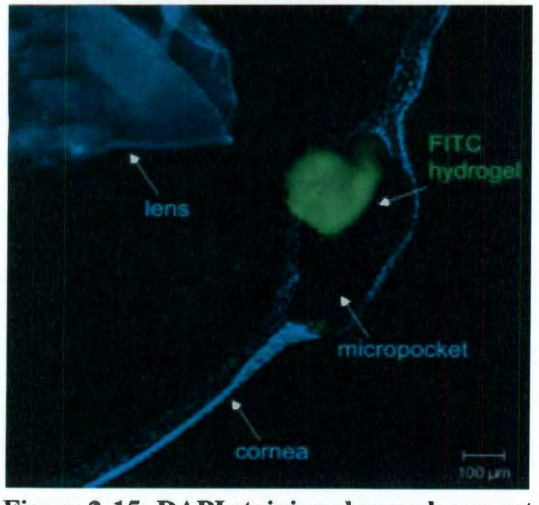

Figure 2-15: DAPI staining shows placement of the hydrogel in between the cornea layers.

Histological sections were stained with DAPI to enable visualization of the nuclei in the cornea layers. The 80 µm thick cornea contains a pocket large enough for the hydrogel and heals itself after implantation of the hydrogel as seen in Figure 2-15. Rehydration of the section allowed the hydrogel to swell to

its original size. Hydrogel shift resulted from the rehydration procedure.

2.3.4 Bioactive Hydrogels Stimulate a Vascular Response *in vivo*

VEGF-releasing hydrogels were used to confirm that implanted hydrogels stimulate a vascular response. Dextran (MW 70,000 Da) was injected in a mouse tail vein to visualize perfused vessels. Limbic vessels were seen in the control PEGDA gel (Figure 2-16) while VEGF-releasing hydrogel promoted limbic vessels branching into the cornea toward the hydrogel six days after implantation. Perfusion of vessels with dextran validates functionality of resultant vessels. In another view, dextran-perfused vessels can be seen surrounding the hydrogel itself (Figure 2-17).

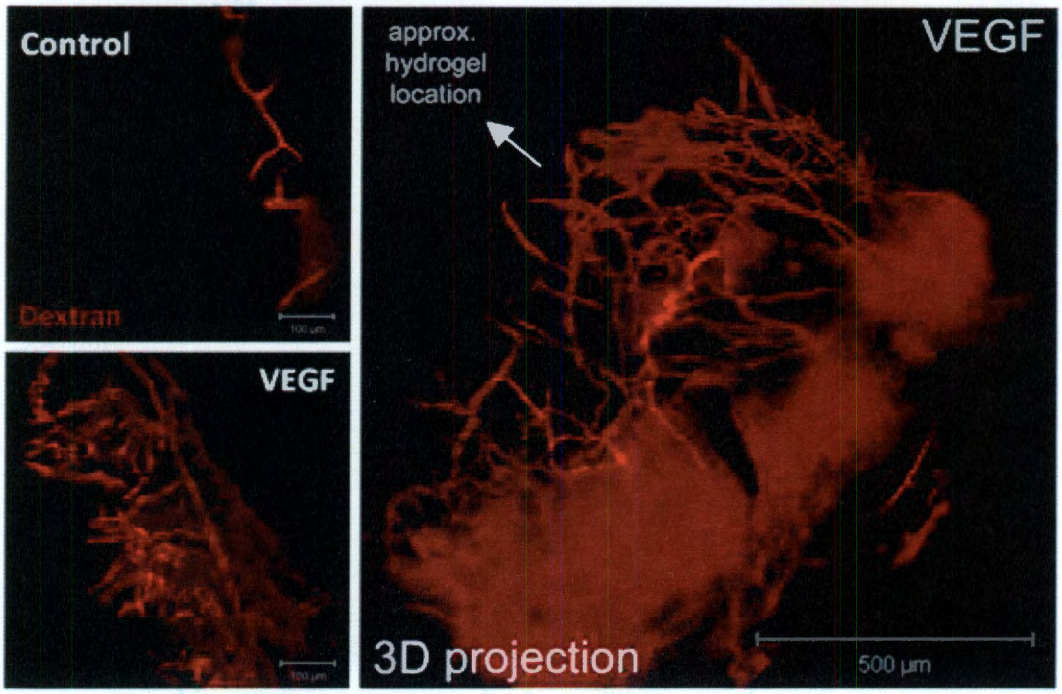

Figure 2-16: VEGF-releasing Hydrogels Induce Angiogenesis in the Cornea. Natural limbic vessels with no enhanced vascularization as a result of PEGDA hydrogel without VEGF are seen in the control as compared to the enhanced vascular response to PEGDA hydrogels releasing VEGF. Functionality of the vessels is suggested by perfusion with fluorescent dextran.

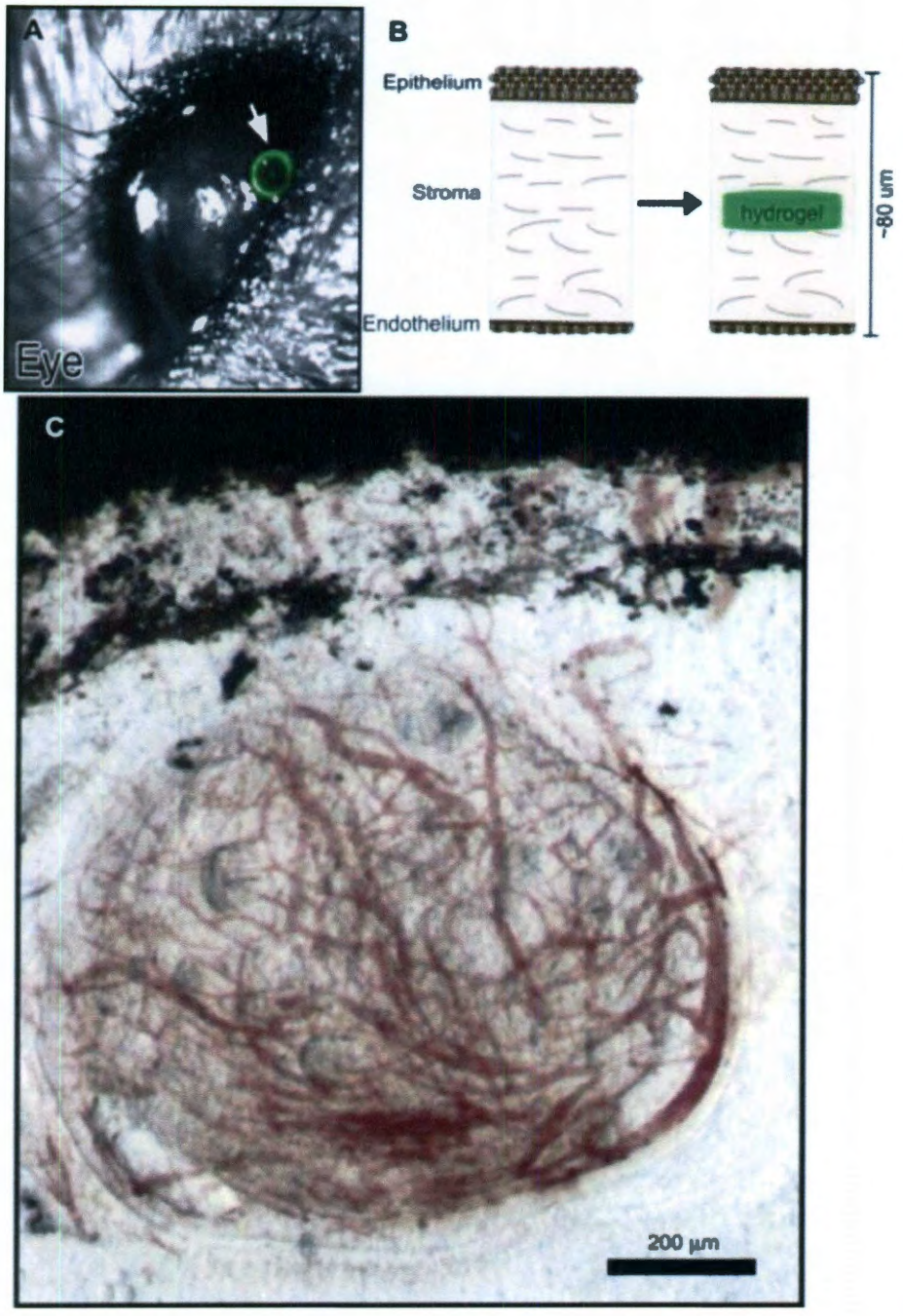

Figure 2-17: Newly formed blood vessels in hydrogels are functional. A,B) Small incision was made in cornea and photopolymerized hydrogels were implanted into the micropocket. C). Blood vessels formed in the hydrogels were perfused with Dextran-Texas red (70 KDa MW) injected intravenously into mice (Moon, Saik, Poche et al., 2010).

The *Flk1-myr::mCherry* genetically modified mouse labels the membrane of endothelial cells with a red fluorescence. This transgenic mouse line creates a novel system for neovascular imaging with subcellular resolution (Poche et al., 2009). Furthermore, the angiogenic response to implanted hydrogels can be monitored *in vivo* over time. An extensive vascular network of myr::mCherry+ vessels can been seen in response to a VEGF-releasing PEGDA hydrogel six days after implantation (Figure 2-18 A-B).

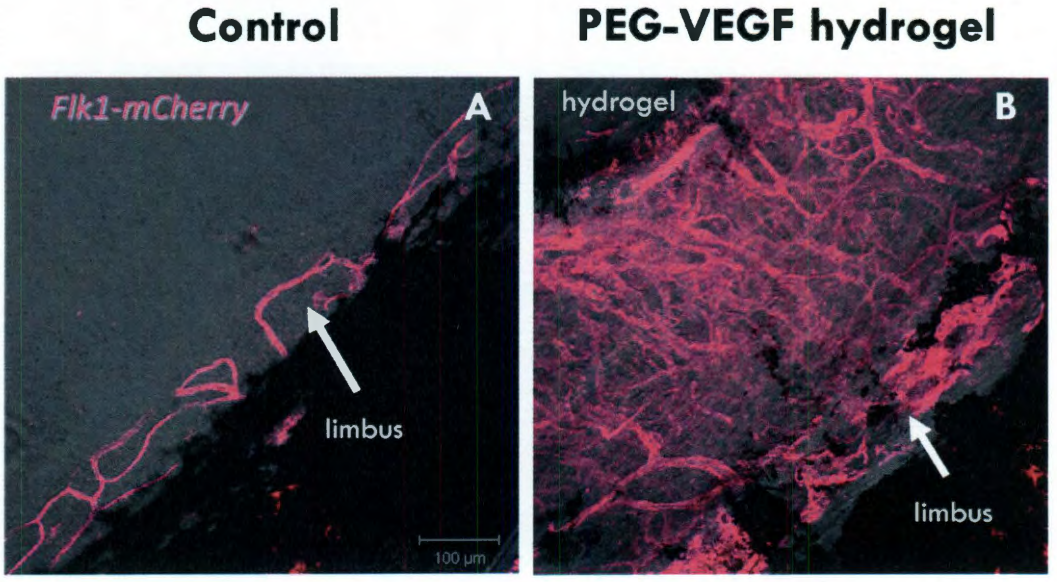

Figure 2-18: VEGF-releasing PEGDA gels stimulate myr::mCherry+ vessels (B) as compared to control gels without VEGF (A). Image from (Poche et al., 2009).

Red blood cells can be seen in the newly formed cherry+ vessels, suggesting functionality of the vessels (Figure 2-19).

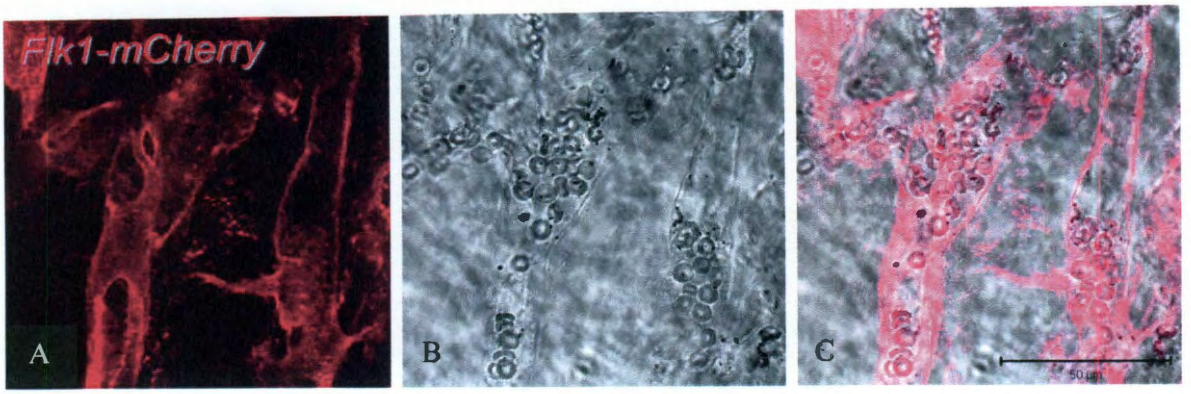

Figure 2-19: Perfused Vessels. (A) Fluorescent endothelial cells showed the angiogenic response to VEGF-releasing hydrogels. Red blood cells were seen in these vessels (B), and an overlay of the images (C) confirmed the presence of red blood cells inside the cherry+ vessels. Image from (Poche et al., 2009).

While VEGF induces a substantial vascular response, the response can be enhanced by releasing both PDGF-BB and FGF-2, which is a previously established synergistic combination (Rogers et al., 2007). After 11 days *in vivo,* PEGDA gels releasing the combination of PDGF-BB and FGF-2 induce a cherry+ neovascular response on both the gel surface (Figure 2-20A) and gel bottom (Figure 2-20B). However, the neovascular response to VEGF-releasing hydrogels was seen only on the hydrogel surface (Figure 2-20C) and not the bottom of the gel (Figure 2-20D).

Another method to confirm successful perfusion of engineered vessels involved injecting fluorescent microspheres into the bloodstream. Vessels were successfully perfused and the rate of perfusion was quantified to be 980 μm/sec (Figure 2-21).

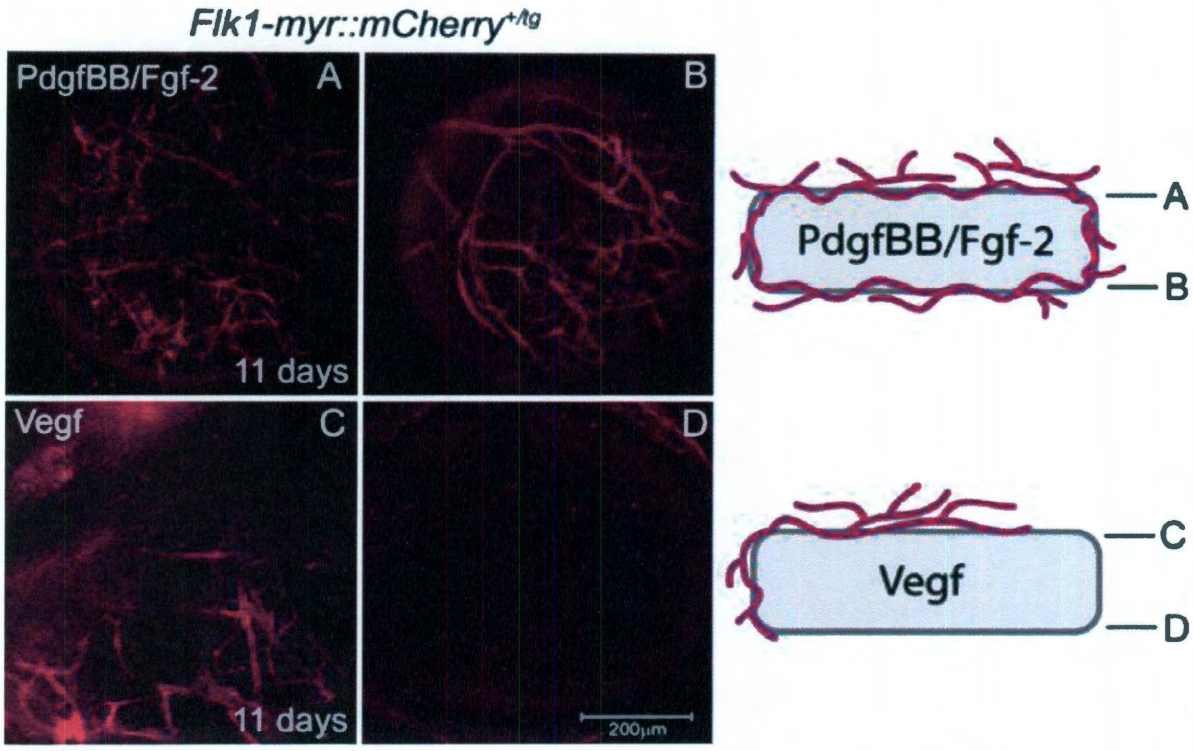

Figure 2-20: PEGDA gels releasing PDGF-BB and FGF-2 (A: top of gel; B: bottom of gel) enhance the neovascular response as compared to gels releasing VEGF (C: top; D: bottom). Furthermore, vessels formed in response to the combination of PDGF-BB and FGF-2 appear more stable and organized.

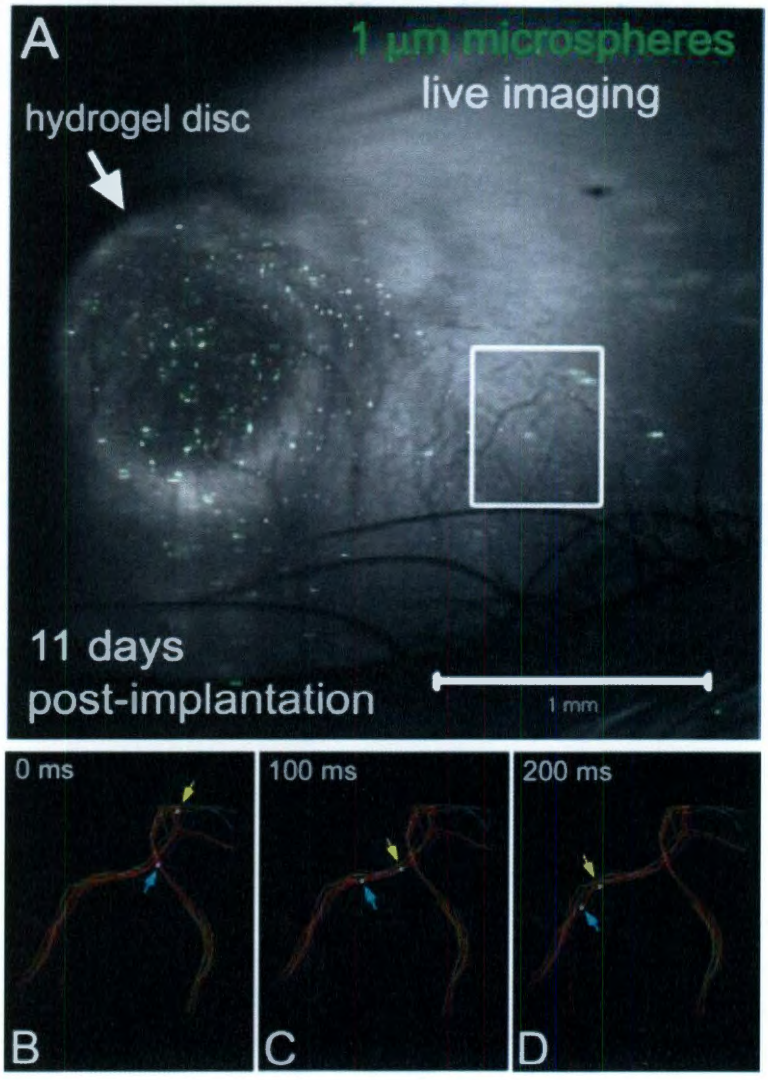

Figure 2-21: High-speed confocal imaging of circulating fluorescent microspheres among an implanted corneal hydrogel. Images were acquired at 50 frames/sec using a Zeiss LSM 5 *LIVE* high-speed confocal microscope with a Zeiss Plan-Neofluar 5X/0.15 NA objective lens, resulting in a movie showing the circulation of microspheres through the newly induced vessels surrounding the hydrogel. (*A*) A single frame taken from the image series. Bright green microspheres are located within the induced vessels and surrounding the hydrogel in the cornea of a live animal. (*B-D*) Images from the Imaris software in which individual spheres (yellow and blue arrows) are tracked in successive frames in an area of interest (white box in *A*). The tracks shown represent the trajectories of 23 microspheres imaged over 15.62 sec (753 images) and are shown as colored lines. The time stamp shows that the elapsed time between each frame (*B* to *D*) is 100 msec. The velocities of fluorescent spheres that were tracked ranged from 0.65 to 1.15 mm/sec (Average = 980.58±147.89 µm/sec) (Poche et al., 2010).

PEG-VEGF and MMP-sensitive hydrogels were combined to enhance the neovascular response. The first column of Figure 2-21 outlines the hydrogel by using fluorescent PEG-RGDS. The middle column shows cherry+ neovessels, and the third column shows the merge of hydrogel and vessels. Degradable gels without any VEGF acted as control gels and caused no vascular response (Figure 2-21).

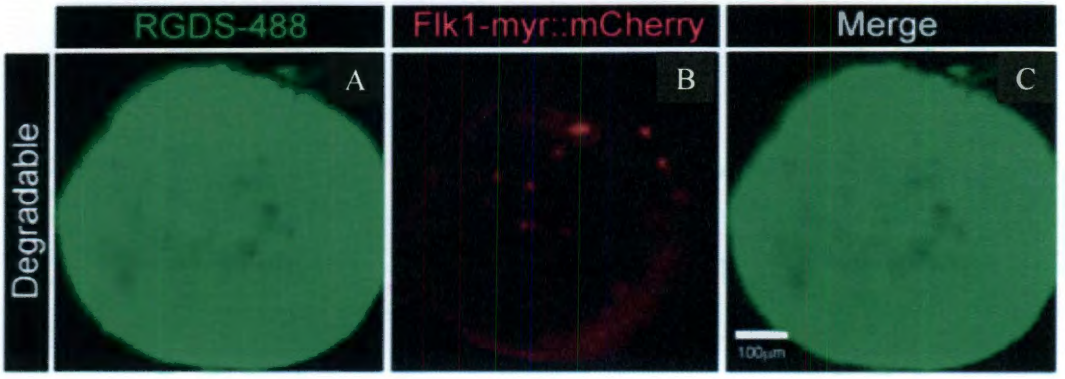

Figure 2-21: Hydrogels without growth factors do not stimulate a vascular response. Fluorescently-labeled RGDS outlines the area of the hydrogel (A) and no vessels are seen in (B). C) An overlay confirms that hydrogels do not stimulate a vascular response without growth factors.

These gels confirm that degradable gels alone cannot stimulate a response. Non degradable 6 kDa PEGDA gels with both PEG-VEGF and releasable VEGF stimulated a response with vessels covering the gel surface (Figure 2-23 A-D). Degradable gels with both releasable and covalently-immobilized VEGF enabled degradation of the matrix as vessels penetrated into the matrix (Figure 2-23 E-H). Degradation was seen in areas of substantial vessel growth.

The effects of tunable mechanical properties were also investigated using a 15% polymer weight percentage degradable gel. The increase in polymer percentage alters hydrogel mechanical properties, creating a stiffer gel with smaller mesh sizes. Previous work has confirmed that increasing polymer weight percentage significantly increases the

compressive moduli of the hydrogels and slows degradation time (Moon, 2008). Lutolf et al. has shown that the rate of fibroblast migration into 3D hydrogels is inversely related to polymer crosslinking density (Lutolf et al., 2003). Furthermore, the mechanical properties also affect cell phenotype, as an increase in matrix stiffness was shown to decrease cardiomyocyte contraction (Shapira-Schweitzer et al., 2007). 15% polymer weight percentage gels were fabricated with both PEG-VEGF and releasable VEGF, and the *in vivo* response was evaluated seven days after implantation. After seven days, a vascular response was seen on the gel surface, and the early stages of scaffold degradation were seen as vessel ingrowth, highlighted by the depth profile image (Figure 2-23 I-L). These studies confirm that the degradation rate can be controlled using tunable mechanical properties, allow precise design of hydrogels for various *in vivo* applications. Moreover, the angiogenic response can also be controlled by altering mechanical properties.

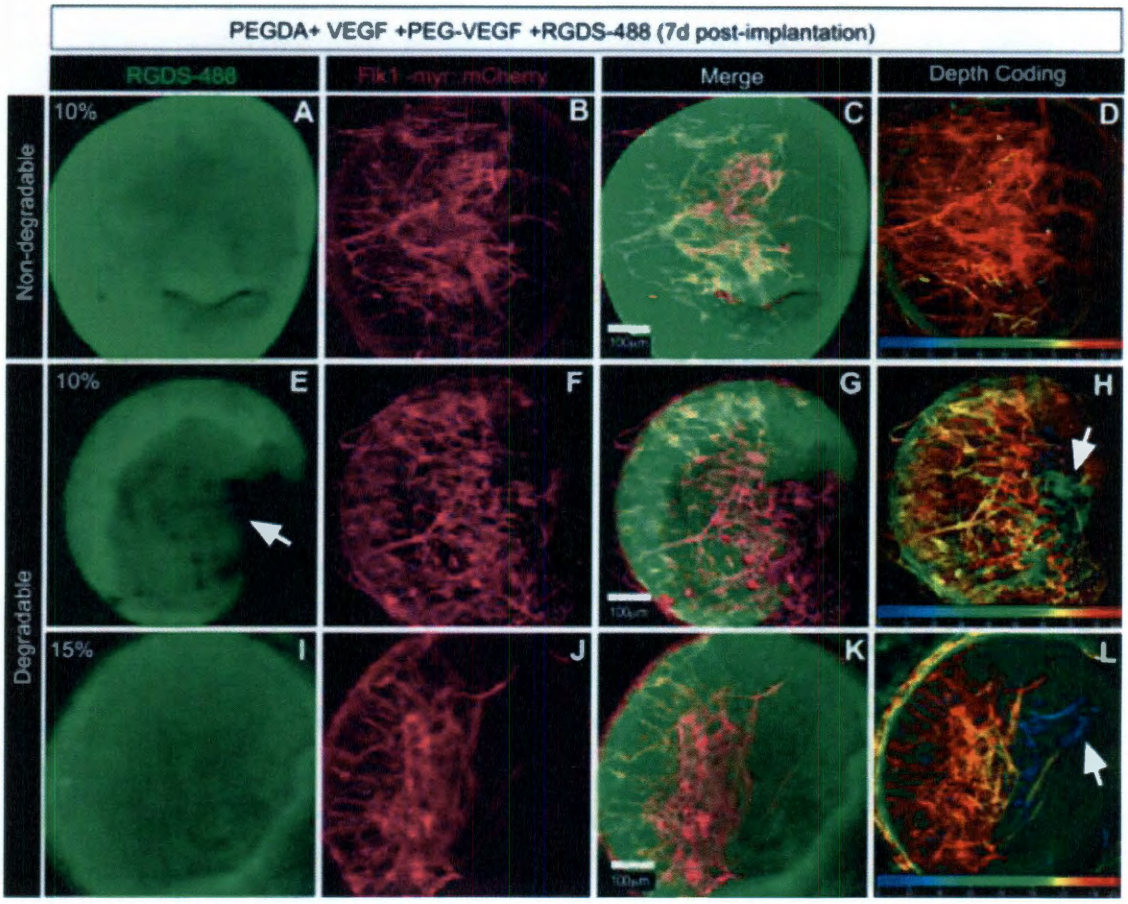

Figure 2-23: Proteolytically-degradable PEG hydrogels promote neovascularization in murine cornea. Hydrogels incorporated with soluble and immobilized forms of VEGF via PEG linkage were implanted into cornea in *Flk1-myr::mCherry* transgenic mice. Newly formed blood vessels were visualized by confocal microscopy, and depth profiles of the vessels were generated to reveal their Z position with respect to the hydrogels. A–D) Non-degradable hydrogels releasing soluble VEGF supported angiogenesis adjacent to the hydrogels, but the depth decoding graph indicates lack of vessel penetration into the hydrogels. E–H) MMP-sensitive PEG hydrogels with 10% polymer weight promoted robust neovascularization adjacent to the hydrogels and extensive infiltration of host vasculature into the hydrogels. The arrow in E) indicates a portion hydrogel undergoing active degradation, and the arrow in H) points to regions within hydrogels with vessel infiltration. I–L) MMP-sensitive PEG hydrogels with 15% polymer weight had blood vessel growth on surface of hydrogels as pointed by the arrow in L), but the hydrogels remained mostly intact (I) without any significant vessel infiltration into the core. Scale bars = 100 μm in A–L) (Moon, Saik, Poche et al., 2010).

Finally, three different doses of PDGF-BB and/or FGF-2 were used to induce vessel formation on PEG-based hydrogels implanted into a cornea micropocket using transgenic mice expressing *Flk1-myr::mCherry* to facilitate characterization of the angiogenic response (Poché, 2009; Poche et al., 2010). Growth factors were used individually to parse out individual effects and in combination to investigate synergistic effects. Resulting vessels were imaged 7 and 14 days after implantation and space-filling morphological parameters including fractal dimension, vessel density, and lacunarity were used to quantify resulting vessel morphology (Gould et al., 2011). Vessel morphology varied based on dose, where high doses of individual factors and combinations of factors induced vessel beds with high vessel density (Figure 2-25 A, B), greater fractal dimension and a higher lacunarity parameter *b*, reflecting less lacunae or open space between vessels versus lower dose treatments (Figure 2-25 D). These trends were confirmed using statistical tests (ANOVA and Tukey post hoc analysis), which confirmed a significant difference between high and low dose groups at 7 and 14 days in all treatment groups, ($p<0.05$) when using the vessel density and fractal dimension analysis. Amongst the various dose and treatment groups, three key findings were present: (1) significant differences existed in all cases between high and low dose groups, indicating a dynamic range of vessel morphology ($p<0.01$), (2) the PDGF-BB / FGF-2 combination group alone at 14 days exhibited significant differences between high, medium and low dose groups using vessel density, fractal dimension, and lacunarity ($p<0.05$), and (3) other groups showed some differentiation between groups, but lacked the same level of differentiation between all groups. At the 7 day timepoints, lacunarity proved significantly different amongst all dose groups. However, at 14 days the

differences between high and low dose groups were not significant except in the PDGF-BB / FGF-2 combination group, which showed differences between all three dose groups ($p<0.01$) at 7 and 14 days. In all treatment cases, the high dose groups were significantly higher in vessel density and fractal dimension, while in some, the medium dose groups were significantly different from either the low or the high dose groups, but not both.

Differences were observed within groups, and examined for trends which might indicate morphological changes from 7 to 14 days. The high dose in all treatment groups exhibited vessel densities of around 40% at 7 days and near 35% at 14 days. Although these trends suggest remodeling, no significant difference within groups and doses in the density from 7 to 14 days was observed. In comparison to the 7 day vessels, the 14 day vessels were visually observed to have lower diameters, and the branching was similarly observed to be slightly lower in some groups (Figure 2-26 A,B).

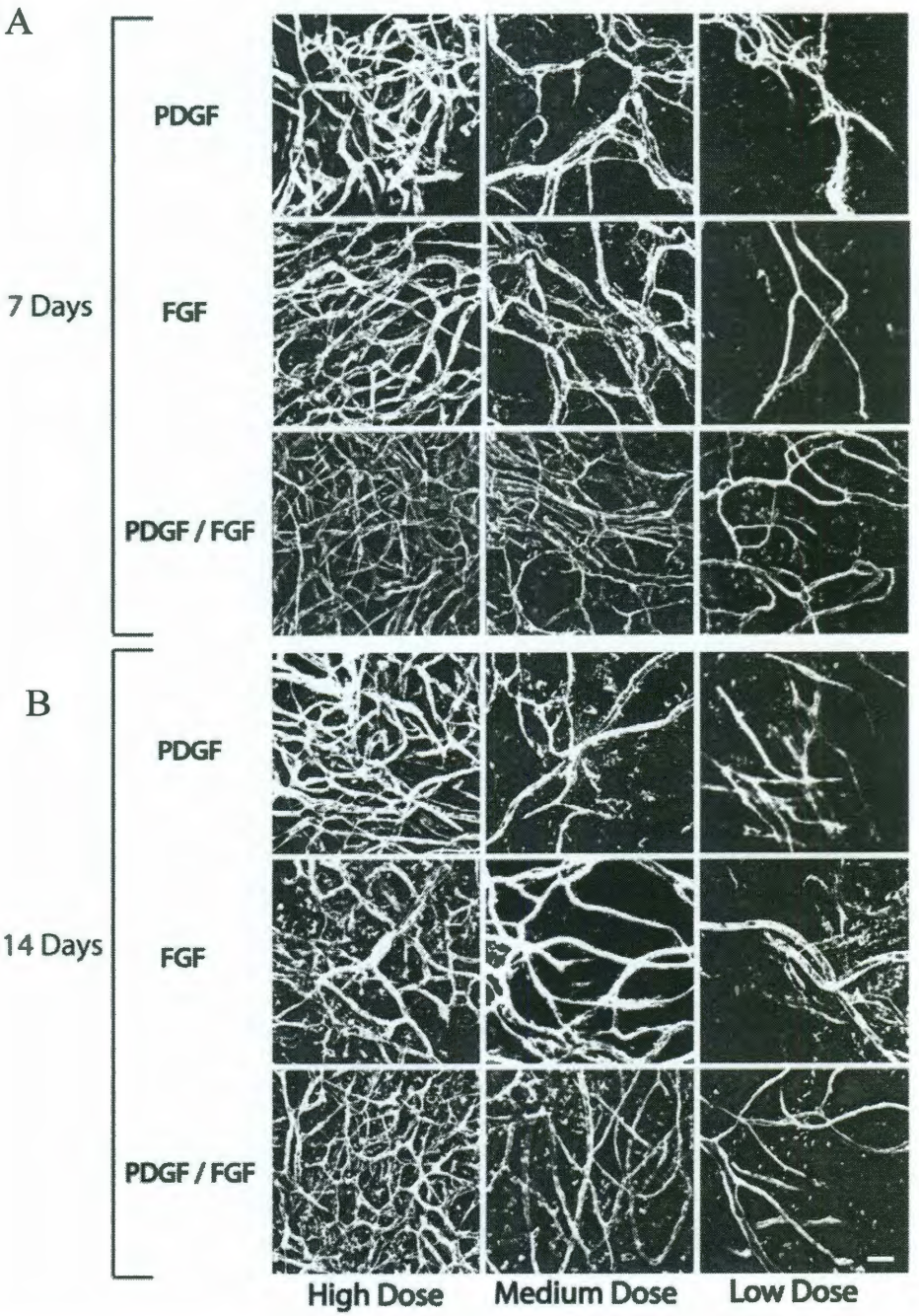

Figure 2-24: Growth Factor Dose Induces Differing Vessel Morphology. 7 days (A) and 14 days (B) after implantation, vessels were visible in response to PDGF-BB and/or FGF-2 at three different concentrations.

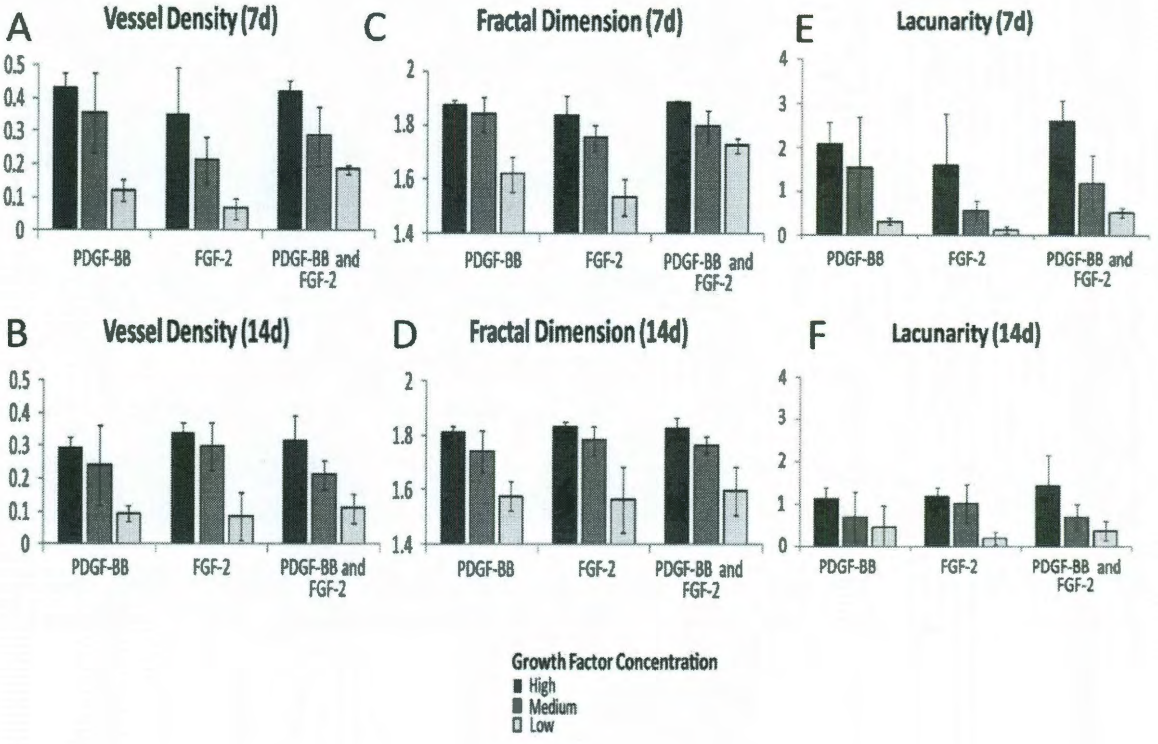

Figure 2-25: Vessel density, fractal dimension, and lacunarity were quantified. Vessel density, fractal dimension, and lacunarity were measured to quantify the vascular response (A-F). 7 Days after implantation, vessel density, fractal dimension and lacunarity parameter b were found to increase as growth factor dose increased (A, C, E). 14 days after implantation, similar trends in vessel density, fractal dimension and lacunarity parameter were observed in response to the growth factors PDGF-BB and FGF-2 at similar dose concentrations (B, D, F). For this study high dose was 640:160ng PDGF-BB: FGF-2, medium was 160:40ng PDGF-BB: FGF-2, low dose was 40:10ng PDGF-BB: FGF-2.

Branching and diameters were quantified and within the PDGF-BB / FGF-2 combination group, the high, medium and low dose groups were significantly different in branching morphology ($p<0.01$) at 7 days, with high dose exhibiting the greatest branching (74±5.5) versus medium (56±3.8) and low (17±5.0) dose groups (Figure 2-26 A). At 14 days similar differences within this treatment group were seen ($p<0.05$). This level of separation between doses with branching was not seen in the FGF-2 and PDGF-

BB alone groups. Similar trends were observed for vessel diameters, within dose groups at 7 days, in that there were differences between high, medium and low dose groups in the case of FGF-2 or PDGF-BB / FGF-2 ($p<0.01$). In the PDGF-BB alone treatment, there was only a significant difference between medium and low dose groups ($p<0.01$) (Figure 2-26 C). One important change highlighted by diameter measurements was the difference within dose groups and within specific dose levels between 7 and 14 days. In each group, with the exception of the PDGF-BB only, high dose group, there was a significant decrease in the average vessel diameter from 7 to 14 days ($p<0.05$). Also at 14 days, the only group which had no significant difference between high, medium and low dose groups was the PDGF-BB / FGF-2 containing group. In contrast, the PDGF-BB alone and FGF-2 alone groups showed significant differences between the high and low dose groups, and medium and high dose groups ($p<0.05$). These data indicate that at fourteen days, the vessel branches are relatively unchanged, and that the vessel diameters are more uniform particularly in the PDGF-BB / FGF-2 combination group. In summary, the key findings were that significant differences in the vessel density, fractal dimension, and lacunarity were supported by similar differences in branching, that the branching differences were only consistently different in the combination treatment, and that the only group with relatively equally distributed vessel diameters in all three treatment groups was the combination treatment group.

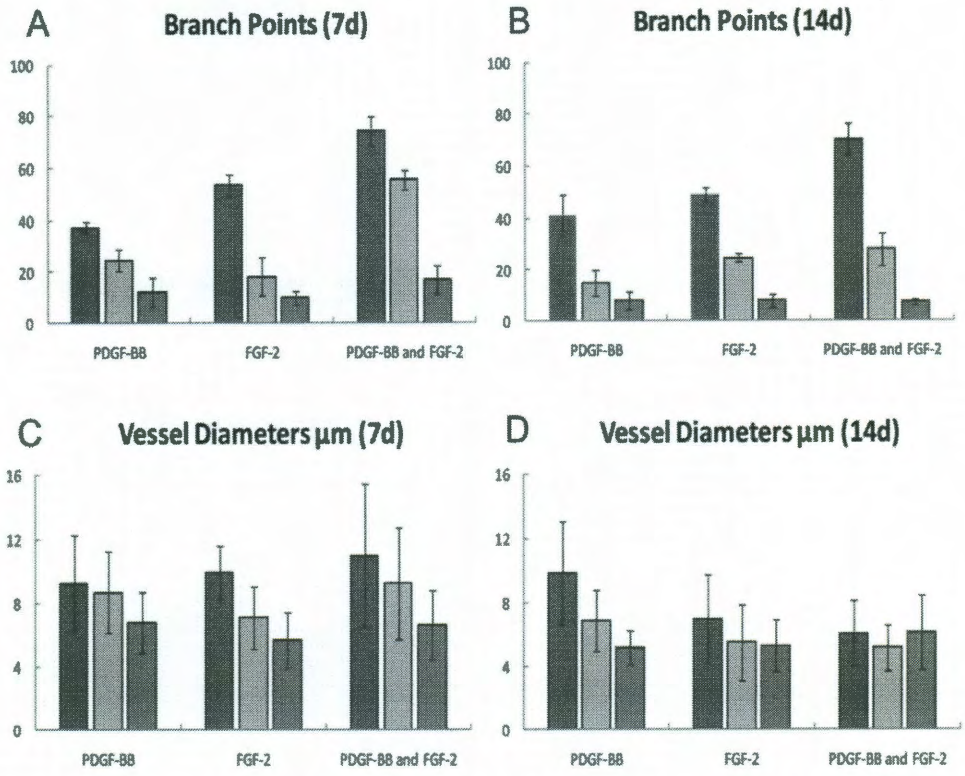

Figure 2-26: Branch point and vessel diameter comparisons. Branching was quantified, by counting the number of branch points using the LSM image browser software in the three dimensional z stacks of the different vessel structures at 7 and 14 days (A, B). Diameters of vessels were measured in similar fashion at 7 and 14 days (C, D) and a histogram was plotted to elaborate on the differences between vessel diameters (E). Interestingly, there were not significant differences between branching from 7 to 14 days in all groups except the medium dose group in the combination PDGF-BB / FGF-2 treatment group ($p<0.05$). In the case of the vessel diameters, there were significant changes in treatment groups between 7 and 14 days, however, the differences that were apparent within treatments, between doses at seven days ($p<0.01$) were not seen in the 14 day timepoint in the PDGF-BB / FGF-2 combination treatment group. This suggests the combination group induces vessels with relatively stable branching and relatively uniform vessel diameter distribution at 14 days, reflected by the histogram in (F) which shows an increased fraction of 6-8um diameter vessels.

The dose of FGF-2/PDGF-BB was shown to have a significant effect on vessel density, fractal dimension and lacunarity. In fact, a linear relationship exists between the dose of FGF-2/PDGF-BB and the values for these three properties for the day 14 data

(Figure 2-27). A fitting function was applied to each set of data at each time point for each recorded parameter (vessel density, fractal dimension, lacunarity). The best fits were seen for all measurements in the combination PDGF-BB / FGF-2 group, which had r^2 values which were greater than those of the FGF-2 only and PDGF-BB only groups (which were no higher than r^2=0.77) at both 7 and 14 days. Importantly, the r^2 values were the highest for the 14 day timepoint in the PDGF-BB / FGF-2 treatment group (r^2=0.94 at 14 days, compared to 0.80 at 7 days). This linear fitting data, in conjunction with the observations about branching and diameter appears to support other researchers claims about the beneficial effect of using PDGF-BB and FGF-2 in combination (Cao, 2003). The fractal dimension from each combination PDGF-BB / FGF-2 group at 14 days was plotted versus the original dose used (Figure 2-27 A). Linear fits were then applied to the data in order to interpolate the dose of PDGF-BB and FGF-2 necessary to induce vessels with a known target fractal dimension (Figure 2-27 A). Figure 2-27 shows the original data (fractal dimension, vessel density, and lacunarity) from the dose escalation using the combination PDGF-BB / FGF-2 treatment group, plotted with the linear fit shown and the 95% confidence intervals plotted above and below. This served as the rationale for choosing the PDGF-BB / FGF-2 treatment group at a 14 day timepoint to tune the vascular response. Fractal dimension alone was used to interpolate the dose needed to recapitulate morphology of known tissues, because this parameter had previously been measured using similar techniques, and is known to be scale-invariant (Gould et al., 2011).

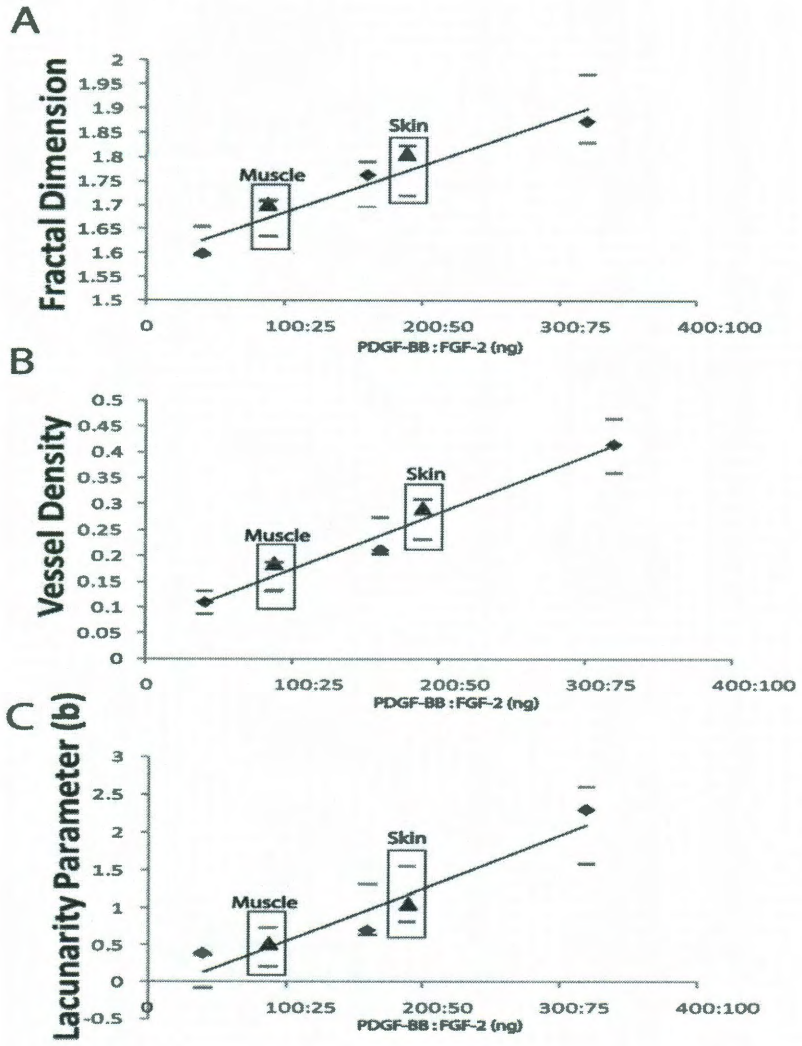

Figure 2-27: Morphological Parameters Used to Calculate a Linear Fit. Fractal dimension (A), vessel density (B) and lacunarity parameter b (C) were plotted against dose released. A linear fit was applied to the data, with R^2 values over 0.9 in each parameter based plot. Linear fit equations were used to back calculate doses necessary to recapitulate vessels with given morphological parameters. The doses were based on the linear plot for the fractal dimension. The measured values for the induced vessels using the interpolated skin and muscle doses are plotted and indicated by the triangle symbols. The 95% confidence intervals are noted as small bars above and below each value. The linear fit for the fractal dimension (A) had an r^2 value of 0.92. For vessel density the fit was $r^2 = 0.96$, for lacunarity $r^2 = 0.92$.

Next, a determination was made as to whether the vessels induced by the range of FGF-2/PDGF-BB doses were similar to vessel beds in endogenous tissues in terms of the fractal dimension. Native skin and muscle tissues from Flk1-myr::mCherry transgenic mice were imaged prior to this study to identify the fractal dimensions at 1.80 ± 0.03 and 1.70 ± 0.05(Table 2-1)(Gould et al., 2011). Thus, the fractal dimension of endogenous vessels within the skin and the muscle fit within the linear range of concentrations tested for FGF-2/PDGF-BB.

Table 2-1: Vessel Parameters for Induced and Native Vessels. Table 2-1 provides the complete set of measured parameters from the induced vessels and the native vessels.

	Vessel Density	Fractal Dimension	Lacunarity Parameter (b)	Vessel Diameter (μm)	Branch Points
Experimental Doses					
320/80 ng (PDGF-BB/FGF-2)	0.41 ± 0.08	1.88 ± 0.03	2.30 ± 0.52	5.42 ± 0.39	84.2 ± 4.02
160/40 ng (PDGF-BB/FGF-2)	0.21 ± 0.04	1.76 ± 0.03	0.70 ± 0.31	6.24 ± 0.22	33.0 ± 5.39
40/10 ng (PDGF-BB/FGF-2)	0.10 ± 0.06	1.59 ± 0.12	0.35 ± 0.23	7.41 ± 0.64	16.0 ± 4.85
Measured Native Vessels					
Skin (native)	0.24 ± 0.01	1.80 ± 0.03	1.03 ± 0.03	7.15 ± 2.05	28.0 ± 2.06
Muscle (native)	0.17 ± 0.01	1.70 ± 0.05	0.73 ± 0.03	5.76 ± 1.20	43.0 ± 1.83
Induced Mimetic Vessels					
Skin Dose	0.29 ± 0.05	1.81 ± 0.04	1.04 ± 0.32	7.65 ± 2.80	32.3 ± 5.00
Muscle Dose	0.18 ± 0.02	1.70 ± 0.05	0.53 ± 0.19	5.97 ± 0.51	47.0 ± 14.2

Since the space-filling properties of vessels within endogenous tissues fit well within the linear range of tested growth factor concentrations, a linear relationship was used to predict the growth factor concentration that would induce vessel structures with space-filling properties that better matched those measured from skin and muscle. Growth factor concentrations necessary to reproduce these fractal dimensions were 184

ng PDGF-BB and 46 ng FGF-2 for skin, and 89 ng PDGF-BB and 22 ng FGF-2 for thigh muscle based on the linear fit of the fractal dimension data. To test whether these doses could indeed induce new vessels with similar properties as those found in skin and muscle, hydrogels were implanted with the predicted concentrations in mouse cornea. The resulting induced vessels are shown in Figure 2-28 (A, C) alongside images of normal vessels in the muscle (B) and skin (D) of a Flk1-myr::mCherry mouse. When the density, fractal dimension and lacunarity of these vessels was measured, a strong correlation existed between the native tissue values and those measured from the vessels induced by FGF-2/PDGF-BB (Table 2-1). Interestingly, even though the fractal dimension was used to tune the vascular response, the muscle and skin vasculature morphological parameters of lacunarity and vessel density also followed a linear fit (Figure 2-27). Interestingly, other parameters such as vessel diameter and the number of branch points also were statistically indistinguishable between native tissue and vessels induced by the optimized dosage of FGF-2/PDGF-BB (vessel diameter ($p=0.55$ and 0.48 for skin and muscle) and branch points ($p=0.11$ and 0.68))(Figure 2-29). Thus, these data show the utility in using space filling morphological parameters such as fractal dimension to define specific growth factor doses to tune the induced angiogenic response.

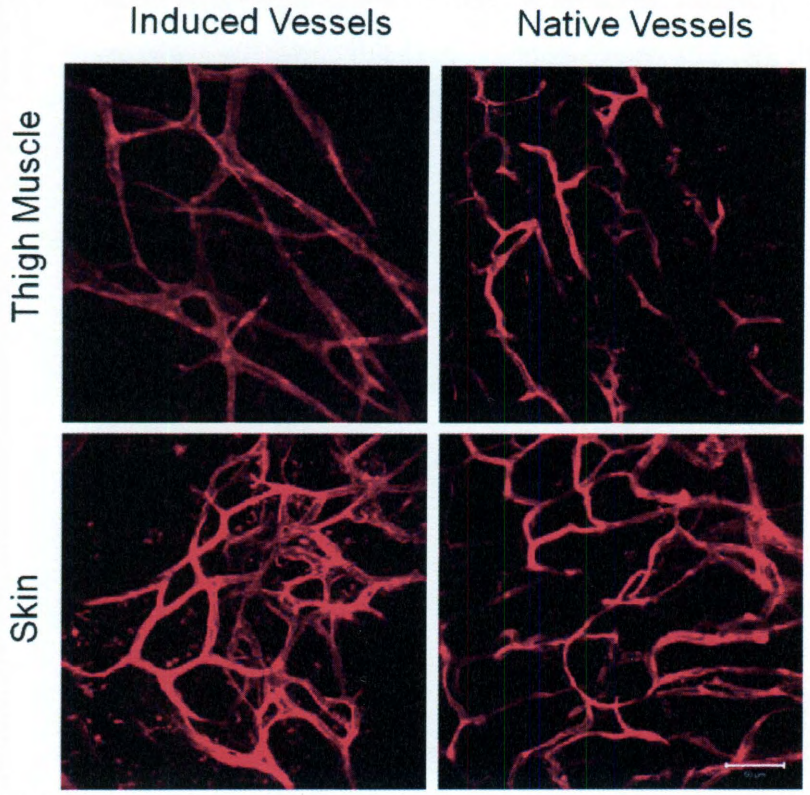

Figure 2-28: Recapitulation of Native Vessels. Vessels in the native mouse skin and thigh muscle (B and D) are visually similar to vessels formed in response to growth factor release from hydrogels (A and C).

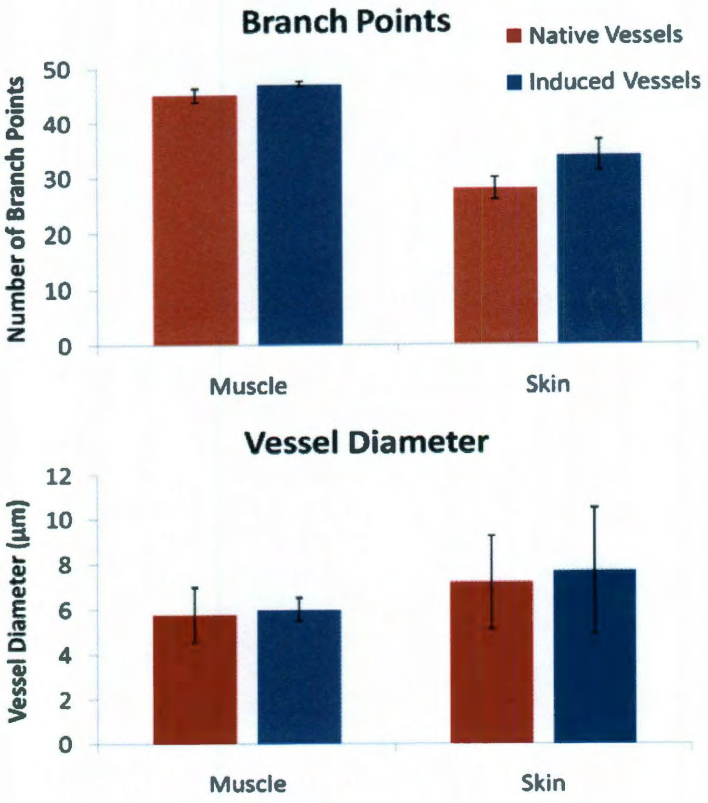

Figure 2-29: Recapitulation of native tissue branch points and vessel diameter. Analysis of vessel diameter and branch points indicates no significant difference between native vessel and induced vessel morphological characteristics.

2.4 Conclusions

Advantages and Disadvantages of the Corneal Micropocket Assay

Due to its external location, immune privilege state, and transparency, the mouse cornea micropocket offers an accessible, high-throughput system in which to rapidly test a variety of tissue constructs in vivo. Using this assay, 70 hydrogel constructs can be

implanted per day based on time to do the surgery. This way, one can quickly screen many candidate tissue constructs and assess specific properties, such as host vessel ingression, perfusion, donor cell survival and integration, and scaffold degradation. Another obvious advantage of the cornea model is that the mouse has two eyes. Thus, one eye can be used as an internal control, thereby reducing the number of mice needed for characterization of test and control constructs. Finally, because the mouse eye is externally localized and the cornea is a transparent tissue, live imaging studies are easily performed. There are two main drawbacks of the cornea as a transplantation site. First, due to the size of the eye, there is an inherent limitation on the size of the implanted tissue construct. Also, the cornea is a highly specialized tissue consisting of a unique microenvironment, and one has to take this into consideration when making comparisons to other transplantation sites. It is important to note that cornea is not the only mouse transplantation site that is amenable to live imaging of tissue constructs. The cranial window (Yuan et al., 1994) and dorsal skin fold (Leunig et al., 1992) have been successfully employed in live imaging studies. Although these methods are better suited for the implantation of larger tissue constructs and constitute more "typical" cellular environments as compared to the highly specialized, avascular cornea, the surgical procedures are fairly laborious for the researcher and invasive to the animal. This combined approach took advantage of the relative ease of the corneal micropocket surgery to analyze many candidate tissue construct designs first in the cornea. Once constructs with the desired properties are identified, larger versions of these constructs can then be generated and validated in other in vivo settings, such as the cranial window and dorsal skin fold (Poche et al., 2010).

Tunability of Implanted Hydrogels

This project has provided a tunable system for angiogenesis *in vivo* in the modified mouse corneal pocket. Importantly, as demonstrated by the linear response of these vessel parameters to loaded protein; it is possible to tune the delivery of angiogenic factors to generate *specific* vascular structures. This tunable system could provide for numerous *in vivo* studies of vasculature and models of vascular disease or remodeling. Beyond the contribution of a tunable system, it has also provided information on the range of doses of factors which may be used for angiogenesis in the corneal micropocket system, and it has demonstrated the utility of scale invariant space filling measures in analysis and design of induced vessel beds for tissue engineering scaffolds. Here, statistical measures including vessel density (Penn et al., 1992), fractal dimension (Mandelbrot, 1982), and lacunarity parameter (*b*) (Tolle et al., 2008; Mandelbrot, 1982) used in conjugation with vessel diameter and density to examine membrane-labeled vessels of the flk1::myr-mCherry mouse, helped to quantify microvascular morphology and remodeling (Gould et al., 2011). These methods have the potential to aid the development of engineered tissues, such as skin, muscle and soft tissue, by providing the important vessel parameters needed to permit physiologic metabolic exchange and to ensure good incorporation of the scaffold with native tissue.

This technique may help to design therapeutic strategies for re-vascularization, in order to control the resultant morphology of induced vessels. It should be noted however, that more complex vessel beds like the 3-5 tufts of capillaries surrounded by Bowman's capsule in the glomerulus or the juxtaglomerular apparatus in the kidney may require more complex methods to recapitulate the vessel architecture and may not be applicable

to the methods described here, because of their complex structures involving several specialized cell types.

The methodology presented in this work has demonstrated utility by informing a formulation parameter necessary to synthesize bioactive scaffolds for a particular angiogenic application. Here, the effect of growth factor concentration was evaluated with respect to influence on the space-filling properties of vessels induced using a hydrogel matrix. In the future, this methodology could be used to optimize other factors within bioactive scaffolds, and to study other angiogenic compounds *in vivo* in applications within tissue engineering, therapeutic angiogenesis, and other applications in regenerative medicine.

Chapter 3: Covalently Immobilized Platelet Derived Growth Factor-BB Promotes Angiogenesis in Biomimetic Poly(ethylene glycol) Hydrogels

A significant portion of Chapter 3 is taken from Saik, JE, DJ Gould, EM Watkins, ME Dickinson, and JL West (2011). *Acta Biomaterialia,* 7, 133-43.

3.1. Introduction

Engineered tissues are often plagued by the regression of tubule networks. When these networks regress, transport of oxygen to the tissue ceases and cells cannot survive. To stabilize the engineered vessel networks, platelet-derived growth factor BB (PDGF-BB) was used in hydrogels for its ability to recruit pericytes and induce anastomosis. To prolong the signaling of PDGF-BB, the protein was covalently immobilized to hydrogels. Immobilized PDGF led to endothelial cell tubule formation on 2D modified surfaces and an increase in cell migration and matrix metalloproteinase (MMP) activation in 3D. Finally, the presence of immobilized PDGF in these bioactive hydrogels significantly increased vessel density in the mouse cornea micropocket angiogenesis assay.

PDGF, originally identified in the 1970s, contains 100 amino acid long A- and B-chains which exhibit 60% sequence identity with eight conserved cysteine residues (Saik et al., 2011). The second and fourth residues form the bond between the two subunits, while the rest form intrachain bonds necessary for proper protein folding. A-chain genes are located on chromosome 7, with B-chain genes on chromosome 22 (Heldin et al., 1999). Exon 6 contains the sequence for interaction with the extracellular matrix, as PDGF binds collagen, thrombospondin, and heparan sulfate. Therefore, the B-chain precursor can be retained in the extracellular matrix (ECM) until cleavage of the retention

sequence. The three-dimensional structure and amino acid sequence show great similarity to VEGF, as well as to nerve growth factor and transforming growth factor β, which have no sequence similarity (Heldin et al., 1999).

Two PDGF receptors exist, α- and β-, both with five extracellular immunoglobulin-like domains and intracellular tyrosine kinase domains. Three amino acids, Asn-115, Arg-154, and Ile-158, are responsible for PDGF-BB binding both receptor types with high affinity as compared to PDGF-AA, which only binds PDGFRα (Ostman et al., 1991, 20]). PDGF receptors form non covalent dimers, held together by the PDGF ligands (Betsholtz, 2003). Ligand-induced receptor dimerization initiates receptor autophosphorylation, which provides SH2 domain docking sites for signal transduction molecules. Approximately 10 signaling molecules bind PDGF receptors, including phosphatidylinositol 3'-kinase (PI3-kinase), Ras, Src, and Phospholipase C_γ (Betsholtz, 2003). The pathway induced by receptor dimerization affects the functional response to PDGF. For example, the PI3-kinase pathway induces cell migration and apoptosis inhibition. Induction of the MAP kinase pathway via Ras and the transcription factor Myc via Src lead to mitogenesis (Heldin et al., 2002). Each receptor type induces different signaling responses. For example, the αβ receptor has a more potent mitogenic effect. Differences are due to more efficient Ras phosphorylation from the ββ receptor via a GTPase-activating protein (Heldin et al., 2002).

Each A- and B- chain is synthesized as precursor molecules, which undergo proteolytic processing. Based on the presence of all three PDGF isoforms from cell lines, PDGF isoforms most probably form by random assembly (Hart et al., 1990). Furthermore, biologically reactive recombinant chains assemble into both homo- and

heterodimers *in vitro* based on mixing conditions (Hoppe et al., 1990) and all three isoforms are seen in cells transfected with both A- and B-chains (Ostman et al., 1988).

PDGF-B, often involved in angiogenesis, is released in high concentrations by endothelial cells at the sprouting tip and mediates pericyte recruitment (Betsholtz et al., 2005). PDGF-B is also expressed in many connective tissue cell types, including fibroblasts, keratinocytes, smooth muscle cells, endothelial cells, neurons, Schwann cells, and macrophages. Expression varies, but can be induced via thrombin, hypoxia, and growth factors. Endothelial cells also increase PDGF expression in response to shear stress via NFκB (Khachigian et al., 1995). Fibroblasts and smooth muscle cells have both α- and β-receptors, but display higher levels of β-receptors. Platelets and liver endothelial cells only express α-receptors, and mouse capillary endothelial cells express only β-receptors (Heldin et al., 1999). Upon dimerization, receptors are internalized into endosomes. In the endosome, the receptor complex dissociates so the receptor can be recycled to the cell membrane or degraded in the lysosome. This thesis immobilized PDGF in order to prevent its degradation. Research involving application to wounds showed increased wound healing, increased wound-breaking strength (Pierce et al., 1988), and an increased rate of reepithelialization due to PDGF (Pierce et al., 1991). The FDA has approved the use of PDGF- BB for use in periodontal bone defects and diabetic ulcers.

PDGF has widespread activities throughout the body, especially in the development of the kidneys, lungs, CNS, and blood vessels. Specific to the vascular system, endothelial cells not only produce PDGF but display PDGF receptors (Bar et al., 1989). Although PDGF is not involved in initial vessel formation, PDGF-BB is involved

in neovessel stabilization and functionalization by inducing functional anastomoses and recruiting pericytes. Vessel stabilization has been shown to be dependent on expression of β-receptors (Zhang et al., 2009). Mice lacking the PDGF-B chain exhibited defective blood vessel development and microaneurysms, likely as a result of the inability of neovessels to attract stabilizing pericytes (Lindahl et al., 1997). PDGF stimulates pericyte production of ECM proteins, including fibronectin, collagen, and proteoglycans, necessary for the basement membrane of capillaries. Furthermore, PDGF stimulates fibroblasts to produce and secrete collagenases, which is further investigated in this thesis. PDGF also increases expression levels of VEGF in mural cells, which target endothelial cells. PDGF can regulate vessel tone by inducing dose-dependent constriction of small blood vessels or relaxation of large blood vessel via nitric oxide (Berk et al., 1986). PDGF maintains tissue interstitial fluid pressure through interactions between the ECM and connective tissue cells (Rodt et al., 1996). Mouse embryonic stem cells even responded to PDGF by forming capillary-like structures with vascular sprouting as a result of Ca^{2+} induced reactive oxygen species generation (Lange et al., 2009).

Growth factors with short half lives and widespread effects, such as PDGF-BB, have seen relatively few clinical successes despite documented *in vitro* efficacy (Kuhl et al., 1996). This is possibly due to a short circulating half-life (Hollinger et al., 2008) or the potential for unintended action due to the ubiquity of PDGF-BB targets. Covalent immobilization enables controlled, spatial presentation of potent growth factors to stimulate a desired response and mediate potential drawbacks. Immobilization of biomolecules can be accomplished by attaching them to a polymer, such as poly(ethylene glycol) (PEG), which is then incorporated into a larger scaffold network. The

conjugation of growth factors to PEG has been shown to improve solubility, decrease immunogenicity, and increase stability (Veronese et al., 2008; Roberts et al., 2002), while at the same time retaining bioactivity of the original molecule. For example, PEG-conjugated epidermal growth factor (EGF), which does not diffuse or become endocytosed, has been shown to be bioactive and capable of inducing DNA synthesis in a manner comparable to soluble EGF (Kuhl et al., 1996). In another study, PEG-VEGF incorporated into a biodegradable gel not only increased endothelial cell tubulogenesis, but also increased endothelial cell motility 14-fold and cell-cell connections 3-fold (Leslie-Barbick et al., 2009).

The work reported in this thesis used bioactive, PEG-based hydrogels modified with covalently immobilized PDGF-BB to promote *in vitro* tubule formation and stabilization, as well as *in vivo* angiogenesis. Bioactive, immobilized PDGF-BB was shown to enhance the angiogenic activities of tubule formation on modified surfaces in 2D and promote cell migration in 3D degradable hydrogels. Since angiogenesis and vessel stabilization *in vivo* require the precise coordination between multiple growth factors, the combination of PDGF-BB with fibroblast growth factor-2 (FGF-2) was also investigated. PDGF-BB and FGF-2 had previously been found to induce a synergistic vascular response in both the mouse cornea and ischemic hindlimb models (Cao et al., 2003). In this thesis, the combination of covalently immobilized PDGF-BB and FGF-2 showed enhanced cell migration in 3D degradable hydrogels (Saik et al., 2011).

Previous research had shown that a co-culture of human umbilical vein endothelial cells (HUVECs) and 10T1/2 pericyte precursor cells formed long-term stable vessels *in vivo* on a fibronectin-type I collagen matrix (Koike et al., 2004). Additionally,

10T1/2s, when cultured with HUVECS, displayed a smooth muscle cell morphology and began expressing pericyte markers, such as α-smooth muscle actin, smooth muscle myosin, and calponin via the transforming growth factor β1 (TGF-β1) pathway (Hirschi et al., 1998). However, FGF-2 has been shown to act as an antagonist of TGF-β1 induced smooth muscle cell gene expression in 10T1/2 cells (Kawai-Kowase et al., 2004). In this thesis, a co-culture of cells resulted in tubule formation independent of surface modifications with covalently immobilized growth factors, and FGF-free media enhanced tubule formation. Finally, bioactive hydrogels containing the combination of both soluble PDGF-BB to initiate angiogenesis and immobilized PEG-PDGF-BB exhibited a significant increase in vessel density when implanted into the mouse cornea micropocket angiogenesis assay. These studies reaffirm that PEG-based hydrogels can be designed with covalently immobilized growth factors to stimulate a desired cellular response.

3.2 Materials and Methods

3.2.1 Cell Maintenance

HUVECs (Lonza, Walkersville, MD) were cultured in endothelial growth medium EGM-2 (Lonza), supplemented with ascorbic acid, epidermal growth factor, fibroblast growth factor (hFGF-2), heparin, hydrocortisone, insulin-like growth factor, GA-1000 (gentamicin, amphotericin-B), 2% fetal bovine serum (Bulletkit, Lonza), 2 mM L-glutamine, 1 U/ml penicillin, and 1 μg/ml streptomycin (GPS, Sigma, St. Louis, MO, USA). 10T1/2 cells (American Type Culture Collection, Manassas, VA) were cultured in

Dulbecco's modified Eagle's Medium with high glucose (DMEM, Gibco, North Andover, MA) supplemented with 10% fetal bovine serum and 2 mM L-glutamine, 1 U/ml penicillin and 1 μg/ml streptomycin (GPS, Sigma). HUVECs were used from passages 4 to 6, and 10T1/2 cells were used from passages 15 to 19. Cells were maintained in an incubator at 37 °C and 5% CO_2 with media replenished every two days and subculturing as necessary.

PEGDA, PEG-RGDS, and PEG-PQ-PEG were synthesized as described in Chapter 2.

3.2.2 Synthesis and Purification of acryloyl-PEG-succinimidyl carbonate (PEG-SMC)

The organic solvents needed to accommodate the short half-life of the succinimidyl carboxymethyl reactive group on the PEG-SCM, which was purchased and used for conjugation of peptides, were not compatible with proteins used in this study. It was therefore necessary to synthesize a heterobifunctional acryloyl-PEG-succinimidyl carbonate (PEG-SMC) in-house. PEG-SMC is functionally similar to the commercially available PEG-SCM, but has a longer reaction half-life and can thus be used under aqueous conditions.

PEG (Fluka/Sigma, MW = 3400 Da) was reacted with Ag_2O (Sigma, St. Louis, MO), acryloyl chloride (Sigma, St. Louis, MO), and KI (Sigma, St. Louis, MO) in anhydrous dichloromethane (DCM; Sigma, St. Louis, MO) at 4 °C overnight, at molar excess ratios of 1.5, 1.1, and 0.3 respectively. Silver was removed by filtering the solution through Celite 521 (Spectrum Chemical Mfg Corp, Gardena, CA). A Rotovap

was used to dry the solution prior to dissolution in di H_20. The pH was adjusted to 3 with HCl, and the solution was heated to 35 °C for 1 h. Iodine was removed by adding activated charcoal (Fisher, Pittsburg, PA), and the solution was filtered through Celite 521. NaCl and DCM were added, followed by DCM extraction. Phase separation with 2 M K_2CO_3 was used to remove acid and chloride ions. Monoacrylated PEG was dried with sodium sulfate (Fisher, Pittsburg, PA), and a Rotovap was used to concentrate the solution followed byethyl ether precipitation and vacuum filtration. A four molar excess of disuccinimidyl carbonate (Sigma) was reacted with the monoacrylated PEG in anhydrous acetonitrile (Sigma) and pyridine (Sigma) under argon overnight. The product was dried using a Rotovap prior to dissolving in anhydrous DCM. The solution was filtered, and PEG-SMC was purified in acetate buffer (0.1 M, pH 4.5, 15% NaCl) via phase separation. The purified PEG-SMC was dried with anhydrous $MgSO_4$. PEG-SMC was precipitated into ethyl ether, filtered, and dried overnight under vacuum. PEG-SMC was characterized by proton nuclear magnetic resonance spectroscopy (^{1}H-NMR, Avance 400 Hz; Bruker, Billerica, MA, USA) and matrix-assisted laser desorption/ionisation-time of flight mass spectrometry (MALDI-TOF; Bruker Daltonics, Dillerica, MA, USA). The final PEG-SMC product was stored at -80 °C under argon.

3.2.3 Synthesis of PEG-PDGF-BB and PEG-FGF-2

In-house synthesized acryloyl-PEG-SMC was dissolved in 50 mM sodium bicarbonate buffer (pH 8.5) and sterilized via filtration (0.2 μm). PDGF-BB (ProSpec Bio, Israel) was conjugated to PEG-SMC using a 400:1 PEG-SMC: PDGF-BB molar

ratio in 200 mM sodium bicarbonate buffer (pH 8.5) at 4 °C for 4 d (Figure 3-1). The resulting PEG-PDGF-BB solution was lyophilized under sterile conditions. PEG-PDGF-BB powder was reconstituted and stored in HEPES Buffered Saline (100 mM NaCl, 10 mM HEPES in deionized water; HBS; pH 7.4) with 0.1% BSA at 4 °C for up to three months. A similar procedure was followed for PEG-FGF-2 (ProSpec Bio) at a 100:1 PEG-SMC: FGF-2 molar ratio. All growth factor conjugations were confirmed via Western Blot analysis on a 15% Tris-HCL precast polyacrylamide gel (Biorad, Hercules, CA). Primary antibodies included rabbit polyclonal anti-PDGF-B antibody (Santa Cruz Biotechnology, Santa Cruz, CA) and rabbit polyclonal anti-FGF-basic antibody (Millipore, Billerica, MA). Secondary antibody HRP-conjugated goat anti-rabbit IgG (Santa Cruz Biotechnology, Santa Cruz, CA) and an ECL™ chemiluminescent western blotting analysis system (GE Healthcare, Buckinghamshire, UK) were used. The western blot membrane was exposed to film (Kodak, Rochester, NY) for 15 s and developed using a Micromax Developer (Hope, Seattle, WA) with T_2 developer and T_2 fixer (White Mountain Imaging, Salisbury, NY). The presence of PEG was confirmed using a PEG stain adapted from (Zhang et al., 2006), which allows barium iodine to react with PEG to form a yellow color.

Unconjugated PDGF-BB was quantified using a PDGF-BB ELISA (R&D systems, Minneapolis, MN). PEG chains mask antibody binding to PEG-PDGF-BB, so the amount of unconjugated PDGF-BB was quantified after running a sample of the reacted solution on an ELISA as compared to a soluble PDGF-BB standard curve. With the amount of soluble PDGF-BB quantified, appropriate concentrations of PEG-PDGF-BB were calculated.

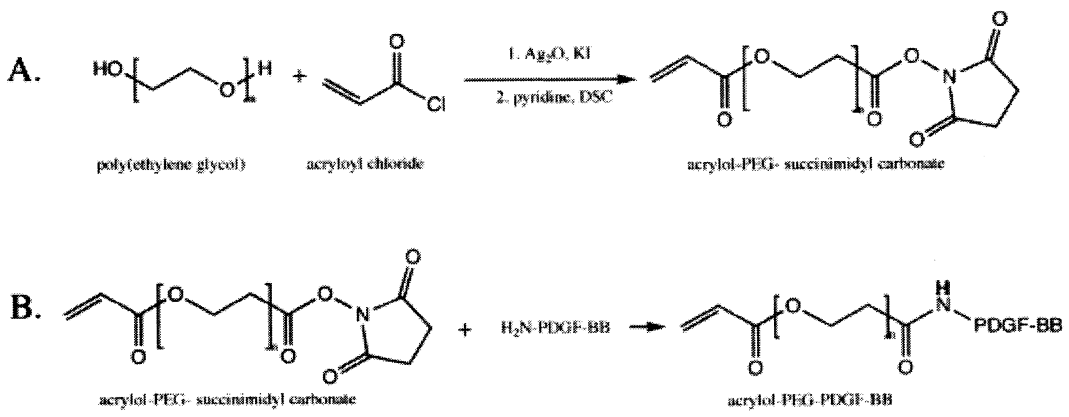

Figure 3-1: Synthesis of conjugated biomolecules. (A) Acryloyl-PEG-succinimidyl carbonate (PEG-SMC) was synthesized by reacting poly(ethylene glycol) with acryloyl chloride in the presence of silver oxide and potassium iodide followed by disuccinimidyl carbonate. (B) acryloyl-PEG-PDGF-BB was synthesized by reacting PEG-SMC with the primary amines of PDGF-BB.

3.2.4 Formation and Surface Modification of PEGDA Hydrogels

Six kDa PEGDA was dissolved in HBS to a 10% polymer weight percentage solution. A stock solution of the photoinitiator 2-dimethoxy-2-phenylacetophenone (acetophenone, Sigma) was prepared by dissolving 300 mg acetophenone in 1 ml N-vinylpyrrolidone (NVP) and then added to the polymer solution at a concentration of 10 µl/ml.

The solution was vortexed and sterile filtered. Hydrogels were polymerized between two glass slides separated by a 0.75 mm thick poly(tetra fluoroethylene) (PTFE) spacer. The glass slides and spacer were secured using clips. Polymer solution was exposed to UV light (B-200SP UV lamp, UVP, 365 nm, 10 mW/cm^2) for 30 s and stored in PBS with 0.1% sodium azide.

The effects of PEGylated proteins in 2D were studied by modifying the surface of bulk PEGDA hydrogels as previously described (Moon et al., 2007). Briefly, 5 mm diameter circles were punched from the hydrogel slabs prepared above. A solution containing 10 µl/ml acetophenone along with PEG-RGDS and PEGylated growth factors was then added in sufficient volume to completely cover the surface of the hydrogel. The exact combination and concentrations of each factor are given in the individual experiments below. Hydrogels were then exposed to UV light for 2 min followed by soaking in sterile PBS to allow for swelling and removal of the photoinitiator solution. A schematic representation of the surface modification process is shown in Figure 3-2.

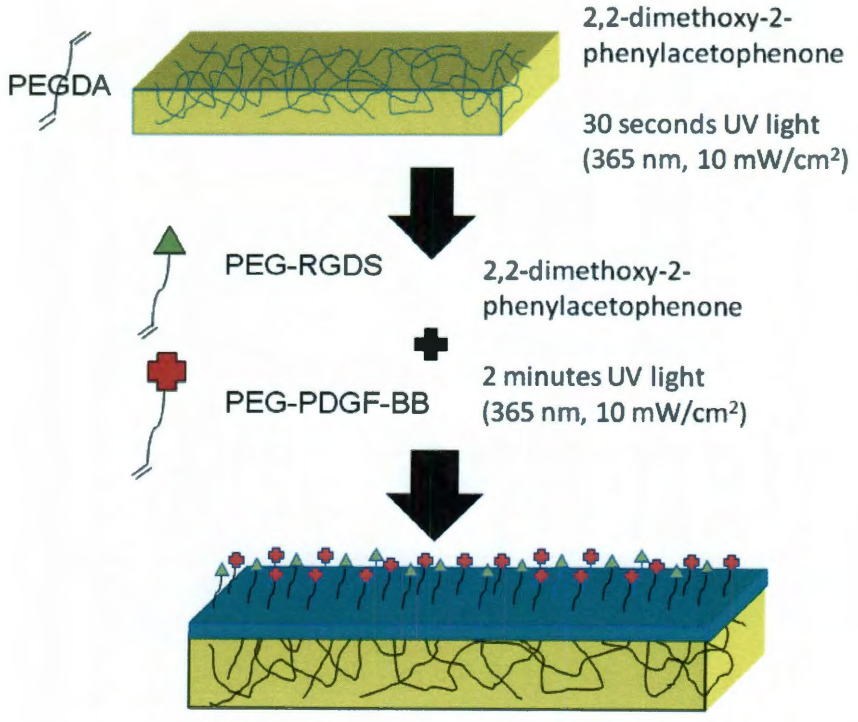

Figure 3-2: To study tubulogenesis in two dimensions, surface modifications of PEGDA hydrogels were performed. PEG-RGDS and PEG-PDGF-BB were covalently immobilized onto the surface of bulk PEGDA hydrogels using the photoinitiator acetophenone.

Patterned hydrogel surfaces were also made to emphasize the utility of spatial control of PEG-PDGF-BB. Hydrogels were patterned by pipetting a solution containing 10 μl/ml acetophenone along with PEGylated growth factors onto the surface of a 5 mm diameter punch of a bulk hydrogel. A black transparency was used to block UV light from part of the gel. Hydrogels were exposed to 2 min of UV light followed by extensive rinsing. PEG-RGDS was then immobilized to the entire surface by adding a solution containing 10 μl/ml acetophenone with PEG-RGDS to completely cover the surface of the hydrogel followed by 2 min UV light exposure.

For all studies, unconjugated PDGF-BB and PEG-SMC were removed via diffusion before the hydrogels were used. Alternatively, soluble PDGF-BB could also be left in place to act as a diffusible growth factor to encourage cell migration in the surrounding tissue for other applications.

To quantify the surface concentration of immobilized PEG-PDGF-BB, hydrogels were synthesized as described above and then degraded in 0.1 N sodium hydroxide for three days. After complete hydrogel degradation, the protein concentration was read on a Nanodrop 2000 (Thermo Scientific, Wilmington, DE).

3.2.5 Bioactivity of Conjugated PDGF-BB via 10T1/2 Proliferation

In order to evaluate the bioactivity of covalently attached PEG-PDGF-BB, 10T1/2 cells (8.5×10^4 cells/cm^2) were seeded onto gels modified with 5 mg/ml PEG-RGDS alone or in combination with 0.70 nmol/ml PEG-PDGF-BB. As a positive control, 0.70 nmol/ml soluble PDGF-BB was added to the media of gels modified with PEG-RGDS

alone. Cells were imaged using an Axiovert 135 (Zeiss) inverted fluorescent microscope after 48 h of culture. Cell nuclei were visualized via incubation with Hoechst 33342 dye (Bis- 119 Benzimide, Sigma) at a concentration of 5 μg/ml in DMEM without serum for one hour at 37 °C. Four fluorescent images were taken per gel at excitation = 350 nm and emission = 460 nm. Cell nuclei were quantified using ImageJ. Cell counts in the presence of PDGF-BB were normalized to counts on surfaces modified with PEG-RGDS alone. Data from three separate experiments using gels with PEG-RGDS (n=31), PEG-PDGF-BB and PEG-RGDS (n=28), and PEG-RGDS and soluble PDGF-BB (n=18) were pooled for statistical analysis as described below.

3.2.6 Quantification of Tubule Formation

To investigate the impact of covalently incorporated growth factors on vascular tubulogenesis, surface-modified PEGDA hydrogels were used. Bulk hydrogels were prepared from 10% 6kDa PEGDA and surfaces were modified as described above. Four modified surfaces were investigated: (1) 7.5 μmol/ml PEG-RGDS, (2) PEG-RGDS and 0.27 nmol/ml PEG-FGF-2, (3) PEG-RGDS and 0.70 nmol/ml PEG-PDGF-BB and (4) PEG-RGDS, PEG-PDGF-BB, and PEG-FGF-2. HUVECs (8.5×10^5 cells/cm^2) or a co-culture of HUVECs and 10T1/2 cells at a ratio of 4:1 were seeded onto the modified gels and cultured in EGM-2 media either with or without FGF-2 and imaged using an Axiovert 135 (Zeiss) inverted fluorescent microscope. Hydrogels were observed over a 30-day period and images of the entire surface of the gels were merged in Adobe Photoshop Elements. Tubules and modified surface areas were traced in Adobe

Illustrator and quantified using ImageJ. For gels seeded with HUVECs alone, data from three separate experiments using gels with PEG-RGDS (n=10); PEG-FGF-2 and PEG-RGDS (n=3); PEG-PDGF-BB and PEG-RGDS (n=10); and PEG-FGF-2, PEG-PDGF-BB, and PEG-RGDS (n=4) was pooled. For the co-culture of HUVEC and 10T1/2 hydrogels, data from three separate experiments using gels in media with FGF-2 with PEG-RGDS (n=10), PEG-FGF-2 and PEG-RGDS (n=3), PEG-PDGF-BB and PEG-RGDS (n=12), and PEG-FGF-2, PEG-PDGF-BB, and PEG-RGDS (n=12) was pooled. Similarly, data from three separate experiments using gels in media without FGF-2 with PEG-RGDS (n=7); PEG-FGF-2 and PEG-RGDS (n=6); PEG-PDGF-BB and PEG-RGDS (n=8); and PEG-FGF-2, PEG-PDGF-BB, and PEG-RGDS (n=7) was pooled.

3.2.7 Immunohistochemistry

To examine tubule morphology, immunohistochemistry was performed to identify endothelial pericyte cell markers. After 30 d in culture, gels were fixed in 4% paraformaldehyde for 30 min and washed with phosphate buffered saline (PBS). Cells were permeabilized with 0.5% Triton-X for 10 min followed by a second PBS wash. 3% normal donkey serum (Sigma) was used as a blocking agent prior to application of the primary antibodies. Gels were incubated overnight at 4 ^{o}C in a 1:200 dilution of mouse anti-alpha smooth muscle actin (R&D systems, Minneapolis, MN) and a 1:100 dilution of goat anti-PECAM-1 (Santa Cruz Biotechnology) in 3% bovine serum albumin solution in PBS. Following incubation, gels were rinsed five times in PBS for 1 h each time. A 1:400 dilution of Alexafluor 488 donkey anti-goat IgG (Invitrogen) and Alexafluor 555

donkey anti-mouse IgG (Invitrogen, Carlsbad, California) was applied overnight at 4 °C in order to visualize the primary antibodies. After washing, gels were incubated in a DAPI solution (2 μM, Invitrogen) for 45 min. Images were taken using a confocal microscope (Zeiss5 LIVE, Plan-Apochromat 20x objective with 0.8 numerical aperture and Plan-Apochromat oil-immersion 63x with 1.4 numerical aperture, for Alexafluor 488: excitation = 489 nm, emission BP filter = 500-525 nm; for Alexafluor 555: excitation = 532nm, emission BP filter = 560-675 nm, for DAPI: excitation = 405 nm, emission BP filter = 415-480 nm).

3.2.8 Cellular Encapsulation into Hydrogels

To further understand the effects of covalently immobilized growth factors on cells in 3D, HUVECs were encapsulated into MMP-sensitive hydrogels containing covalently immobilized growth factors. HUVECs were fluorescently labeled the day before encapsulation by incubation with 10 μg green CMFDA Cell Tracker® (Invitrogen, Eugene, Oregon) in the culture media for 1 h. Following incubation, cells were rinsed with PBS and fresh media was added.

Polymer solution was prepared in HBS (10 mM, pH 7.4) with a final formulation of 10% PEG-PQ-PEG, 3.5 μmol/ml PEG-RGDS, and 0.3% w/v Irgacure 2959 (Ciba Corporations, Based, Switzerland). Four treatment groups were observed, including hydrogels containing: (1) PEG-RGDS alone, (2) PEG-RGDS and PEG-FGF, (3) PEG-RGDS and PEG-PDGF-BB, and (4) PEG-RGDS, PEG-FGF-2, and PEG-PDGF-BB. 0.03 nmol/L PEG-FGF and 0.08 nmol/L PEG-PDGF-BB were used for both the individual

factor groups and the combination of factors. Fluorescently-labeled HUVECs were harvested using trypsin-EDTA and counted using a Coulter counter to determine the cell concentration. After counting, the cells were pelleted by centrifuging at 2700 RPM for 4 min and resuspended in polymer solution to a concentration of 30,000 cells/μl. 5 μl droplets of cell-laden polymer were formed and exposed to UV light for 7 min and the resulting cell-laden hydrogels were immediately immersed in EGM-2 media for *in vitro* analysis.

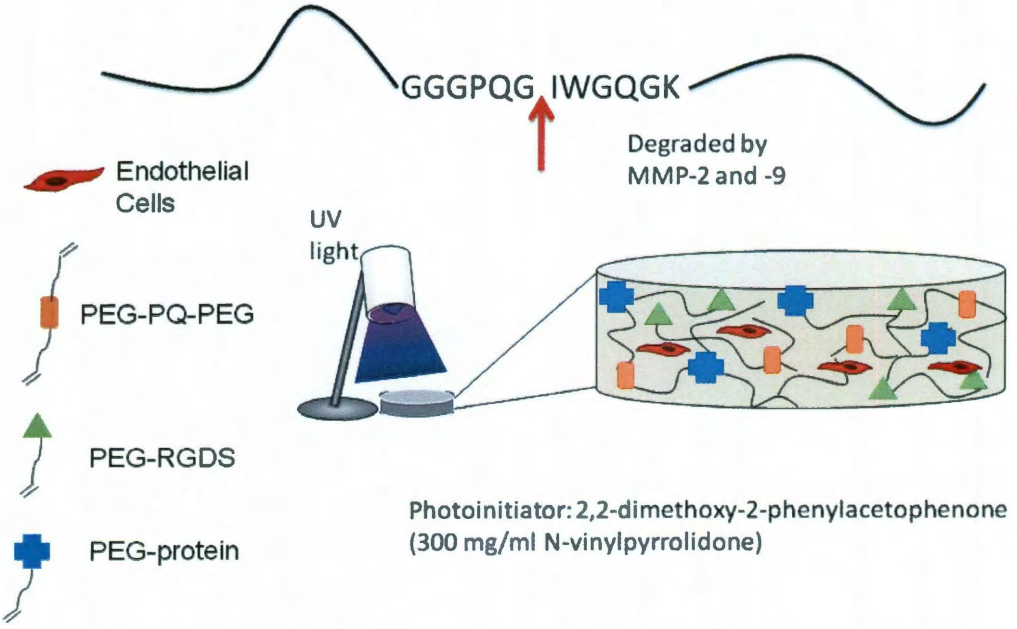

Figure 3-3: Cellular encapsulation into degradable hydrogels. To study tubulogenesis in three dimensions, endothelial cells were encapsulated into MMP-sensitive hydrogels containing covalently immobilized cell adhesive peptides and proteins.

Activity of the cells in the hydrogels was monitored for 60 h using a Zeiss LSM 5 LIVE confocal microscope. Images were captured every hour and analyzed using Logger

Pro Software to track cell movement. Data from three separate experiments was pooled (n=30) for data analysis.

3.2.9 Zymography

To determine MMP activity, media was collected from gels with encapsulated HUVECs 60 h after encapsulation. Standard zymography was performed on a 10% precast polyacrylamide gel with gelatin (Biorad, Hercules, CA) following a Millipore protocol. Briefly, after running electrophoresis, gels were immersed in a 25% triton-X-100 solution in water with gentle mixing for 30 min. After decanting the solution, a developing buffer (50 mM Tris base, 50mM Tris-HCl, 0.2 M NaCl, 5 mM $CaCl_2$, 5 mM Brij 35) was applied overnight at 37 ^{o}C. Gels were then stained with Coomassie Blue and destained with Methanol:acetic acid:water (50:10:40). Gel images were obtained using a Fujifilm LAS 4000 and analyzed for the presence of MMP bands.

3.2.10 Hydrogel Implantation into the Mouse Cornea

Hydrogels were prepared following the protocol outlined in Poche *et al.* (Poche et al., 2009). Briefly, the prepolymer solution contained a 10% polymer weight percentage (100 mg/ml) of PEG-PQ-PEG, 3.5 μmol/ml PEG-RGDS, 10 μl/ml acetophenone stock solution, and 160 ng soluble PDGF-BB per gel with or without 1.6 ng PEG-PDGF-BB per gel (n=8). Hydrogels were prepared by injecting 0.12 μl polymer solution in between the glass slides spaced by a 0.005 in thick PTFE spacer secured with binder clips and exposed to UV light for two min.

Bioactive hydrogels were implanted into the cornea following a modified mouse cornea micropocket angiogenesis assay (Poche et al.). All animals were used under an approved protocol of the Institutional Animal Care and Use Committee at Baylor College of Medicine. Briefly, mice were anesthetized and a partial thickness incision of approximately 50 μm in depth was made in the eye. A Von Graff knife was used to create a micropocket in the cornea stroma into which a hydrogel was implantated immediately after crosslinking. The *Flk1-myr::mCherry* transgenic mice utilized in this study enabled visualization of vessel invasion via endothelial cell specific florescence (Larina et al., 2009). Fourteen days after implantation, mice were euthanized and corneas were collected and fixed in 4% paraformaldehyde. Flatmounts of tissue were made and imaged on a Zeiss LSM 510 META confocal microscope using a 40x/1.2NA C-Apochromat water immersion objective lens with a working distance of 0.28 mm and corrected for UV vis IR. A 543 nm laser was used to excite the mCherry fluorophore. Images of vessels on the hydrogel were compiled from projections of z-stacks exactly 22 μm in thickness, spaced 1.1 μm apart.

3.2.11 Statistics

One-way ANOVA and subsequent Tukey's Least Significant Difference (LSD) tests were used to statistically analyze the bioactivity of PEG-PDGF-BB and HUVEC tubulogenesis on surface-modified hydrogels and the movement of cells inside the hydrogels. In the tubulogenesis study, a generalized linear model in Minitab was used to analyze statistical differences in tubule formation of the co-culture of HUVEC and 10T1/2 cells. For each analysis, $p<0.05$ was considered significant.

3.3 Results

Immobilized PDGF-BB was used in bioactive hydrogels to induce tubule formation. First, the successful conjugation and bioactivity of PEG-PDGF-BB were confirmed followed by the application of PEG-PDGF-BB for angiogenesis in 2D, 3D, and *in vivo*.

3.3.1 Polymer Characterization

Conjugation of acryloyl PEG-SMC to the primary amines of PDGF-BB was confirmed using a western blot. Conjugated PDGF-BB was compared to unmodified PDGF-BB, with an increase in molecular weight representing conjugation of PEG chains to the protein (Figure 3-4). The presence of an intense PEG band in the PEG stain (arrow, Figure 3-4B) at the same molecular weight as the conjugated PDGF-BB band on the western blot further verified PEG-conjugation (Saik et al., 2011).

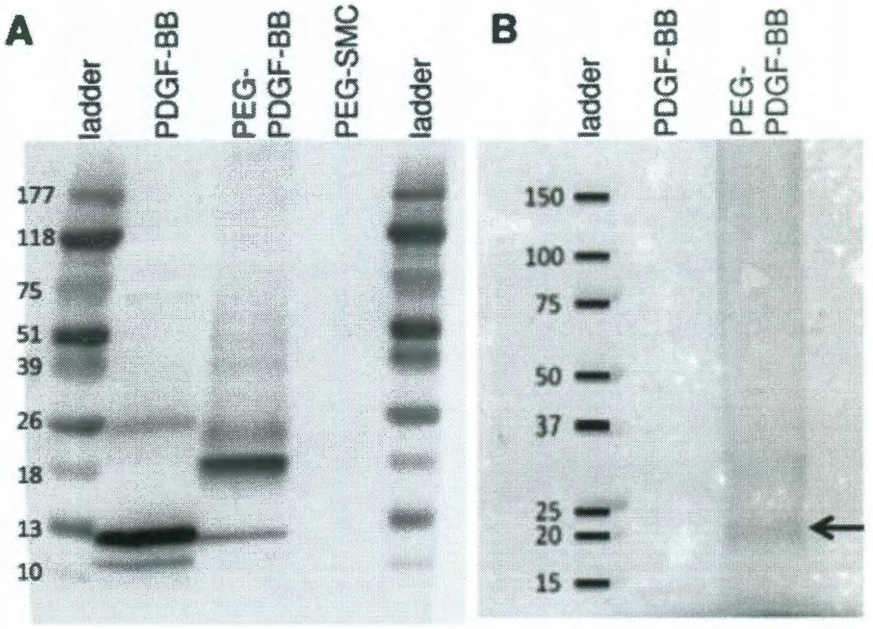

Figure 3-4: Successful Conjugation of PEG to PDGF-BB (A) Successfully conjugated PDGF-BB was confirmed on a western blot by the increase in molecular weight after conjugation. (B) A PEG stain confirmed the presence of a PEG band at the same molecular weight (arrow) as PEG-PDGF-BB in the western blot, further validating PEG-PDGF-BB conjugation.

3.3.2 PEG-PDGF-BB Bioactivity

Bioactivity of the conjugated PDGF-BB was confirmed by quantifying 10T1/2 proliferation on hydrogel surfaces modified with PEG-RGDS and PEG-PDGF-BB as compared to those with PEG-RGDS alone. Soluble PDGF-BB was added to the media of some gels modified with PEG-RGDS to serve as a positive control. As shown in Figure 3-5A, 10T1/2 proliferation significantly increased in the presence of either soluble or bound PDGF-BB at 48 h (ANOVA, $p<0.05$). There was no significant difference in proliferation in the presence of soluble PDGF-BB compared to PEG-PDGF-BB, suggesting that bioactivity of this growth factor is not adversely affected by conjugation

to PEG. The capability to spatially control immobilized PDGF-BB was demonstrated on hydrogels patterned with immobilized PDGF-BB (Figure 3-5 B-C). 10T1/2 cells evenly adhered to surfaces with and without PEG-PDGF-BB at 4 hours (Figure 3-5B). By 48 hours, 10T1/2 cells seeded onto these patterned hydrogels proliferated more on areas with immobilized PDGF-BB (Figure 3-5C).

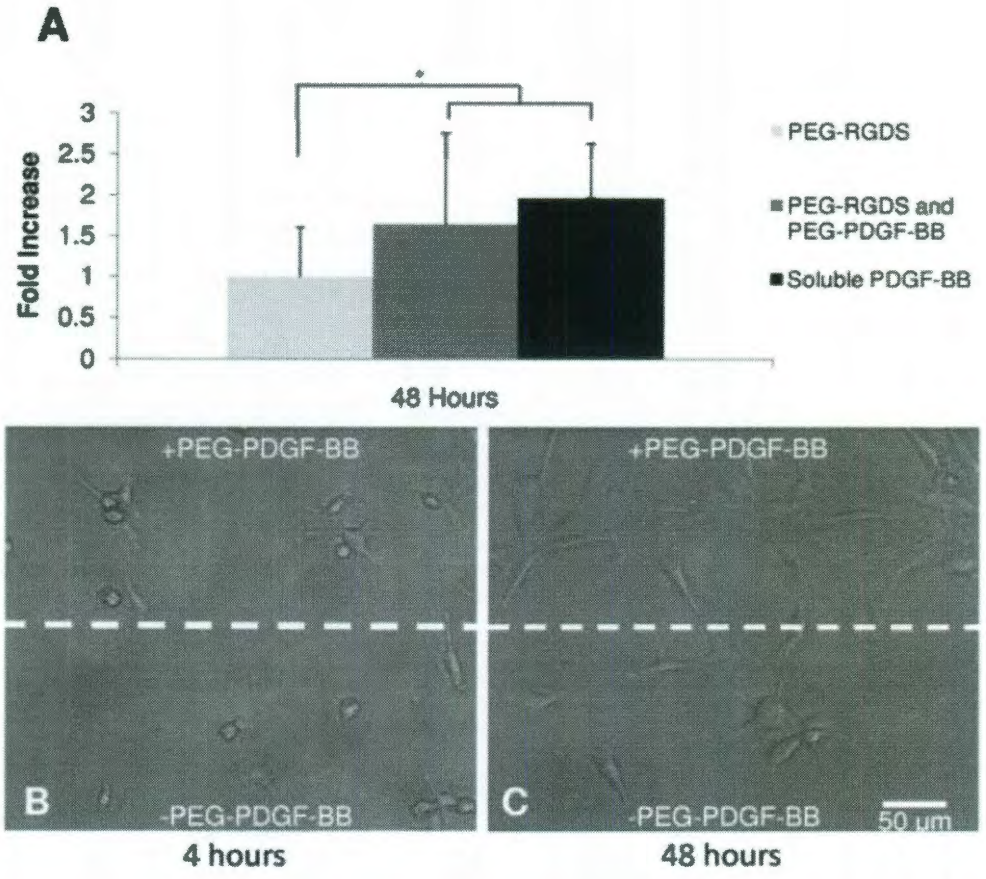

Figure 3-5: Bioactivity of PEG-PDGF was confirmed by seeding 10T1/2 cells onto modified surfaces. (A) By 48 hr, 10T1/2 proliferation had significantly increased in the presence of PDGF-BB (ANOVA, # $p<0.05$). No significant difference between soluble and bound forms of PDGF-BB indicated that covalently-immobilized PEG-PDGF-BB retained its bioactivity. (B-C) Hydrogels with patterned regions of PEG-PDGF-BB demonstrated the utility of spatial control of PDGF-BB. 10T1/2 cells seeded onto these patterned gels were evenly dispersed at 4 hours (B) but exhibited increased proliferation on regions patterned with PDGF-BB after 48 hours (C).

3.3.3 Covalently Immobilized PDGF-BB Promotes Tubulogenesis

Thirty days after seeding HUVECs on surfaces modified with PEG-RGDS and PEG-PDGF-BB, endothelial cell tubules and branching networks were visible (Figure 3-6A). HUVECs on surfaces modified with PEG-RGDS alone exhibited the normal cobblestone morphology of the cell type (Figure 3-6B). Early tubulogenesis was apparent after 18 d, with robust tubulogenesis at day 30. The presence of tubulogenesis after 30 d suggests that the bioactivity of covalently immobilized PEG-PDGF-BB was maintained. Statistical analyses indicated significantly higher tubule formation on surfaces modified with PEG-RGDS and PEG-PDGF-BB (1122 $\mu m/mm^2$) as well as surfaces modified with the combination of PEG-RGDS, PEG-PDGF-BB, and PEG-FGF-2 (983 and 807 $\mu m/mm^2$, respectively) when compared to surfaces modified with PEG-RGDS alone (384 $\mu m/mm^2$; ANOVA with Tukey's LSD, $p<0.05$, Figure 3-6C).

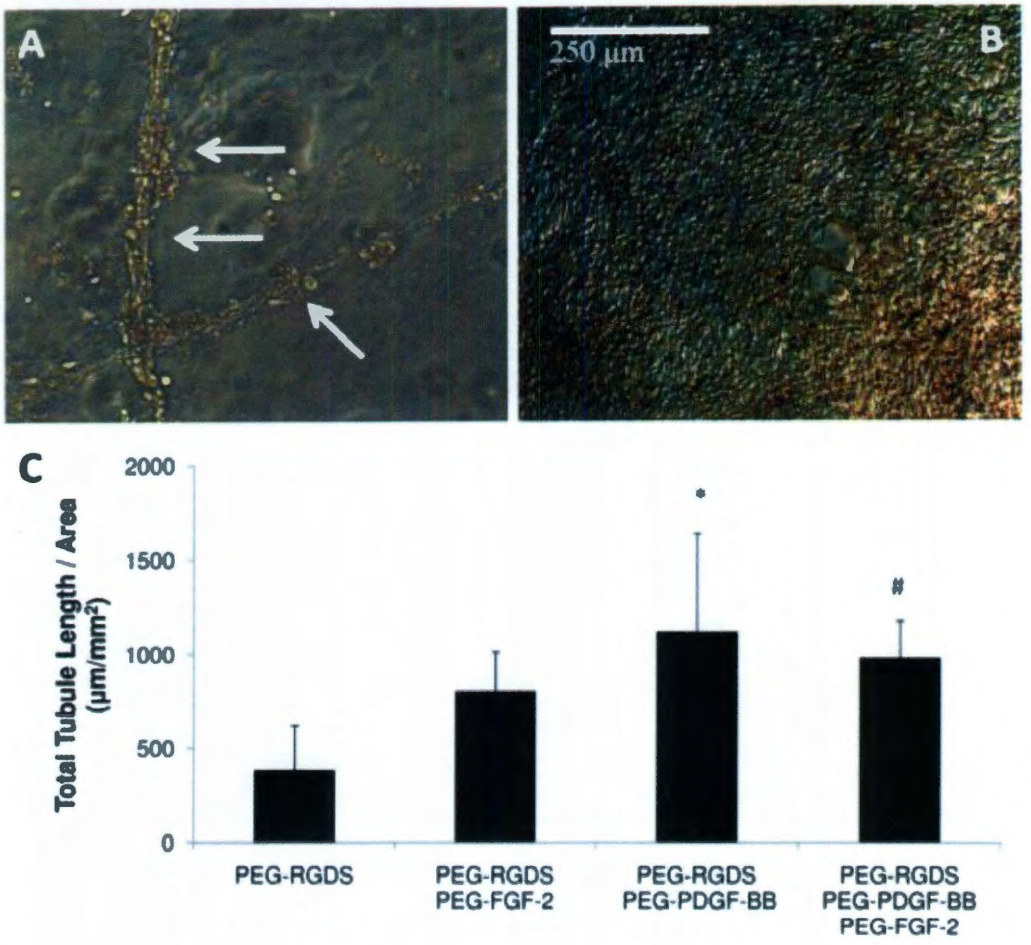

Figure 3-6: Modified surfaces significantly enhanced endothelial cell tubule formation. (A) HUVECs seeded onto modified surfaces exhibit extensive tubule formation (arrows) as early as 18 days compared to the cobblestone appearance of HUVECs seeded on surfaces with only PEG-RGDS (B). (C) A significant increase in tubule formation on surfaces with covalently immobilized PDGF-BB (* $p<0.01$) and surfaces with both covalently immobilized PDGF-BB and FGF-2 (# $p<0.05$) is seen as compared to surfaces modified with PEG-RGDS alone.

3.3.4 Tubule Formation by Co-cultures of HUVEC and 10T1/2 Cells is Independent of Surface Modification

The co-culture of HUVEC and 10T1/2 cells in a 4:1 ratio was seeded onto PEGDA hydrogels modified with cell adhesive peptides and growth factors. Cells in these studies formed tubules within 6 d, with some tubule formation visible by 2 d. Tubulogenesis was independent of surface modifications, indicating that covalently-immobilized FGF-2 and PDGF-BB are not necessary to stimulate tubule formation. Additionally, because FGF-2 is known to antagonize the TGF-β1 dependent differentiation of 10T1/2 into pericytes, cultures were maintained in media both with and without this additive. A generalized linear model in Minitab showed a significant difference in tubule formation between these two experimental groups (Figure 3-7, $p<0.0005$), with FGF-2 free media resulting in the greatest degree of tubulogenesis.

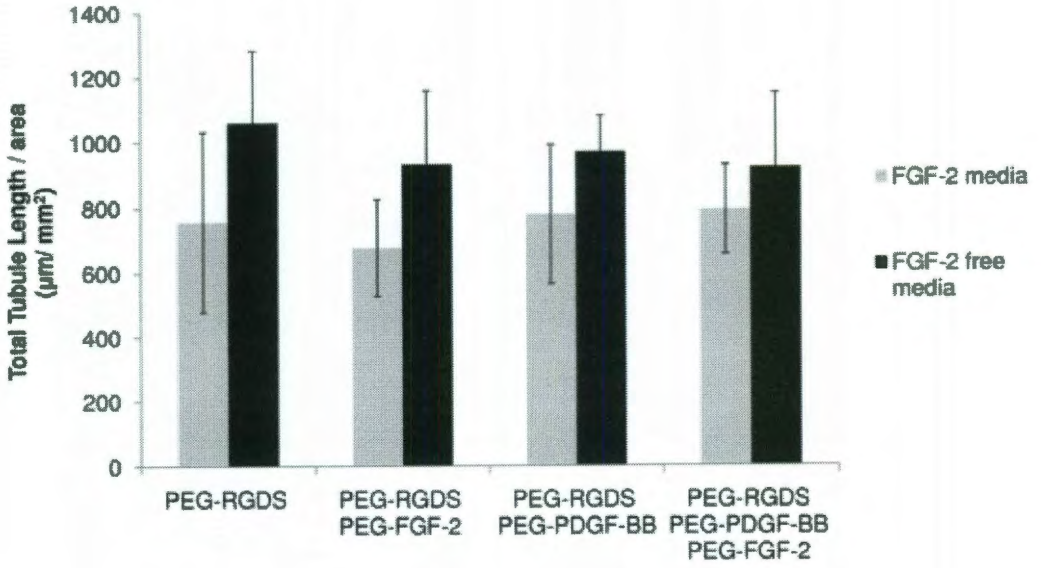

Figure 3-7: Analysis of total tubule length using a generalized linear model confirmed a significant difference between cells cultured in media with and without FGF-2 ($p<0.0005$). The co-culture of HUVECs and 10T1/2 cells exhibited robust tubule formation independent of surface modifications with covalently immobilized growth factors.

3.3.5 Endothelial and Smooth Muscle Cell Marker Expression Induced by Immobilized PEG-FGF-2 and PEG-PDGF-BB

Immunohistochemistry confirmed the expression of endothelial and smooth muscle cell markers in tubules formed by co-cultures of HUVEC and 10T1/2 cells on modified surfaces. 10T1/2 cells were found to express alpha smooth muscle actin, suggesting a pericyte phenotype (Figure 3-8). PECAM-1 labeled HUVECs formed extensive and branching tubule networks throughout the surface. No visible difference in tubule formation was observed between cells seeded on surfaces modified with PEG-RGDS alone or with the cell adhesive peptide in combination with PEG-PDGF-BB

and/or PEG-FGF-2. This suggests that tubule formation in the co-culture of HUVECs and 10T1/2 cells is independent of surface modification (Figure 3-8A and B).

Upon closer examination, single 10T1/2 cells were found to associate with multiple HUVECs in a typical pericyte "umbrella-like" morphology (Figure 3-8C). In addition, the appearance of large vacuoles within HUVECs in these networks (arrows, Figure 3-8D) is suggestive of the early stages of capillary lumen formation. Both of these features confirm the successful formation of stable and functional tubule networks. The presence of pericytes is necessary to prevent tubule regression, and lumen formation is required for red blood cell perfusion.

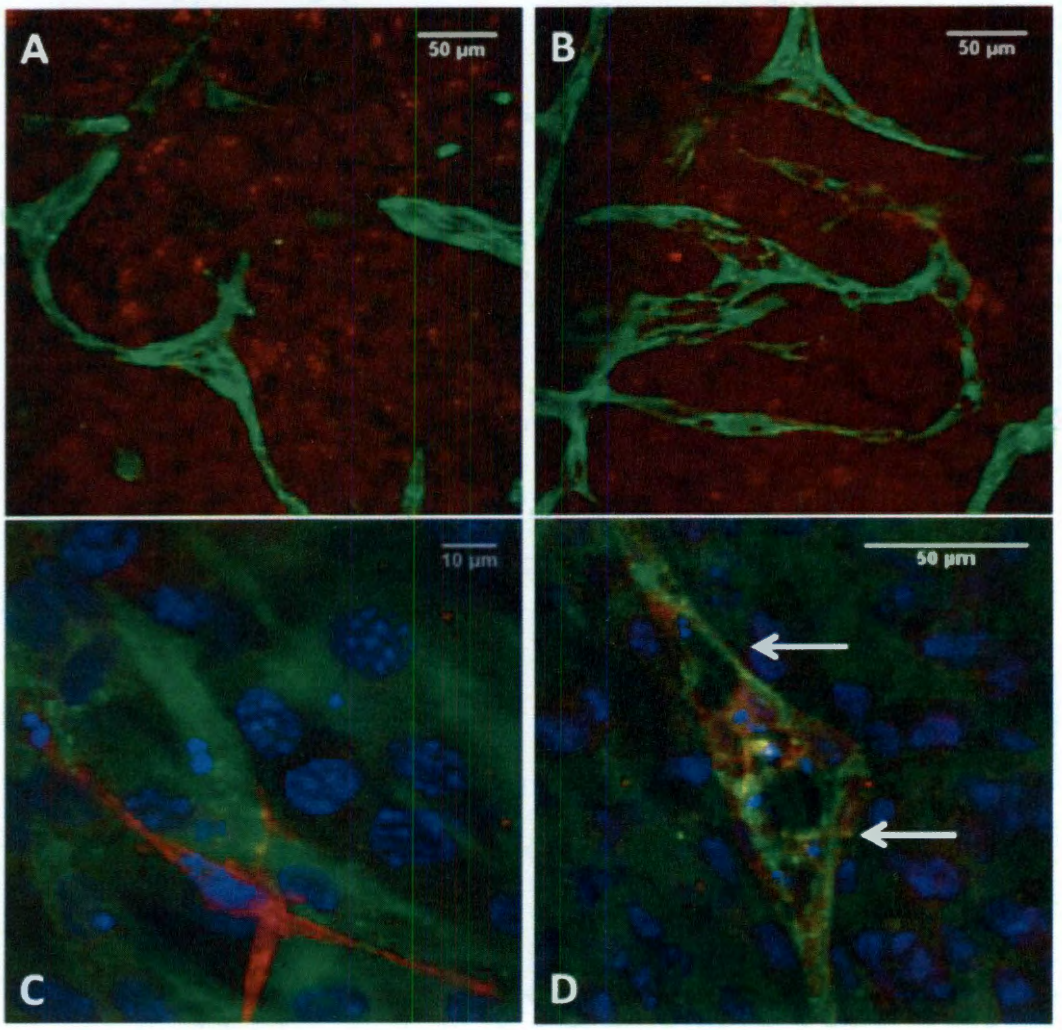

Figure 3-8: Immunofluorescent staining showing tubule morphology. Staining showing PECAM-1 (green), alpha smooth muscle actin (red) and cell nuclei (blue). No significant difference in tubule formation was visible between surfaces modified with RGDS (A) and surfaces modified with covalently immobilized PDGF-BB (B). 10T1/2 cells exhibiting a pericyte morphology can be seen encompassing an endothelial cell and associating with multiple endothelial cells on surfaces modified with RGDS (C). Vacuole formation (arrow) is visible as an early step toward lumen formation on surfaces modified with covalently immobilized PDGF-BB (D).

3.3.6 Covalently Immobilized PEG-PDGF-BB Promotes Cell Migration in 3D Degradable Hydrogels

Timelapse confocal microscopy of fluorescently-labeled HUVECs encapsulated in 3D degradable hydrogels exhibited a significant increase in migration distance per hour in the presence of covalently immobilized growth factors. Single images at 0, 10, 20, and 30 hours are provided to illustrate the cell locations (Figure 3-9). At the starting time, cells are evenly dispersed throughout the hydrogels. By 20 hours, cell movement is visible in the presence of PEG-PDGF-BB. Significant cell clumping is visualized by 30 hours, especially as the gel containing both PEG-PDGF-BB and PEG-FGF-2 collapsed. Cell movement was quantified for the first 14 h, after which time extensive cell clumping and eventual gel collapse hindered measurement. Endothelial cells encapsulated in 3D degradable hydrogels exhibited significantly higher migration in the presence of covalently immobilized PEG-PDGF-BB and PEG-FGF-2 compared to hydrogels containing only PEG-RGDS (Figure 3-10A, *$p<0.01$). Also, PEG-FGF-2 significantly increased migration relative to PEG-PDGF-BB (Figure 3-10A, #$p<0.05$), most likely due to FGF-2's role as a chemoattractant (Bikfalvi et al., 1997). The combination of covalently immobilized PEG-PDGF-BB and PEG-FGF-2 was found to significantly increase migration (Figure 3-10A, *$p<0.01$) and decrease the time to gel collapse (Figure 3-10B, *$p<0.01$) as compared to the presentation of either of the factors alone.

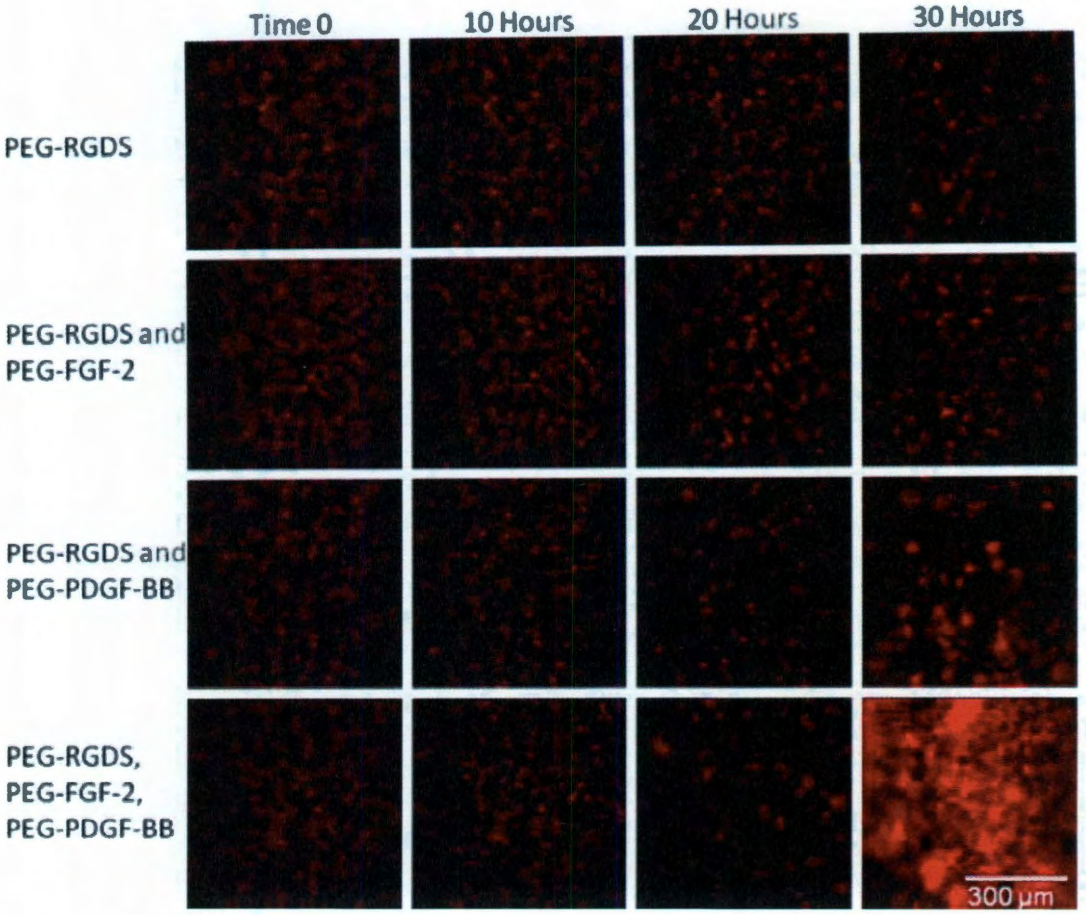

Figure 3-9: Images from timelapse confocal microscopy illustrating cell movement. Fluorescently labeled HUVECs are evenly dispersed at the beginning of the experiment. In the presence of PEG-PDGF-BB, cells begin to move by 20 hours and significant cell clumping is visualized at 30 hours.

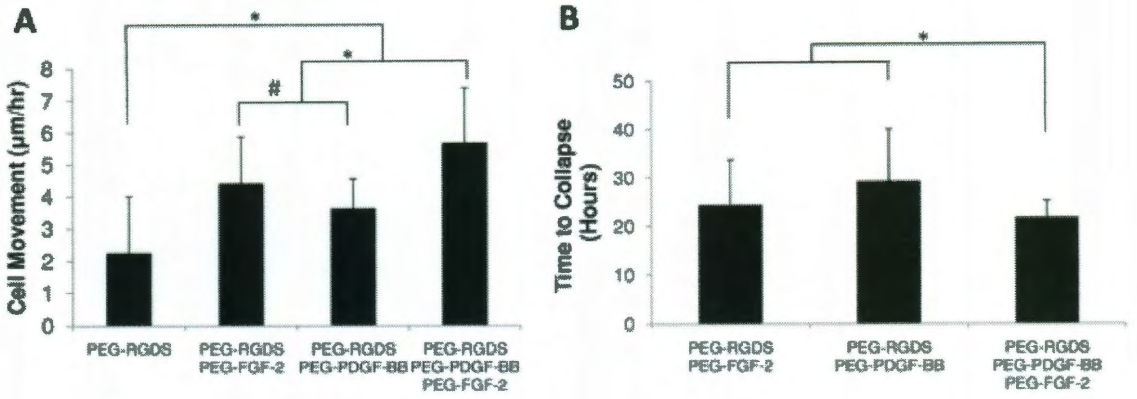

Figure 3-10: Endothelial cells exhibit angiogenic characteristics in 3D. (A) HUVECs encapsulated into 3D degradable hydrogels exhibited greater cell movement in gels containing covalently immobilized growth factors (* $p<0.01$). PEG-FGF-2 significantly increased migration as compared to PDGF-BB (# $p<0.05$), and the combination of PEG-PDGF-BB and PEG-FGF-2 induced significantly increased cell migration as compared to PDGF-BB and FGF-2 alone (* $p<0.01$). (B) Hydrogels containing covalently immobilized growth factors collapsed after 20-40 hr. The combination of PDGF-BB and FGF-2 lead to earlier gel collapse as compared to each growth factor alone (* $p<0.01$).

3.3.7 MMP Activation in Response to Covalently Immobilized Growth Factors

Gelatin zymography was performed to analyze the presence of matrix metalloproteinase-2 (MMP-2) in hydrogels containing encapsulated HUVECs with covalently immobilized growth factors (Figure 3-11). Interestingly, the 72 kDa pro-form of MMP-2 was present in all samples, but only samples with covalently immobilized PEG-PDGF-BB and/or PEG-FGF-2 contained active MMP-2 (68 kDa), a finding which corroborates the increase in cell movement in the same materials.

Figure 3-11: Immobilized growth factors induce MMP cleavage. Gelatin zymography confirmed the presence of pro-MMP-2 (MW 72 kDa) in all samples, but active MMP-2 (MW 68 kDa, arrow) was seen only in the presence of covalently immobilized growth factors.

3.3.8 PEG-PDGF-BB Enhances *In Vivo* Vascular Response

To confirm the bioactivity of PEG-PDGF-BB during angiogenesis *in vivo*, hydrogels containing PEG-PDGF-BB were implanted into the mouse cornea, a well defined method to assess angiogenesis (Kenyon et al., 1996). Hydrogels containing soluble PDGF-BB initiated an angiogenic response by stimulating vessels from the surrounding limbus to invade into the normally avascular cornea. Once vessels reached the bioactive hydrogel, the immobilized PEG-PDGF-BB (Figure 3-12B) induced a more robust vascular response than hydrogels with soluble PDGF-BB alone (Figure 3-12A), including an increase in quantified morphological parameters (Figure 3-12 C-F).

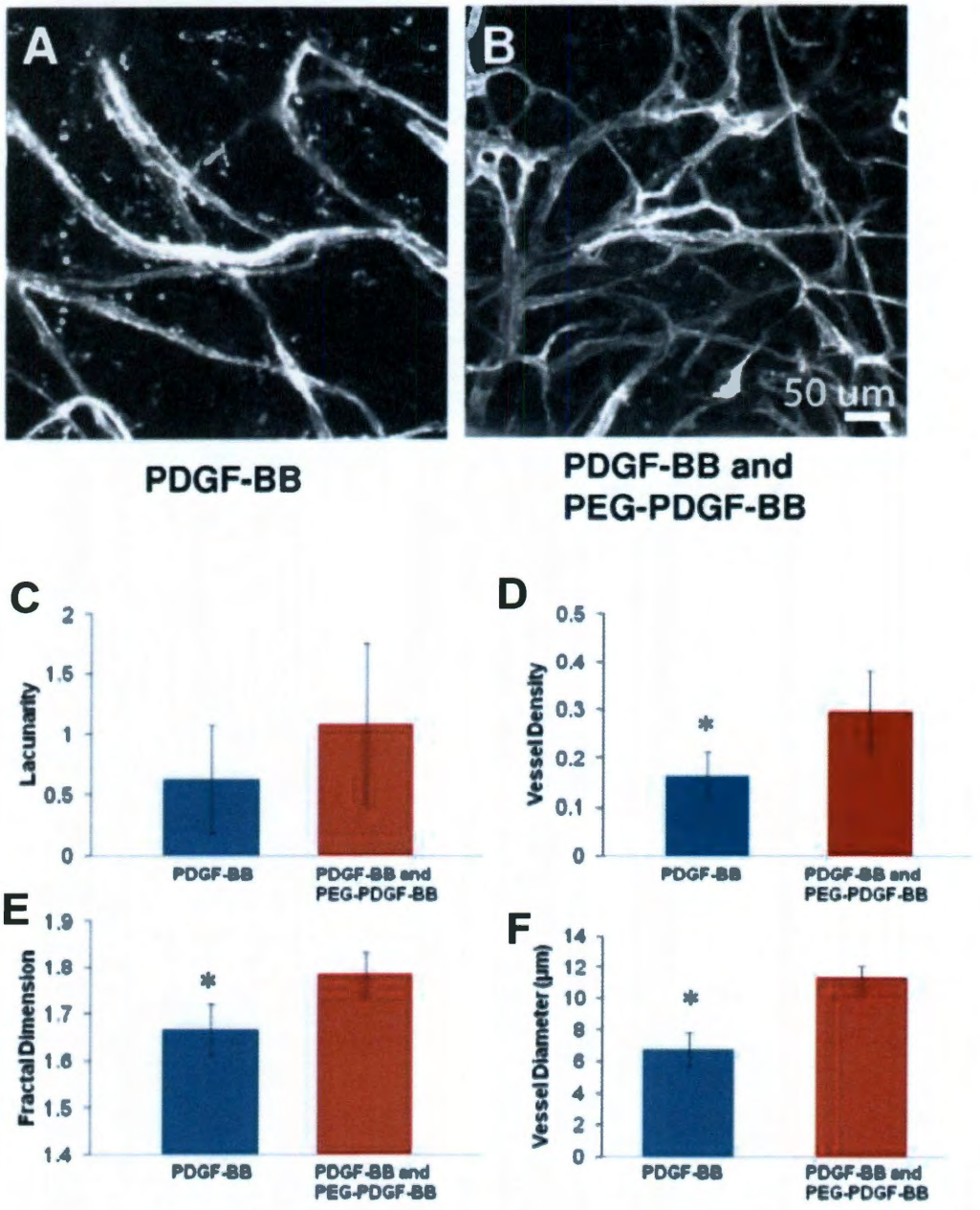

Figure 3-12: Immobilized PDGF-BB enhances the in vivo vascular response. Bioactive hydrogels incorporating both releasable and covalently immobilized PDGF-BB (B) were implanted into the mouse cornea micropocket and resulted in a more robust vascular response than hydrogels with releasable PDGF-BB alone (A). Statistical analysis highlights a significant increase in the vessel density, fractal dimension, and vessel diameter (D-F) with the addition of immobilized PDGF-BB ($p<0.05$).

3.4 Discussion

Controlled delivery of PDGF, such as the work in this thesis, has been investigated in several forms. Primarily, biomaterials have been employed as slow release delivery mechanisms (De la Riva et al., 2009). Rather than relying on growth factor release, fibrin matrices using heparin-binding to mimic the body's delivery system have also been designed to deliver PDGF-BB and FGF-2, a delivery system which increased fibroblast proliferation in tendon tissue (Thomopoulos et al., 2009). However, heparin binding does not provide as controlled an environment as the immobilization technique used in this thesis because other proteins can bind to heparin, and proteins can release and rebind. Recently, two groups have immobilized PDGF, enabling more prolonged delivery than that achieved with soluble release only. Aizawa *et al.* immobilized PDGF-AA, which induces PDGF receptor αα homodimers, as opposed to PDGF-BB which binds all three dimeric combinations of α- and β- receptors. Maleimide functionalized PDGF-AA was immobilized to a natural material, agarose, containing sulfhydryl groups and used for PDGF-AA's known effect in regulating the differentiation of neural stem cells (Aizawa et al., 2008). Chen *et al.* introduced sulfhydryl groups into collagen scaffolds and used them to immobilize PDGF-BB, which stimulated fibroblast proliferation and increased blood vessel density after subcutaneous implantation (Chen et al., 2009).

As opposed to previous work, this thesis focused on PDGF-BB for its involvement in inducing stable and functional neovessel formation. PDGF-BB was conjugated to PEG and immobilized in synthetic PEG-based scaffolds, which allow precise control over incorporated biological molecules, as well as mechanical properties

(Saik et al., 2011). PEG-PDGF-BB was shown in a cell proliferation assay to maintain bioactivity. In addition, PEG-PDGF-BB and PEG-FGF-2 stimulated angiogenesis in engineered PEG-based hydrogels.

To form stable and functional vessels, angiogenesis requires the precise coordination of various signaling molecules. While combinations of growth factors have been used in releasable form, they have never been presented in an immobilized form. This work demonstrates the feasibility using immobilized PDGF-BB with FGF-2, a previously established synergistic combination (Cao et al., 2003), to promote endothelial migration in 3D. HUVECs seeded onto hydrogels exhibited significantly higher tubule formation on surfaces modified with PEG-RGDS and PEG-PDGF-BB and the combination of PEG-RGDS, PEG-PDGF-BB, and PEG-FGF-2 as compared to surfaces modified with PEG-RGDS alone. The work presented in this thesis confirms that growth factors can assist endothelial cells in forming tubes, with robust tubule formation for 30 days.

In addition to the necessary growth factors, capillary formation requires two cell types where stabilizing pericytes promote endothelial cell survival (Reinmuth et al., 2001) and form the basement membrane required for vessel stabilization and function (Diaz-Flores et al., 2009). In order to more rapidly form stable tubule networks, this work made use of a co-culture of HUVEC and 10T1/2 cells, which has previously been shown to form stable vessels *in vivo* (Koike et al., 2004). Mouse pericyte precursor 10T1/2 cells are known to differentiate into pericytes in the presence of HUVECs via the TGF-β1 pathway (Hirschi et al., 1998). The co-culture of HUVEC and 10T1/2 cells confirmed the role of stabilizing pericytes as the presence of 10T1/2 cells was sufficient

to induce tubule formation independent of surface modification as early as two days after cell seeding. Pericytes, first described in 1873 (Edelman et al., 2006), function to contract in order to regulate blood flow but also to regulate permeability. With less than 20 nm between pericytes and endothelial cells, each pericyte covers several endothelial cells in an "umbrella-like" manner (Edelman et al., 2006). Furthermore, vessels lacking pericytes exhibit abnormal features, such as leakage and impaired perfusion due to abnormal endothelial junctions, endothelial hyperplasia, and hypervariable diameter (Betsholtz et al., 2005).

Direct contact with HUVECs induces 10T1/2 cell differentiation into stabilizing pericytes. However, FGF-2 is a known antagonist of the TGF-β1 dependent differentiation of 10T1/2 cells into pericytes, and thereby an important factor in the stabilization of new vessels. In this work, the removal of FGF-2 from culture media resulted in increased tubule formation by HUVECs and 10T1/2 cells seeded on modified surfaces, suggesting that the critical pericyte differentiation had occurred. Confirmation of the presence of endothelial pericyte markers via immunohistochemistry further supports this reasoning. As demonstrated, tubule-like networks were visible on all surfaces, with alpha smooth muscle actin-positive cells seen extending over several endothelial cells in a pericyte-like fashion. Furthermore, the presence of multiple, large vacuoles within endothelial cells suggests lumen formation and capillary development (Kamei et al., 2006) on these functionalized hydrogels.

Reduced tubule formation in the presence of FGF-2 *in vitro* may affect the design of the hydrogels for *in vivo* use. Koike *et al.* have shown that a co-culture of HUVEC and 10T1/2 cells is capable of forming functional tubule networks *in vivo*, which is

supported by the tubule formation seen in this *in vitro* work (Koike et al., 2004). However, to enhance tubule formation, local FGF-2 may need to be reduced, possibly through design of hydrogels with FGF-2 antibodies. As an alternative, hydrogels could be designed with only HUVECs with the addition of immobilized PDGF-BB as the immobilized PDGF-BB induces HUVEC tubule formation.

Based on the success of PEG-PDGF-BB in 2D, its effects were also studied in 3D. It has been well established that growth factors, and in particular FGF-2 and PDGF-BB, effectively increase the migratory behavior of cultured endothelial cells. Soluble factors have been shown to induce a migratory phenotype, characterized by cytoskeletal rearrangement and pseudopodia formation, and to increase random movement in wound healing models of endothelial cells cultured in monolayer (Lee et al., 2006; Zhang et al.). In the presented thesis work, a similar effect was observed in degradable hydrogels containing immobilized PEG-FGF-2 and PEG-PDFG-BB. HUVECs encapsulated in these MMP-sensitive hydrogels exhibited a significant increase in random migration distance per hour as compared to materials without the growth factors. In addition, the combination of PEG-FGF-2 and PEG-PDGF-BB resulted in a decreased time to gel collapse (33 hours as opposed to 52 and 43 hours, respectively), likely due to FGF-2 induced PDGF receptor expression in vascular endothelial cells (Cao et al., 2008). Also, PDGF-BB is capable of inducing a positive feedback signal to amplify FGF-2 expression in vascular mural cells, which in turn enhances mural PDGF receptor β expression (Kano et al., 2005; Cao et al., 2008).

In addition to stimulating migration, growth factors such as PDGF-BB stimulate the release of MMP-2 and MMP-9. The degradable hydrogels used in this work

comprised crosslinked polymer chains that contain a protease-sensitive, PQ peptide segment. As such, when MMPs are secreted near or within the hydrogel material, the PQ peptide is degraded, causing the polymer backbone to fragment. As more peptides are cleaved, polymer fragments are released to solution and the hydrogel loses its integrity. In the current study, the increase in cell motility in the presence of growth factors appears to have hastened the collapse of the collagenase-sensitive hydrogel, presumably due to the secretion of MMPs by migrating cells. This reasoning is supported by results from gelatin zymography, which confirmed the presence of MMP-2 in hydrogels containing encapsulated HUVECs. MMPs play an active role in angiogenesis, particularly MMP-2, by enabling sprouting endothelial cells to migrate and by regulating growth factor release and activation (Stamenkovic, 2003). In addition, MMP activity is often controlled by proteolytic cleavage, in which a propeptide is cleaved to generate an active form of the enzyme. Interestingly, only samples with covalently immobilized growth factors contained active MMP-2 (68 kDa), corroborating the increase in cell movement and earlier hydrogel collapse in the same materials.

Controlled delivery of PDGF-BB is particularly useful for *in vivo* applications. Soluble PDGF-BB was necessary to stimulate the initial angiogenic response of the surrounding limbic vessels into the cornea. Since soluble PDGF-BB degrades very rapidly *in vivo,* the presence of PEG-PDGF-BB enables prolonged angiogenic signaling on the hydrogel, leading to an increase in vessel density and diameter. This manuscript presents the first work with a PEGylated growth factor *in vivo.*

3.5 Conclusion

Biomimetic hydrogels can be designed to incorporate cell adhesive sequences and covalently immobilized growth factors to stimulate a desired cellular response in tissue engineered constructs. This thesis work demonstrates that PEG-PDGF-BB is bioactive and can be successfully incorporated into PEG-based hydrogels alone and in combination with PEG-FGF-2. HUVECs seeded onto hydrogel surfaces modified with covalently immobilized growth factors formed extensive and branching networks of tubules. Additionally, a co-culture of HUVEC and mouse pericyte precursor 10T1/2 cells seeded onto modified surfaces induced tubule formation independent of growth factor modification as early as two days after cell seeding. Endothelial cells encapsulated in MMP-sensitive hydrogels with covalently immobilized growth factors exhibited key steps in angiogenesis, such as a significantly higher migration rate and MMP-2 activation. Finally, bioactive hydrogels containing both soluble PDGF-BB and immobilized PEG-PDGF-BB led to a significant increase in vessel density when implanted into the mouse cornea as compared to hydrogels with soluble PDGF-BB alone. Further work is necessary to determine optimal combinations of cell types as well as both bound and soluble growth factors to form stable and functional vascular networks. The results presented here demonstrate the potential of biomimetic, PEG-based hydrogels containing immobilized growth factors as a promising methodology to engineer a microvascular system within tissue engineered constructs for regenerative medicine applications.

Chapter 4: Biomimetic Hydrogels with Immobilized EphrinA1 for Therapeutic Angiogenesis

A significant portion of this chapter is from Saik, JE, DJ Gould, AK Keswani, ME Dickinson, and JL West. *Biomacromolecules.* In press 2011.

4.1 Intoduction

The formation of a microvascular system requires precise coordination between cells and their environment. In order to influence cell-cell interactions during microvascular formation, the receptor tyrosine kinases family of Eph receptors and their ephrin ligands were utilized for their involvement in growth, differentiation, and patterning of tissues. Most commonly expressed on neuron and endothelial cells, ephrinA1 is notably involved in the formation of the neuronal system as well as organization of the vasculature (Pasquale, 2008). Unlike other receptor tyrosine kinases, Eph receptors bind to membrane bound ephrin ligands. Ephrin ligands are categorized as type A for having a Glycosylphosphatidylinositol-anchor or type B for having a transmembrane domain. Eph receptors of the A class usually interact with ephrin ligands of the A class. Signaling can occur in a forward manner by ephrin ligands activating Eph receptors or in reverse by Eph receptors activating ephrin ligands (Heroult et al., 2006).

The Eph receptors, the largest family of receptor tyrosine kinases, were first identified in 1987 as organ receptors with no known ligands. Several years later, ephrins were identified. The extracellular structure for the Eph receptor includes a NH_2-terminal ephrin-binding domain with a cysteine-rich domain and two fibronectin-type III repeats

(Wykosky et al., 2008). The receptor then passes through the cell membrane and the intracellular structure contains two tyrosines, enabling autophosphorylation, and a tyrosine kinase domain. The COOH terminal end of the receptor provides a docking site for downstream signaling proteins (Wykosky et al., 2008). Reverse signaling via the ephrinA ligand may involve protein interactions, including the Src family, with the GPI linker (Wykosky et al., 2008). Signaling requires clustering of receptors, naturally done via membrane linkage. This thesis will use an Fc-conjugated ephrinA1 to enable clustering. The specific interaction between EphA2 and eprhinA1 likely occurs between the serine or alanine at the 109th position on ephrinA1 with the glutamine or methionine at the 38th position on EphA2. EphA2 is a 130 kDa, 976 amino acid receptor expressed on chromosome 1p36. ephrinA1 is a 22 kDa, 205 amino acid ligand from chromosome 1q21-2. Tumor necrosis factor α is capable of inducing ephrinA1-mediated endothelial cell migration (Ogawa et al., 2000).

Since both Ephs and ephrins are membrane bound and involve cell-cell contacts, signaling occurs in both a forward and reverse manner. Forward signaling generally repels two cells apart while reverse signaling generally adheres cells (Himanen et al., 2007). The interaction between ephrinB2 and EphB4 is widely known to pattern arterial versus venous endothelial cells, respectively. Similar to PDGF, stabilization of vessels may also be due to recruitment of pericytes. Only ephrinB2 has been specifically shown to recruit pericytes, but ephrinA1 may also be involved. Furthermore, ephrinA1 is known to induce formation of actin stress fibers for smooth muscle cell contractility in regulating blood pressure (Kuijper et al., 2007). Interestingly, as Ephs and ephrins are known to be involved in both axonal guidance and angiogenesis, similarities between endothelial tip

cells and axon growth cones have recently been made. For example, peripheral nerves guide artery pattern formation and arteries will continue to form along disrupted nerves (Mukouyama et al., 2002). Therefore, the endothelial tip cells resemble axon growth cones by displaying a similar morphology, responding to similar growth factors including ephrins, and comprising a necessary component to form new cell-cell connections (Adams et al., 2010).

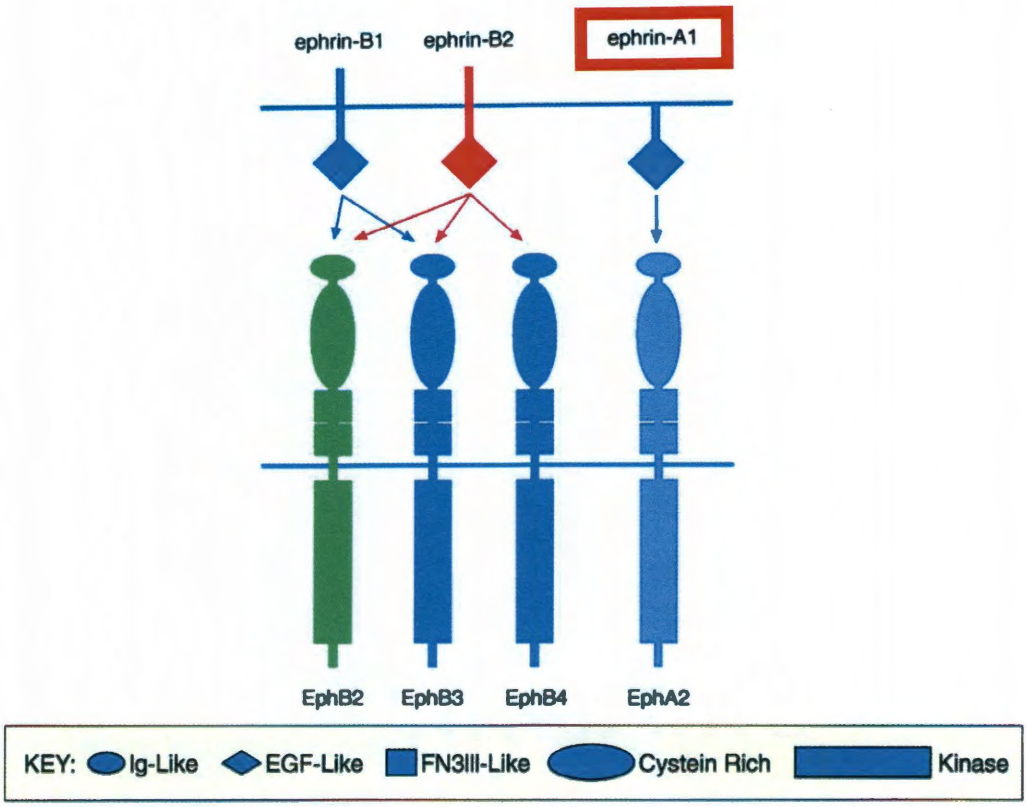

Figure 4-1: Ephrins and their Eph receptors involved in vascular development. Membrane bound ephrin ligands interact with membrane bound Eph receptors. In this thesis, a covalently immobilized ephrinA1 (red box) was used to induce tubule formation in PEG-based hydrogels. Figure adapted from (Gale et al., 1999)

Although initially discovered in 1990 for involvement in the nervous system, the interaction between ephrinA1 and its EphA2 receptor first elicited the role of ephrins and their Eph receptors in angiogenesis (Pandey et al., 1995). Activation of ephrin-A1 and its EphA2 receptor has been shown to initiate endothelial cell migration and capillary invasion by regulating vascular cell shape, migration, adhesion, and proliferation (Brantley et al., 2002). Expression of ephrinA1 is induced by tumor necrosis factor-α, interleukin-1 beta, and vascular endothelial growth factor (Cheng, Brantley, and Chen, 2002). Soluble ephrin-A1 has been shown to induce human umbilical vein endothelial cells (HUVECs) to form capillary-like structures (Daniel et al., 1996). Furthermore, a dominant-negative form of EphA2 inhibited HUVECs from forming capillary-like structures (Ogawa et al., 2000). Soluble ephrinA1 has also induced endothelial cell migration (Brantley et al., 2002) and capillary sprouting (Cheng, Brantley, Liu et al., 2002) and *in vivo* angiogenesis in a variety of assays, including the cornea micropocket (Cheng, Brantley, Liu et al., 2002) and subcutaneous implantation of ephrinA1 soaked sponges (Brantley-Sieders et al., 2004). Alternatively, an immobilized ephrinA1 may be used to induce the formation of a microvascular system in tissue engineering constructs (Moon et al., 2007), specifically PEG-based hydrogels.

Immobilized growth factors and signaling peptides have been used to induce precise local effects. Previously, basic fibroblast growth factor was immobilized onto PEGDA hydrogels and induced vascular smooth muscle cell proliferation and migration (DeLong et al., 2005). Immobilized ephrinA1 lead to dose-dependent endothelial cell adhesion to PEGDA hydrogels via $a_v\beta_3$ integrins as well as tubule formation with lumen formation (Moon et al., 2007). In this work, the role of immobilized ephrinA1 was

highlighted in microvascular formation via 2D tubule formation of HUVECs on hydrogels modified with PEG-ephrinA1 and in three dimensional degradable matrices. Extensive tubule formation was visualized as early at 24 hours and up to 7 days. Tubule deposition of collagen IV was found to be dependent upon immobilized ephrinA1 concentration, and laminin deposition was dependent upon immobilized ephrinA1 concentration and time. To confirm the role of the EphA2-ephrinA1 interaction in tubule formation, soluble EphA2 reduced tubule formation in a co-culture of HUVEC and human brain vascular pericytes on modified hydrogels. Finally, hydrogels incorporating immobilized ephrinA1 in a mouse cornea micropocket exhibited a significant increase in vessel density and the number of branch points as well as space filling parameters of fractal dimension and lacunarity. Based on these findings, immobilized ephrinA1 represents a promising molecule to regulate cell adhesion and migration for the formation of a microvasculature in tissue engineered constructs.

4.2 Materials and Methods

4.2.1 Cell Maintenance

Human Umbilical Vein Endothelial Cells (HUVEC, Lonza, Walkersville, MD) were cultured in endothelial growth medium EGM-2 (Lonza), supplemented with the EGM-2 bullet kit containing ascorbic acid, epidermal growth factor, fibroblast growth factor (hFGF-2), heparin, hydrocortisone, insulin-like growth factor, GA-1000 (gentamicin, amphotericin-B), and 2% fetal bovine serum (Bulletkit, Lonza). Human brain vascular pericytes (HBVP, ScienCell, Carlsbad, CA) were cultured in pericyte

medium (ScienCell) on poly-L-lysine coated flasks (2 μg/cm^2). HUVECs were used from passages 4 to 6, and HBVP cells were used from passages 4 to 9. Cells were incubated at 37 °C and 5% CO_2 with media replenishment and subculturing as necessary. Immunohistochemistry was performed to confirm ephrinA1 expression on HBVP and EphA2 expression on HUVECs (Figure 4-2).

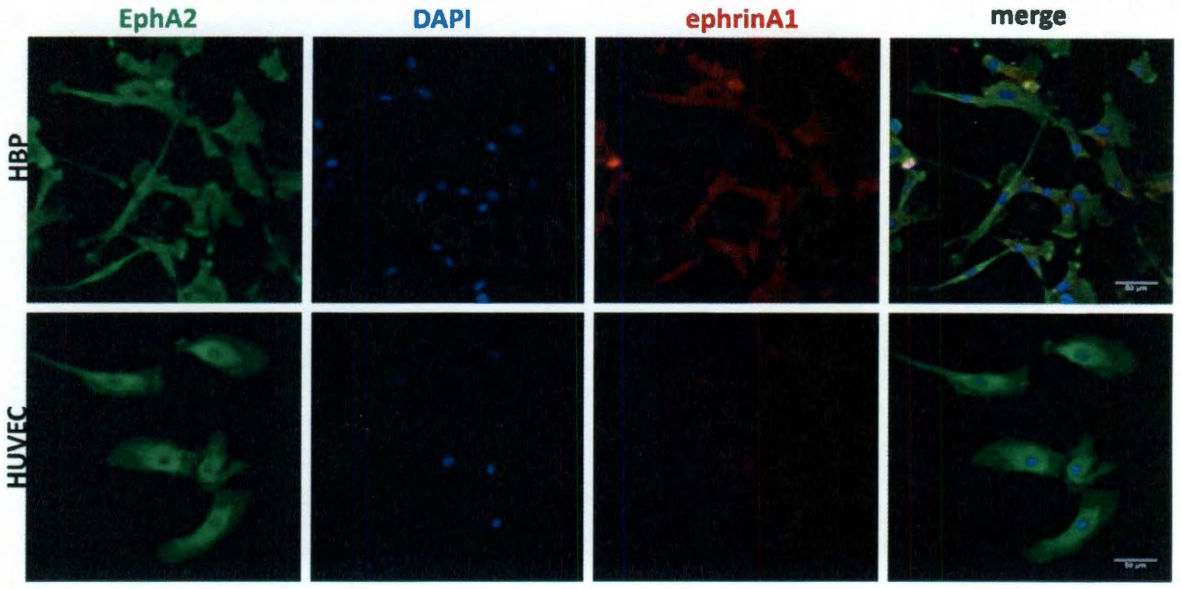

Figure 4-2: HBVP positively label for expression of EphA2 (green) and ephrinA1 (red) while HUVECs only express EphA2.

4.2.2 Seeding Cells on Modified Hydrogel Surfaces with Soluble EphA2

Hydrogel surfaces were modified as described in Chapter 2 with 50 mg/ml PEG-RGDS. 8.5 x 10^5 cells/cm^2 HUVEC and HBVP cells were seeded onto the modified surfaces at a ratio of 4:1 HUVEC:HBVP. Cells were seeded in media with 0, 500 ng/ml, 1500 ng/ml, or 5000 ng/ml soluble EphA2 (R&D Systems) based upon previously established effective levels of EphA2 (Dobrzanski et al., 2004). Six days after cell

seeding, hydrogels were imaged using an Axiovert (Zeiss) inverted fluorescence microscope. Hydrogel area and tubule length were quantified as described above.

4.2.3 PEG-ephrinA1 Synthesis

Acryloyl-PEG-succinimidyl carbonate (PEG-SMC) was synthesized in house in order to formulate a product that was capable of reacting in aqueous conditions, amenable for protein conjugations. Synthesis followed procedures previously outlined. (Leslie-Barbick et al., 2009)

EphrinA1 was obtained from R&D Systems (Minneapolis, MN) as a recombinant fusion protein containing the extracellular binding portion of ephrinA1 and the Fc fragment of human IgG. This protein, now referred to as ephrinA1, was reacted with in-house synthesized acryloyl-PEG-SMC to form PEG-ephrinA1 (Figure 4-2 A and B). 200 mM sodium bicarbonate buffer (pH 8.5) was used to dissolve synthesized acryloyl-PEG-SMC. The solution was sterile filtered (0.2 μm) and combined with ephrinA1 at a 1:100 molar ratio of ephrinA1:PEG-SMC. The reaction was placed on a rocker for four days at 4°C before lyophilization under sterile conditions. The PEG-ephrinA1 powder was reconstituted and stored in HEPES Buffered Saline (100 mM NaCl, 10 mM HEPES in deionized water; HBS; pH 7.4) for up to three months at 4°C. A western blot was used to confirm successful conjugation on a 4-15% Tris-HCL precast polyacrylamide gel (Biorad, Hercules, CA). The primary antibody used was anti-ephrinA1 produced in goat (Sigma, St. Louis, MO) with secondary antibody HRP-conjugated rabbit anti-goat IgG (Sigma). Using an ECL™ chemiluminescent western blotting analysis system (GE

Healthcare, Buckinghamshire, UK) images were taken on an LAS 4000 (FujiFilm, Little Rock, AK).

4.2.4 Surface Modification of Hydrogels with PEG-ephrinA1

6 kDa PEGDA hydrogels were synthesized by dissolving polymer (10% w/v) in HBS with 10 μl/ml acetophenone stock solution (300 mg acetophenone in 1 ml n-vinyl pyrrolidone (NVP)). Prepolymer solution was injected between glass slides separated by a 0.75 mm polytetrafluoroethylene spacer secured by binder clips. Hydrogels were crosslinked via exposure to UV light for 30 s and allowed to swell by soaking in HBS with 0.1% sodium azide.

Circular disks of diameter 5 mm were punched from the bulk hydrogels using a #2 biopsy punch. A solution containing 50 mg/ml PEG-RGDS and 10 μl/ml acetophenone stock solution with 0, 0.0392, 0.216, 0.392 μg PEG-ephrinA1 was added to the gel surface and exposed to UV light for 2 minutes to achieve conjugation. Hydrogels were soaked in sterile HBS before use. HUVECs (8.5×10^5 cells/cm^2) were seeded onto the modified surfaces and imaged using an Axiovert (Zeiss) inverted fluorescence microscope 2, 3, and 4 weeks after cell seeding. Images of the hydrogels were merged using Adobe Photoshop Elements, and modified surface area and tubule lengths were traced using Adobe Illustrator. Modified surface are and tubule lengths were quantified using ImageJ.

4.2.5 Endothelial Cell Encapsulation into Degradable Hydrogels

To delineate the effects of PEG-ephrinA1 on endothelial cells in 3D, HUVECs were encapsulated into MMP-sensitive hydrogels containing PEG-ephrinA1. Polymer solution was prepared with a final formulation of 10% PEG-PQ-PEG, 3.5 μmol/ml PEG-RGDS, 1.5% triethanolamine (v/v), 10 μl/ml eosin Y stock solution (10 mM Eosin Y in MilliQ H_2O), and 3.95 μl/ml NVP in 10 mM HBS. Three concentrations of PEG-ephrinA1 were used in combination with PEG-RGDS, including 0.25 ng/ml, 2.5 ng/ml, and 25 ng/ml. Hydrogels containing PEG-RGDS alone were used as a control group. Cells were harvested using trypsin-EDTA and counted using a Coulter counter. After counting, the cells were pelleted by centrifuging at 2700 RPM for 4 min and resuspended in polymer solution to a concentration of 10,000 cells/μl. Five μl droplets of cell-laden polymer were formed between a Sigmacoted (Sigma) glass slide and an acrylated coverglass spaced by a 380 nm strip of polydimethylsiloxane and exposed them to white light for 30 second. Hydrogels were immediately immersed in EGM-2 media.

4.2.6 Immunohistochemistry for Extracellular Matrix Proteins

To examine tubule morphology, immunohistochemistry was performed to identify tubule structure and extracellular matrix production. Gels were fixed in 4% paraformaldehyde for 20 min and washed with phosphate buffered saline (PBS). 0.5% Triton-X was used to permeabilized cells for 10 min followed by a second PBS wash. Hydrogels were blocked with 3% bovine serum albumin (BSA). Gels were incubated with a 1:100 dilution of rhodamine phalloidin (Invitrogen) with 2 μM DAPI in 1% BSA for 2 hrs. Images were obtained on a confocal microscope (Zeiss5 LIVE, Plan-

Apochromat 20x objective with 0.8 numerical aperture). To quantify resulting tubule formation using phalloidin stainin, Farsight was used to calculate the percent of each cell's borders that were shared with other cells (Roysam et al., 2008; Bjornsson et al., 2008).

To identify collagen IV and laminin production, 3% normal donkey serum (Sigma) was used as a blocking agent. Primary antibodies were diluted in 3% BSA in PBS and incubated over night at 4 °C on a rocker table. Primary antibodies included anti-collagen IV produced in rabbit (Abcam, Cambridge, MA) and anti-laminin produced in chicken (Sigma). Gels were rinsed five times in PBS for 1 h each time. Gels were incubated with a 1:500 dilution of Alexafluor 488 donkey anti-rabbit IgG (Invitrogen) or Alexafluor 488 goat anti-chicken IgG (Invitrogen) overnight at 4 °C in order to visualize the primary antibodies. PBS washing was repeated and gels were imaged using a confocal microscope. Alexafluor 488 pixel intensity in 3D projections of 20 μm in thickness with 1 μm in between slices were quantified in ImageJ and normalized to cell number using DAPI pixel intensity.

4.2.7 Hydrogel Implantation into the Mouse Cornea Angiogenesis Assay

Hydrogel preparation and implantation followed the protocol outlined in Poche *et al.* (Poche et al., 2009). Briefly, hydrogels were prepared to a 10% polymer weight percentage of degradable PEG-PQ-PEG, 3.5 μmol/ml PEG-RGDS, 10 μl/ml acetophenone stock solution, and 160 ng soluble platelet derived growth factor BB per gel with or without 1.6 ng PEG-ephrinA1 per gel (n=5 and 6, respectively). Images of

vessels on the hydrogel were compiled from projections of z-stacks exactly 22 μm in thickness, spaced 1.1 μm apart.

Confocal z-stacks were used to quantify vessel parameters. Vessel branch points and diameters were quantified using the image browser in the LSM software. Fractal dimension, lacunarity, and vessel density were quantified as previously described (Gould et al., 2011). The fractal dimension was quantified to describe the complexity of the vessel network and lacunarity to examine nonuniformity of cell distribution in a scale-invariant manner (Mandelbrot, 1982; Lopes et al., 2009).

4.2.8 Statistics

Two-way ANOVA and subsequent Tukey's Least Significant Difference (LSD) tests were used to statistically analyze vessel formation and extracellular matrix production. For each analysis, $p<0.05$ was considered significant.

4.3 Results

4.3.1 Soluble EphA2 Downregulates PEG-ephrinA1-induced Tubule Formation

To investigate the role of the EphA2-ephrinA1 interaction in tubule formation, soluble EphA2 was used to inhibit PEG-ephrinA1 induced tubule formation. A co-culture of HUVEC and HBVP was used since it has previously been shown to form tubule networks (Stratman et al., 2010). Six days after cell seeding, the co-culture of HUVEC and HBVP exhibited a reduction in tubule formation dependent upon dose of soluble EphA2 (Figure 4-3; $p<0.05$), confirming the importance of the EphA2-ephrinA1 interaction in tubule formation.

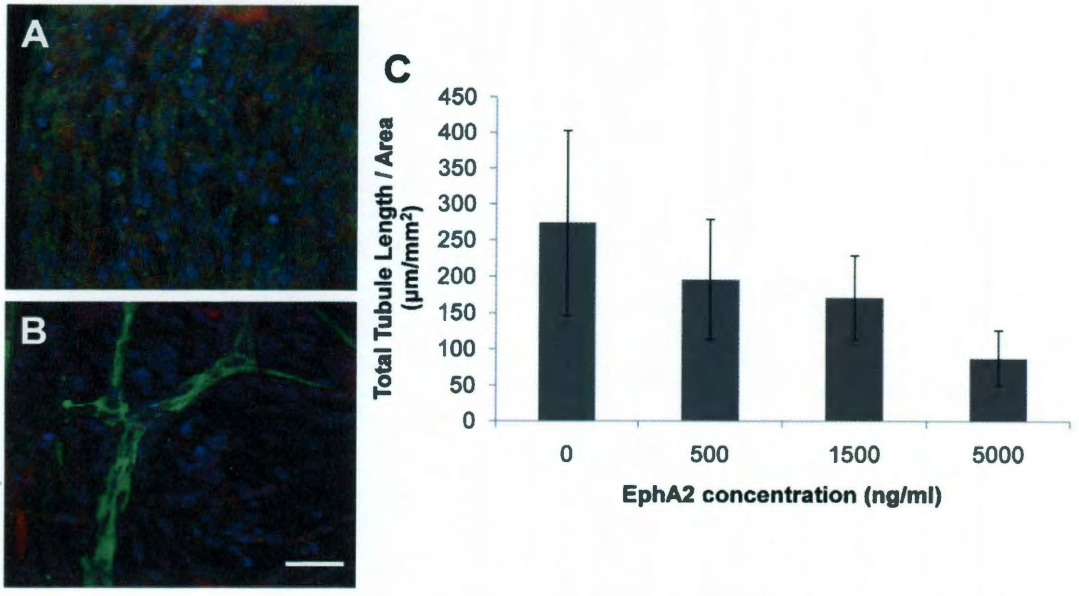

Figure 4-3: Soluble EphA2 confirms the role of EphA2-ephrinA1 in tubule formation. CD31-labeled vessels (green) are visible only in the lowest dose of 500 ng/ml EphA2 (B) while no vessels are visible in the highest dose of 5000 ng/ml EphA2 (A; nuclei=blue, α- smooth muscle actin=red; scale bar= 50 μm). Disruption of the EphA2-ephrinA1 interaction between the cells via soluble EphA2 in the media induced a dose dependent decrease in tubule formation between HBVP and HUVECs (C). All dose pairings exhibit statistical significance except 1500 and 500 ng/ml ($p<0.05$).

4.3.2 Polymer Characterization

PEG-ephrinA1 was synthesized by reacting acrylol-PEG-succinimidyl carbonate (Figure 4-4 A) with the primary amines of ephrinA1 to form a conjugated biomolecule (Figure 4-4 B). Successful conjugation of acrylyl-PEG-SCM to ephrinA1 was confirmed using a western blot where the increase in molecular weight confirms conjugations of PEG chains to ephrinA1 (Figure 4-4 C).

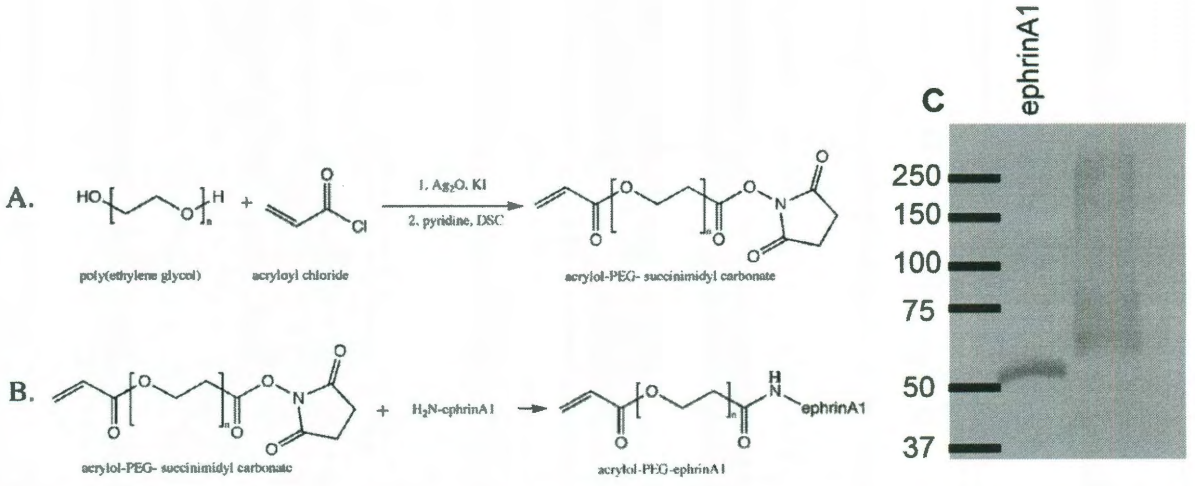

Figure 4-4: Successful conjugation of ephrinA1. Immobilized ephrinA1 was synthesized by reacting acrylol-PEG-succinimidyl carbonate (A) with primary amines on ephrinA1 (B). Successful conjugation of PEG to ephrinA1 was confirmed with a western blot where an increase in molecular weight is visualized via the addition of PEG chains to the protein (C).

4.3.3 HUVEC Tubule Formation on Hydrogel Surfaces Modified with PEG-ephrinA1

HUVECs seeded onto surfaces modified with three concentrations of PEG-ephrinA1 exhibited robust tubule formation with branching networks. Using a two way ANOVA and Bonferroni post hoc analysis, a significant effect of the PEG-ephrinA1 concentration was observed (Figure 4-5, $p<<0.001$). As early as 14 days, a direct relationship existed between the concentration of PEG-ephrinA1 and tubule formation with a significant difference between the highest concentration of 0.392 μg and both 0 and 0.039 μg ($p<0.05$). Prolonged ephrinA1 signaling via immobilization onto the surface maintained tubule formation, especially for the highest concentration of PEG-ephrinA1.

A significant difference between the control group and both 0.216 and 0.392 μg PEG-ephrinA1 groups confirms the concentration affect ($p<0.05$).

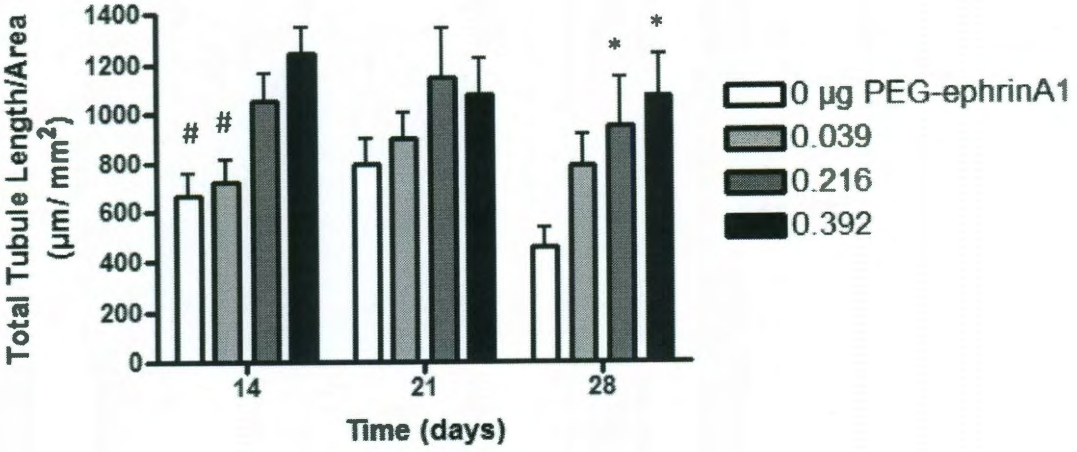

Figure 4-5: HUVECs seeded onto surfaces modified with PEG-ephrinA1 exhibited robust tubule formation where PEG-ephrinA1 concentration had a significant effect ($p<<0.05$). As early as 14 days, the 0.392 μg PEG-ephrinA1 induces significantly more tubule formation when compared to 0 and 0.039 μg (#, $p<0.05$). By 28 days, the presence of PEG-ephrinA1 maintains tubule formation, and a significant difference is visible between the control and both 0.216 and 0.392 μg PEG-ephrinA1 (*, $p<0.05$).

4.3.4 Encapsulated HUVECs with PEG-ephrinA1 form tubule networks

HUVECs encapsulated in degradable hydrogels with PEG-ephrinA1 formed tubule networks, visualized from 6 hours to 7 days via staining for actin and nuclei. Three different concentrations of PEG-ephrinA1 were used, including 0.25, 2.5, and 25 ng/ml and compared to the presence of no PEG-ephrinA1 (Figure 4-6). At early timepoints including 24 and 48 hours, the low concentration of 0.25 ng/ml PEG-ephrinA1 induced the most tubule formation. However, by 5 and 7 days, the highest concentration of 25

ng/ml PEG-ephrinA1 induced robust tubule formation. In order to quantify tubule formation, the percentage of shared borders was calculated for all cells. Using a two way ANOVA, the concentration of PEG-ephrinA1, the time elapsed, and the interaction between the concentration and time were found to affect HUVEC tubule formation. Using a Bonferroni post hoc test, individual comparisons were made. For example, the low concentration of 0.25 ng/ml PEG-ephrinA1 was significantly different from all other treatments at 24 hours ($p<0.05$). This finding corresponds to the images, which clearly show tubule formation only in the low concentration. By 7 days, the control with no PEG-ephrinA1 was statistically significant from all concentrations of PEG-ephrinA1.

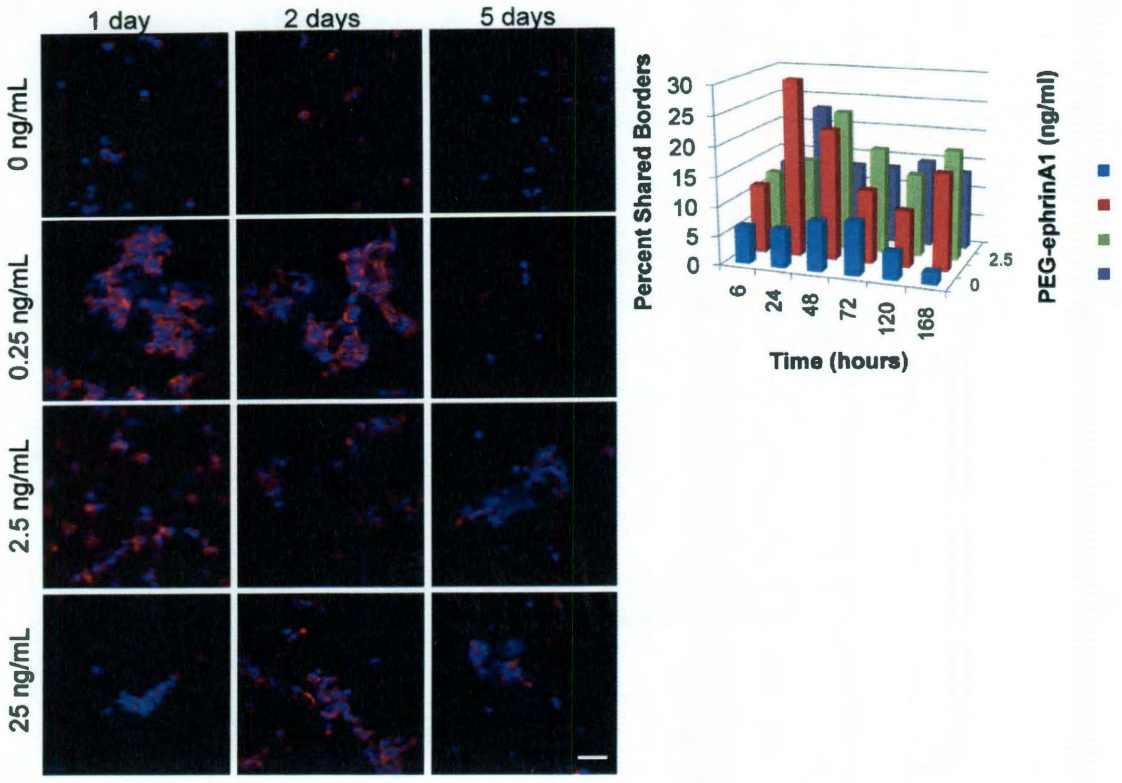

Figure 4-6: PEG-ephrinA1 enhances 3D tubule formation. HUVEC tubule formation in 3D degradable hydrogels with 0, 0.25, 2.5, or 25 ng/ml PEG-ephrinA1 was visualized with staining for nuclei (blue) and actin filaments (red; scale bar= 50 μm; 3D projects of 20 μm with 1 μm in between slices). Robust tubule formation was seen as early as 24 hours with 0.25 ng/ml PEG-ephrinA1; however, tubule formation at this lower concentration of PEG-ephrinA1 regressed by 5 days. More robust long term tubule formation was visualized with 25 ng/ml PEG-ephrinA1, seen at 2 and 5 days. In order to quantify the resulting tubule formation, the parameter percent shared borders was calculated to examine the percentage of each cell's edges that were interacting with other cells to form tubule networks. As the graph corresponds to the images, robust tubule formation was seen at early timepoints using low PEG-ephrinA1 concentrations and at late timepoints using higher PEG-ephrinA1 concentrations. A two-way ANOVA shows a significant effect of PEG-ephrinA1 concentration and time. Additional images are available in the supplemental material.

4.3.5 Collagen IV and Laminin Expression by Tubule Networks

Immunohistochemistry was performed to investigate the role of extracellular matrix production, specifically collagen IV and laminin, production in tubule formation and stabilization. In order to allow time for collagen IV and laminin synthesis and deposition, staining began with the 2 day timepoint. The peak fluorescence intensities of the collagen IV graph were found to correspond to visually identified areas of high tubule formation (Figure 4-7). Specifically, 0.25 ng/ml PEG-ephrinA1 at 2 days and 25 ng/ml PEG-ephrinA1 at 7 days showed the highest expression (Figure 4-7). Laminin deposition was found to be dependent upon PEG-ephrinA1 concentration and time ($p<0.05$) with laminin deposition increasing over time (Figure 4-8). For example, laminin expression increased as more PEG-ephrinA1 was included at both 5 and 7 days, confirming the dependence upon PEG-ephrinA1 concentration (Figure 4-8). Looking specifically at images of 0.25 and 2.5 ng/ml, the increase in pixel intensity from 5 to 7 days is also clearly visible, highlighting the dependence upon time.

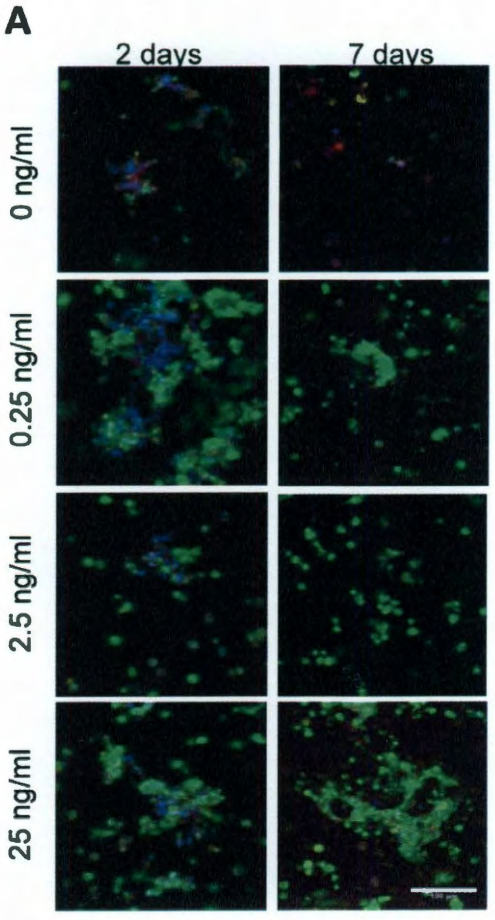

Figure 4-7: Collagen IV deposition is affected by PEG-ephrinA1 concentration. Collagen IV deposition (green) in addition to nuclei (blue) illustrated the effect of PEG-ephrinA1 concentration of collagen IV deposition, where areas of high tubule formation correspond to areas of high collagen IV deposition. This effects is noticeable at 2 days using the 0.25 ng/ml PEG-ephrinA1 concentration as well as the 7 days 25 ng/ml PEG-ephrinA1 concentration (Scale bar = 100 μm).

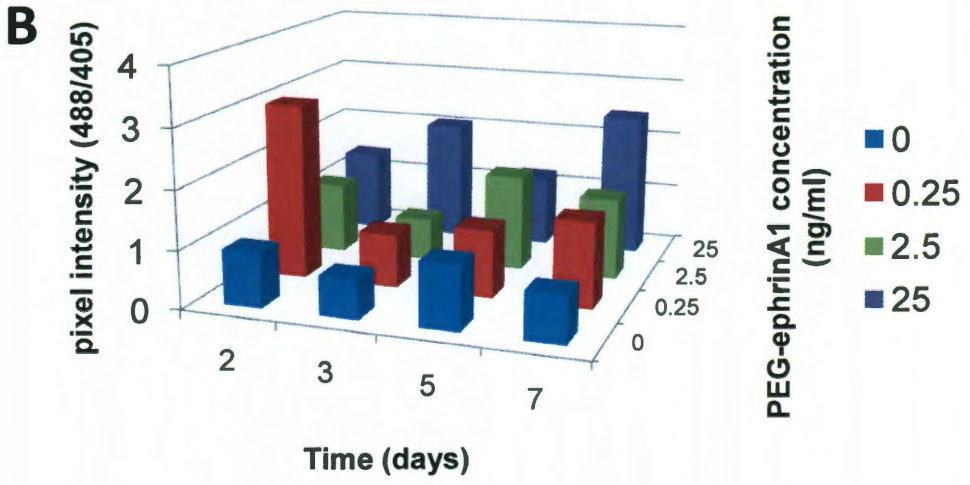

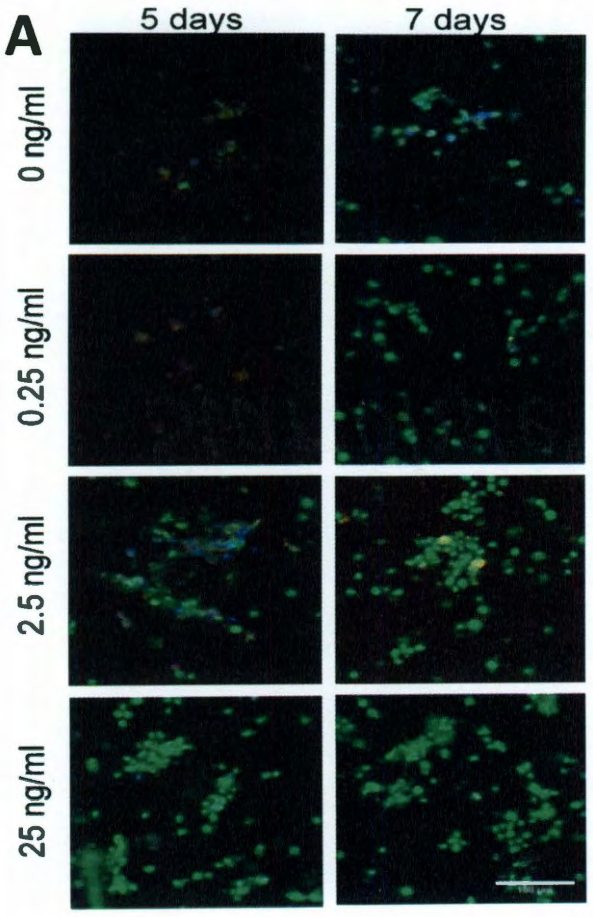

Figure 4-8: Laminin deposition is dependent upon PEG-ephrinA1 concentration. Laminin deposition (green) in addition to nuclei (blue) was shown to be dependent upon both PEG-ephrinA1 concentration and time (scale bar= 100 μm) (B). For example, at 5 days, 25 ng/ml PEG-ephrinA1 expresses the most laminin and laminin deposition decreases with PEG-ephrinA1 dose (A). The effects of time are visible in 2.5 ng/ml PEG-ephrinA1 where there is a notable increase in laminin deposition.

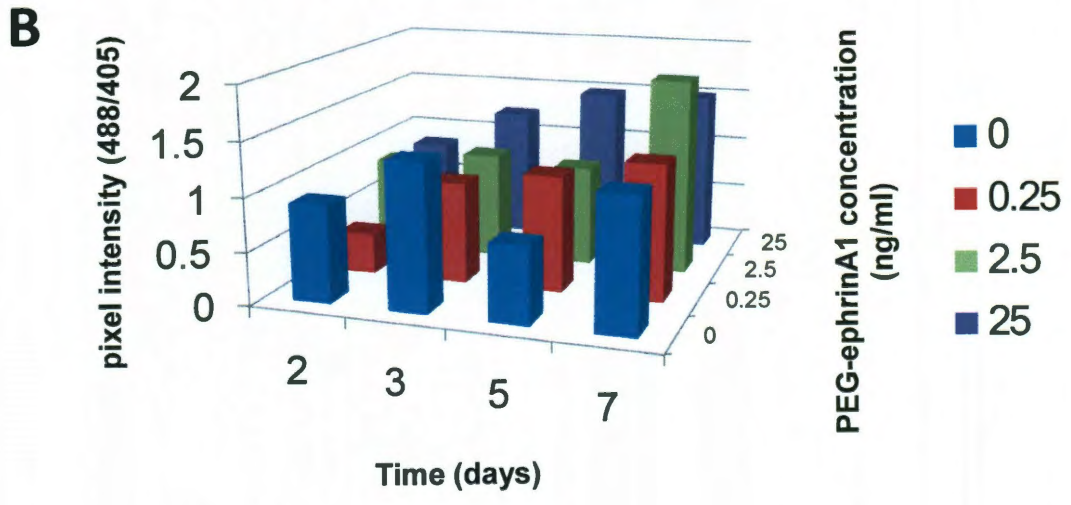

4.3.6 PEG-ephrinA1 Enhances the *In vivo* Vascular Response

Hydrogels were implanted into the mouse cornea micropocket to investigate the impact of PEG-ephrinA1 *in vivo*. The mouse cornea micropocket facilitates image analysis of angiogenesis, using an established and reproducible assay. Using the *Flk1-myr::mCherry* transgenic mouse, soluble PDGF was used to stimulate fluorescently labeled angiogenic processes to grow onto the gel from the surrounding limbus. The addition of immobilized ephrinA1 allowed prolonged signaling once the vessels had reached the hydrogel, resulting in a very different vascular morphology in response to PEG-ephrinA1 (Figure 4-9B) as compared to no PEG-ephrinA1 (Figure 4-9A). Fourteen days after implantation, this vascular morphology was quantified, resulting in a significant increase ($p<0.05$) in vessel density (Figure 4-9C) and vessel branch points (Figure 4-9D) with the addition of PEG-ephrinA1. Additionally, space filling parameters were also used to quantify vessel morphology (Gould et al., 2011). The addition of PEG-ephrinA1 significantly increased both ($p<0.05$) fractal dimension (E) and lacunarity (F), indicating a greater complexity among the vessel networks where immobilized PEG-ephrinA1 was included. Interestingly, PEG-ephrinA1 induced smaller diameter vessels.

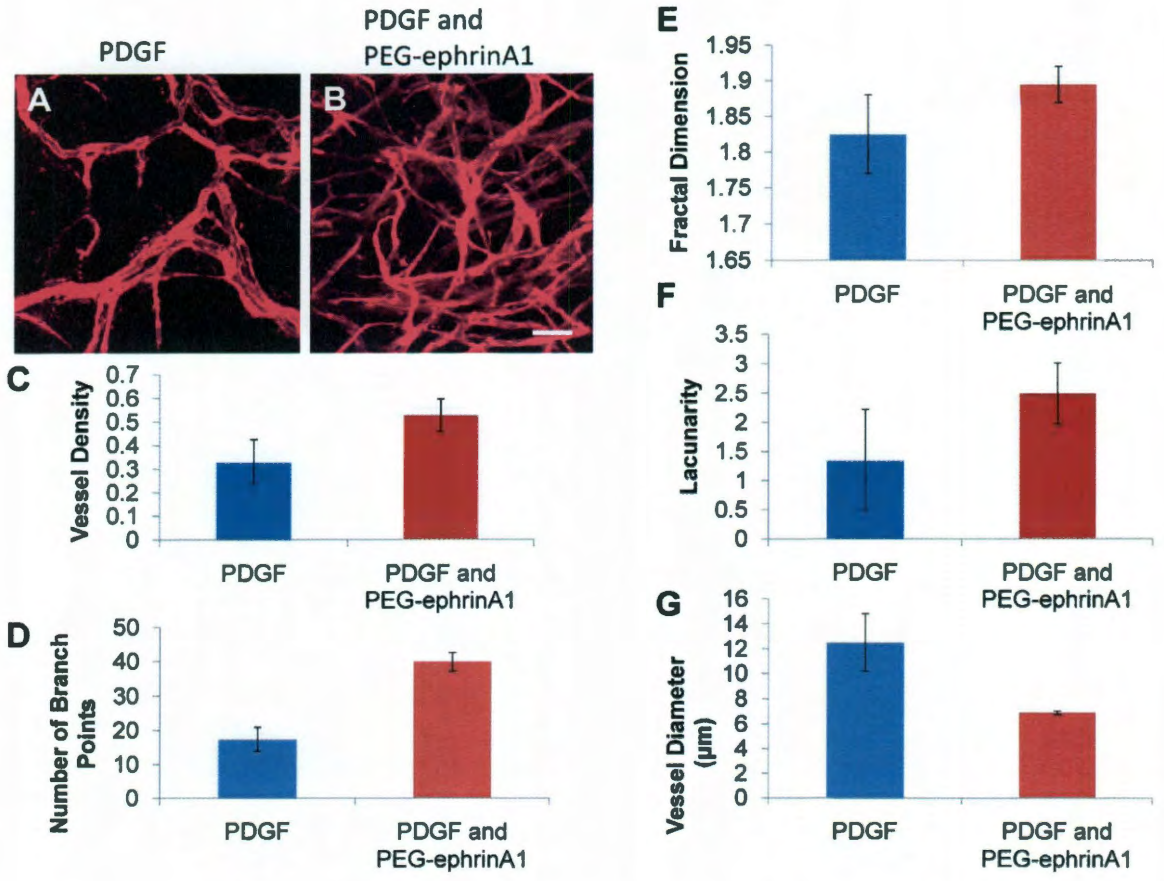

Figure 4-9: Immobilized ephrinA1 enhances the in vivo vascular response. Bioactive hydrogels incorporating releasable PDGF and PEG-ephrinA1 (B) showed a more robust vascular response than hydrogels with releasable PDGF alone (A) when implanted into the mouse cornea. The presence of PEG-ephrinA1 induced a significant increase in vessel density (C), branch points (D) fractal dimension (E), and lacunarity (F). PEG-ephrinA1 also stimulated a significant decrease in vessel diameter.

4.4 Discussion

Rapid vessel formation and perfusion is key to the survival of implanted cells (Hegen et al., 2010; Laschke et al., 2006). While stable vessels have been formed in engineered constructs using multiple cell types (Chen et al., 2008; Koike et al., 2004), the

use of PEG-ephrinA1 removes the necessity for a supportive cell type. Exploiting the cell-cell interactions for vessel development offers an alternative approach for forming long-lasting stable tubule structures in engineered constructs (Jain et al., 2005; Francis et al., 2008). Specifically, an immobilized ephrinA1 has been used to induce tubule formation for its ability to influence endothelial cell migration and invasion. In 2D, immobilized ephrinA1 lead to prolonged tubule formation and branching networks for 4 weeks after cell seeding. In 3D degradable scaffolds, PEG-ephrinA1 induced HUVEC tubule formation as early as 24 hours with persistent tubules up to 7 days. The dose of PEG-ephrinA1 incorporated into the scaffold can also be tailored based on the specific application.

The mechanism by which ephrinA1 stabilizes tubule formation may be basement membrane production, including laminin and collagen IV, as the basement membrane connects cells to the interstitial matrix and is necessary for tissue development and vessel stabilization (Kruegel et al., 2010). Samples were stained for the deposition of laminin and collagen IV to determine vessel stabilization via basement membrane formation, and laminin deposition was found to be statistically dependent upon PEG-ephrinA1 concentration and time while collagen IV deposition was found to be dependent upon PEG-ephrinA1 concentration. While laminin deposition indicates vessel maturation (Risau et al., 1988), collagen IV is largely responsible for the mechanical properties of the basement membrane (Kruegel et al., 2010). Laminins are critical in regulating cell adhesion, migration, and matrix-mediated signaling (Hamill et al., 2009) via interacting with their integrin receptors. Similarly, endothelial cell binding to collagen IV is mediated by integrins, and is necessary for cell adhesion, migration, and proliferation

(Khoshnoodi et al., 2008). Interestingly, cell binding to both laminin and collagen IV is regulated by $\alpha_v\beta_3$ integrins, which is the same integrin that was shown induce endothelial cell adhesion in response to immobilized ephrinA1 (Durbeej, 2010; Moon et al., 2007). The link between ephrinA1 and laminin production has been previously established in tumor formation as ephrinA1 and EphA2 play a role in tumor neovascularization, enabling tumor growth (Ogawa et al., 2000). Heptocellular carcinoma cell lines that overexpressed ephrinA1 also increased expression of laminin (Iida et al., 2005), and aggressive melanoma cells have also been found to overexpress EphA2 and laminin (Hendrix et al., 2003).

To confirm the role of the EphA2-ephrinA1 interaction in tubule formation, soluble EphA2-Fc was used to prevent EphA2-ephrinA1 interaction between HUVECs and HBVP cells (Figure 4-3). Soluble EphA2-Fc was found to decrease tubule formation on modified hydrogel surfaces in a dose dependent manner. Similar findings have been illustrated when soluble EphA2-Fc inhibited vessel formation in two *in vitro* assays in a dose dependent manner (Dobrzanski et al., 2004). Soluble EphA2 has also been targeted in cancer therapy, where delivery of soluble EphA2 receptors inhibited tumor angiogenesis and disease progression (Cheng et al., 2003).

The presence of PEG-ephrinA1 in *in vivo* hydrogel implants in the mouse cornea induced vessel coverage of the hydrogel with an increase in vessel density and branch points but a decrease in vessel diameter. This phenomenon has been illustrated previously when Lee et al. generated an MMP-resistant form of vascular endothelial growth factor and these MMP-resistant VEGF tumors displayed an increase in branch points but decrease in diameter (Lee et al., 2005). Vessel remodeling involves alterations to

cytoskeletal organization, extracellular matrix composition, and cell-cell connections to stabilize vessels. Inhibition of $\alpha_v\beta_3$ integrins has been shown to prevent remodeling, and $\alpha_v\beta_3$ integrin binding is likely involved in determining vascular diameter (Martinez-Lemus et al., 2009; Iruela-Arispe et al., 2009). Smooth muscle cell recruitment during vessel stabilization has also been linked to the $\alpha_v\beta_3$ integrin receptor, and may be an area for future investigation (Bendeck et al., 2000). Interestingly, embroid bodies lacking laminin γ1 displayed an increase in lumen size, consistent with findings in laminin α4 deficient mice (Jakobsson et al., 2008). The increase in lumen is possibly due to a weakening of the vessel wall or because laminin-rich basement membrane is important in polarization of endothelial cells, which is required for lumen formation.

4.5 Conclusion

The formation of a microvascular system is highly regulated by cell-cell interactions for capillary sprouting and remodeling. An immobilized ephrinA1 was used to exploit the cell signaling interaction of EphA2 and ephrinA1 seen in angiogenesis. PEG-ephrinA1 was then shown to induce HUVEC tubule formation on surfaces modified with PEG-ephrinA1 as well as in 3D degradable hydrogels in a dose dependent manner. Collagen IV and laminin, extracellular matrix proteins involved in vessel stabilization, production was also found to be dependent upon PEG-ephrinA1 concentration. The presence of soluble EphA2 prevented EphA2-ephrinA1 interactions between HUVEC and HBVP cells, reducing tubule formation in a dose dependent manner while confirming the importance of ephrinA1 in tubule formation. Finally, hydrogels incorporating PEG-

ephrinA1 *in vivo* resulted in vessels with a statistically significant increase in vessel density, branch points, lacunarity, and fractal dimension. The results presented demonstrate the utility of an immobilized cell adhesion and patterning molecule ephrinA1 in inducing microvascular network formation for use in tissue engineered constructs for applications in regenerative medicine.

Chapter 5: Encapsulated Cells Anastomose to Host Vasculature

A significant portion of this chapter is from JE Saik and DJ Gould, ME Dickinson and JL West. "Building Vascular Bridges: Advances in Tissue Engineering." *Nature Biotechnology.* Submitted 2011

5.1 Introduction

The formation of stable and functional vessels in replacement tissues remains a tremendous challenge, and a deeper understanding of functional vessels is necessary to further tissue engineering, vessel biology, and cancer. Vascularized tissue constructs have a wide variety of applications in the replacement of damaged or diseased tissues including peripheral limb ischemia and chronic diabetic wounds. While many approaches utilize potent growth factors to induce angiogensis, an alternative employs cells themselves to recruit vessels via naturally secreted chemokines. Cell-based approaches eliminate the time-delay inherent in recruiting host vessels into the biomaterial and reduce the necessary concentration of potent growth factors.

For example, Chen et al. allowed a co-culture of human umbilical vein endothelial cells (HUVECs) and fibroblasts to form tubes *in vitro* for seven days before *in vivo* implantation. Scaffolds containing pre-formed tubes led to anastamosis with the host vasculature within 5 days as compared to 14 days for scaffolds without pre-formed tubes. Additionally, the number and area of perfused lumens was significantly higher in prevascularized scaffolds (Chen et al., 2008). Koike et al. formed long-term stable vessels when HUVECs were used alone and in combination with pericyte precursor cells (10T1/2) on a fibronectin-type I collagen matrix (Koike et al., 2004). HUVECs alone

formed vessels with minimal perfusion, but HUVECs and 10T1/2 cells formed a functional vascular network capable of anatosmosing with host circulatory system up to one year later (Au et al., 2007). When HUVECs were cocultured with 10T1/2 cells, 10T1/2 cells displayed a smooth muscle cell morphology and began expressing pericyte markers, such as α-smooth muscle actin, smooth muscle myosin, and calponin (Hirschi et al., 1998).

Cellular response has been enhanced with the addition of growth factors. Lower doses of growth factors than currently used in clinical trials can be used to act upon the transplanted vessel-forming cells, promoting survival, proliferation, and differentiation. Peters et al. showed that functional vessels were formed after seven days when human microvascular endothelial cells were seeded with VEGF in PLG (Peters et al., 2002). The combination of dermal fibroblasts and HUVECs showed significantly more capillary formation in response to FGF-2 and VEGF (Hudon et al., 2003). Frerich et al. enhanced capillary formation by combining two cell types, HUVECs and stromal cells from adipose tissue, along with two growth factors, VEGF to stimulate angiogenesis and insulin-like growth factor (IGF)-1, to stabilize the capillary structures (Frerich et al., 2001).

In the thesis research, cell-laden hydrogels were evaluated using a mouse cornea micropocket angiogenesis assay (Poche et al., 2010; Moon, Saik, Poche et al., 2010), a reproducible and quantifiable assay in a normally avascular tissue (Kenyon et al., 1996). Flk1-myr::mCherry transgenic mice were utilized, which display endothelial specific fluorescence to enable imaging of capillary invasion (Poche et al., 2009). This thesis research improved upon existing research by reducing the *in vitro* incubation time before

in vivo implantation, making the research more clinically applicable. Additionally, sites of anastomosis were identified as early as 24 hours after implantation, earlier than any other reports in the literature. Finally, most of the cell form tubes contained red blood cells, confirming their connection to the host vasculature. This system can be used to further probe the process of anastomosis to identify precise locations and timepoints.

5.2 Materials and Methods

5.2.1 Cellular Encapsulation

To confirm that a co-culture of encapsulated cells forms tubules networks in response to growth factors, HUVEC and 10T1/2 cells at a 4:1 ratio were incorporated into hydrogels at a concentration of 30,000 cells/μl. Cells were centrifuged at 2700 RPM for 4 min and resuspended in polymer solution containing 10% PEG-PQ-PEG, 3.5 μmol/ml PEG-RGDS, 10 μmol eosin Y, and 3.5 μl/ml NVP. Hydrogels were exposed to white light for 30 sec and immediately immersed in EGM-2 media. Four days later, cells were fixed with 4% formaldehyde, permeabilized with 0.5% Triton X-100, and blocked with 1% bovine serum albumin. Cells were then incubated with a 1:20 dilution of rhodamine phalloidin (Invitrogen) in 300 nM DAPI for 2 h. Hydrogels were imaged on a confocal microscope (Zeiss5 LIVE, Plan-Apochromat 20x objective with 0.8 numerical aperture, for rhodamine: excitation = 532nm, emission BP filter = 560-675 nm, for DAPI: excitation = 405 nm, emission BP filter = 415-480 nm).

5.2.2 Encapsulated Cell Implantation into the Mouse Cornea

Poly(ethylene glycol) (PEG) based hydrogels comprised of a biocompatible polymer with tunable mechanical properties (Hahn et al., 2007) were used to encapsulate a co-culture of bEnd.3 endothelial cells and 10T1/2 pericyte precursors under mild photocrosslinking conditions. Gels with individual cell types were also crosslinked as controls. PEG-based hydrogels, normally resistant to protein adsorption and cellular adhesion, were cross-linked with immobilized fibronectin-derived peptide RGDS to enable cell adhesion. Hydrogels were rendered biodegradable by incorporating a matrix metalloproteinase-sensitive peptide into the polymer backbone (West et al., 1999). Encapsulated cells were allowed to culture for 48 hours before implantation. Prior to implanting the tubule containing constructs, mouse corneas were prevascularized by implanting hydrogels containing 320 ng of soluble platelet-derived growth factor-BB and 80 ng fibroblast growth factor-2 which induced robust angiogenesis toward the hydrogel. Two weeks later, the growth factor implants were surgically excised (Figure 5-1). Cell-laden implants were soaked in media containing 12 mol/ml PDGF for 2 hours before being implanted into the pre-vascularized cornea. Corneas were examined for anastomosis and perfusion one day and three days after implantation using confocal microscopy.

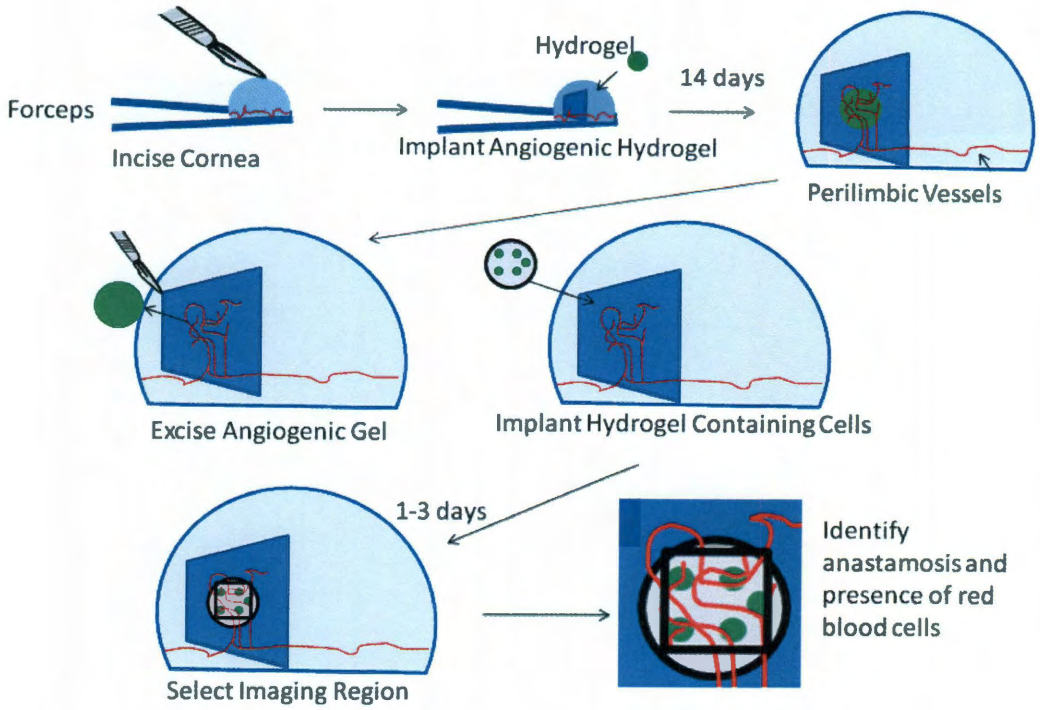

Figure 5-1: Protocol for Implanting Encapsulated Cells. A hydrogel containing soluble growth factors was implanted in a mouse cornea micropocket. 14 days after implantation, the angiogenic hydrogel was excised and replaced with a cell-laden hydrogel. 1-3 days after implantation, the hydrogel was examined for anastomosis between cell formed tubules and host vasculature and the presence of red blood cells in tubule networks.

5.2.3 Viability Staining and Tubule Formation of Encapsulated Cells

At the time of implantation, some gels were stained to determine cell viability and tubule formation. Cell viability was assessed using a LIVE/DEAD Viability/Cytotoxicity kit for mammalian cells (Invitrogen, Carlsbad, California). Media was removed from cells and replaced with phosphate buffered saline (PBS, Sigma) solution containing 2 μM calcein AM (ex/em: 495 nm/515 nm) and 4 μM ethidium homodimer (ex/em: 495

nm/635 nm). Cells with LIVE/DEAD solution were incubated at 37°C and 5% CO_2 for 30 minutes before imaging with a 5LIVE confocal microscope.

Tubule structures were visualized by staining nuclei with DAPI and actin with phalloidin. Hydrogels were incubated in 4% formaldehyde for 20 minutes and rinsed with PBS three times. Gels were incubated with a 0.5% Triton X solution for 30 minutes and rinsed three times again. A 1% bovine serum albumin (BSA) solution was placed on the gels for 40 minutes followed by a rinsing step. A 1:100 dilution of rhodamine-phalloidin was incubated on the gel overnight. After rinsing, a 1:100 dilution of DAPI was incubated on the gels for one hour followed by rinsing and visualization under fluorescence microscopy.

5.3 Results

5.3.1 Encapsulated Cells form Tubule Networks

Hydrogels containing encapsulated endothelial cells and mouse pericyte precursor cells demonstrate the bioactive efficacy of these releasable angiogenic growth factors. Hydrogels containing either VEGF, PDGF, or FGF induced encapsulated cells to initiate tubule formation as early four days after encapsulation; whereas, hydrogels without growth factors did not exhibit this response (Figure 5-2). This finding is supported by previous work, which exhibited the effects of angiogenic factor release and further supports the development of a tunable system for delivery. For example, VEGF release from PLGA/PEG microspheres increased HUVEC proliferation (King et al., 2000), FGF release from poly(ester urethane) urea scaffolds induced more smooth muscle cell

mitogenicity (Guan et al., 2007), and PDGF release from PLGA microspheres resulted in increased blood vessel number in an *in vivo* soft tissue wound repair model (Jin et al., 2008).

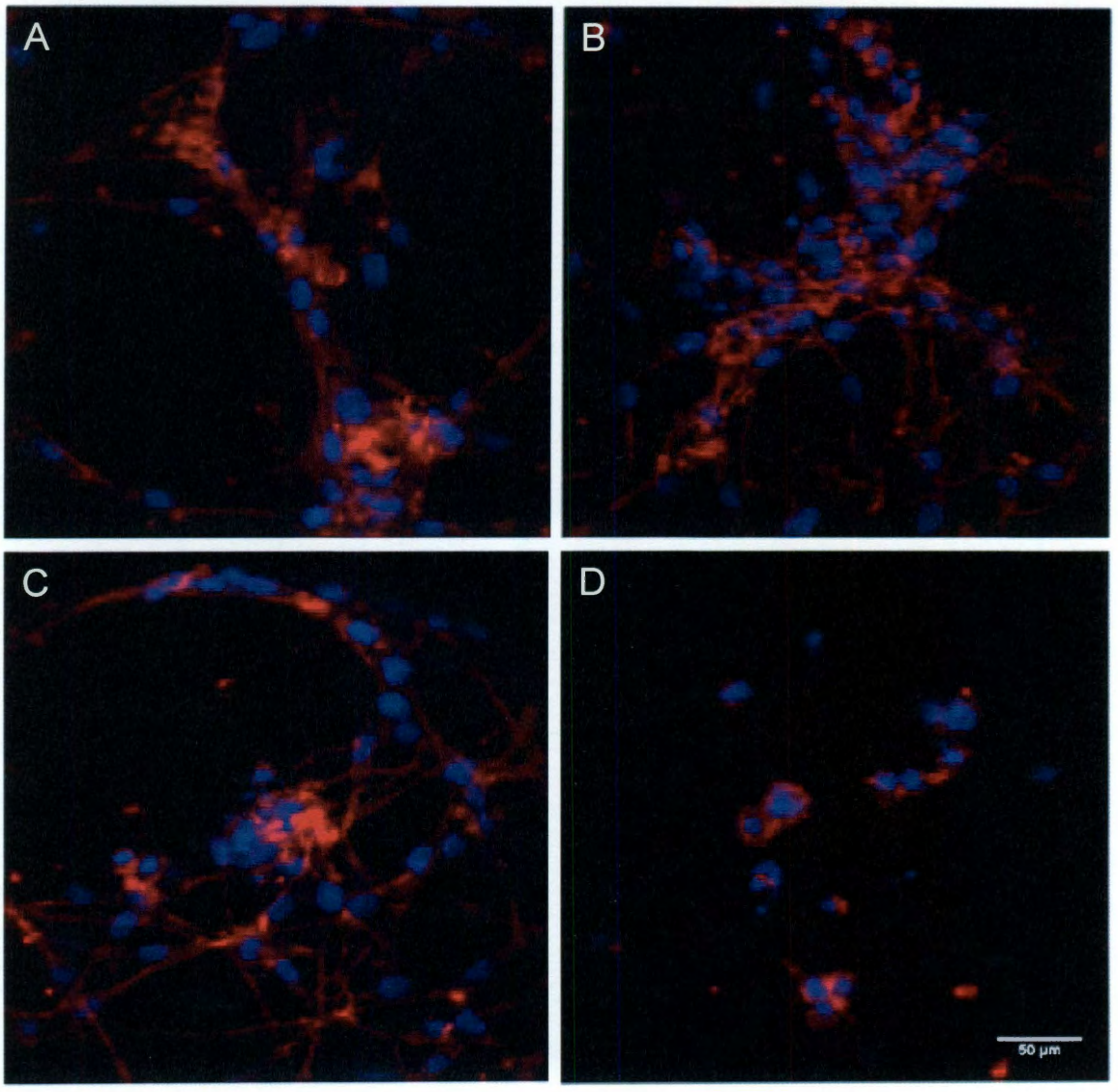

Figure 5-2: Encapsulated cells form tubule networks. Endothelial cells and pericyte precursor cells were encapsulated into degradable hydrogels with VEGF (A) PDGF (B), FGF (C), and no growth factor (D). In the presence of growth factors, tubules are visible after four days in culture, suggesting the utility of releasable growth factors in PEG hydrogels to initiate a desired biological response.

5.3.2 Encapsulated Cells Exhibit High Viability

Using the co-culture of bEnd.3 and 10T1/2 cells, staining confirmed high viability of 82% $\pm$ 1.5%. Extensive tubule formation with branching, cell-cell interconnections, and network formation was visualized via actin staining (Figure 5-3).

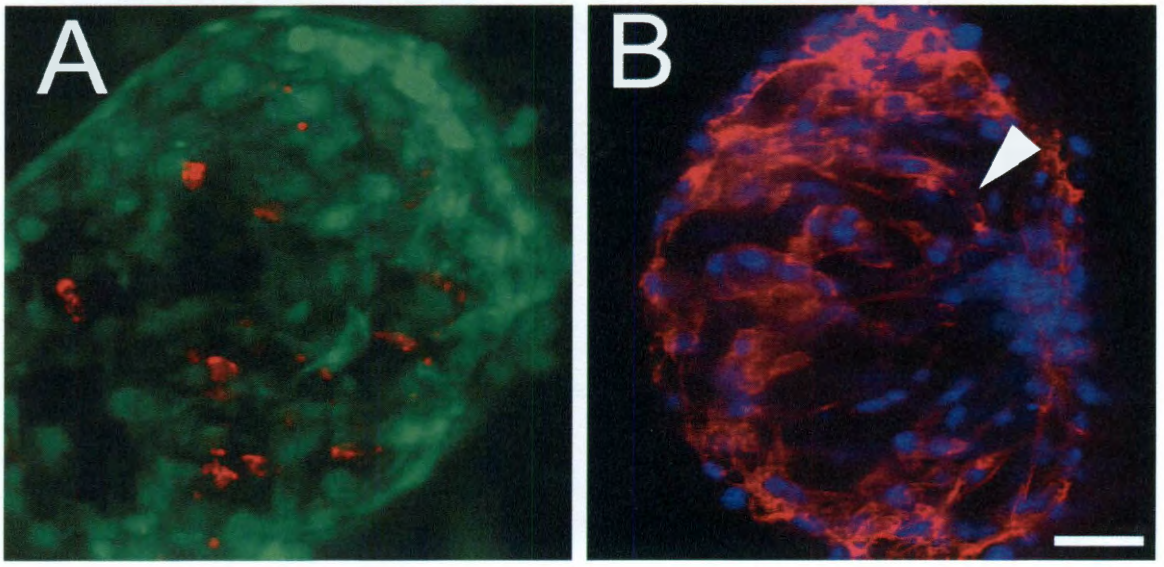

Figure 5-3: Encapsulated cells display high viability and robust tubule formation *in vitro*. A co-culture of bEnd.3 and 10T1/2 cells at a 4:1 ratio in matrix metalloproteinase-sensitive PEG-based hydrogels demonstrate 82% $\pm$ 1.5% viability (A, green= live; red = dead) after culturing for 48 hours. B) Cells also form robust tubules (arrow) as visualized via actin (red) and nuclei (blue) staining. The white arrow highlights an example of a tubule with interconnecting cells. Scale bar = 50 μm.

Additionally, each cell type was encapsulated individually to look for differences in cell viability. High cell viability was equally maintained for both cell types. Individual cell types were also examined for their ability to form tubule networks. 10T1/2 cells alone remained balled without elongating or forming networks. bEnd.3 cells elongated and formed cell-cell connections, but did not form robust tubule networks as seen in the co-culture of cells.

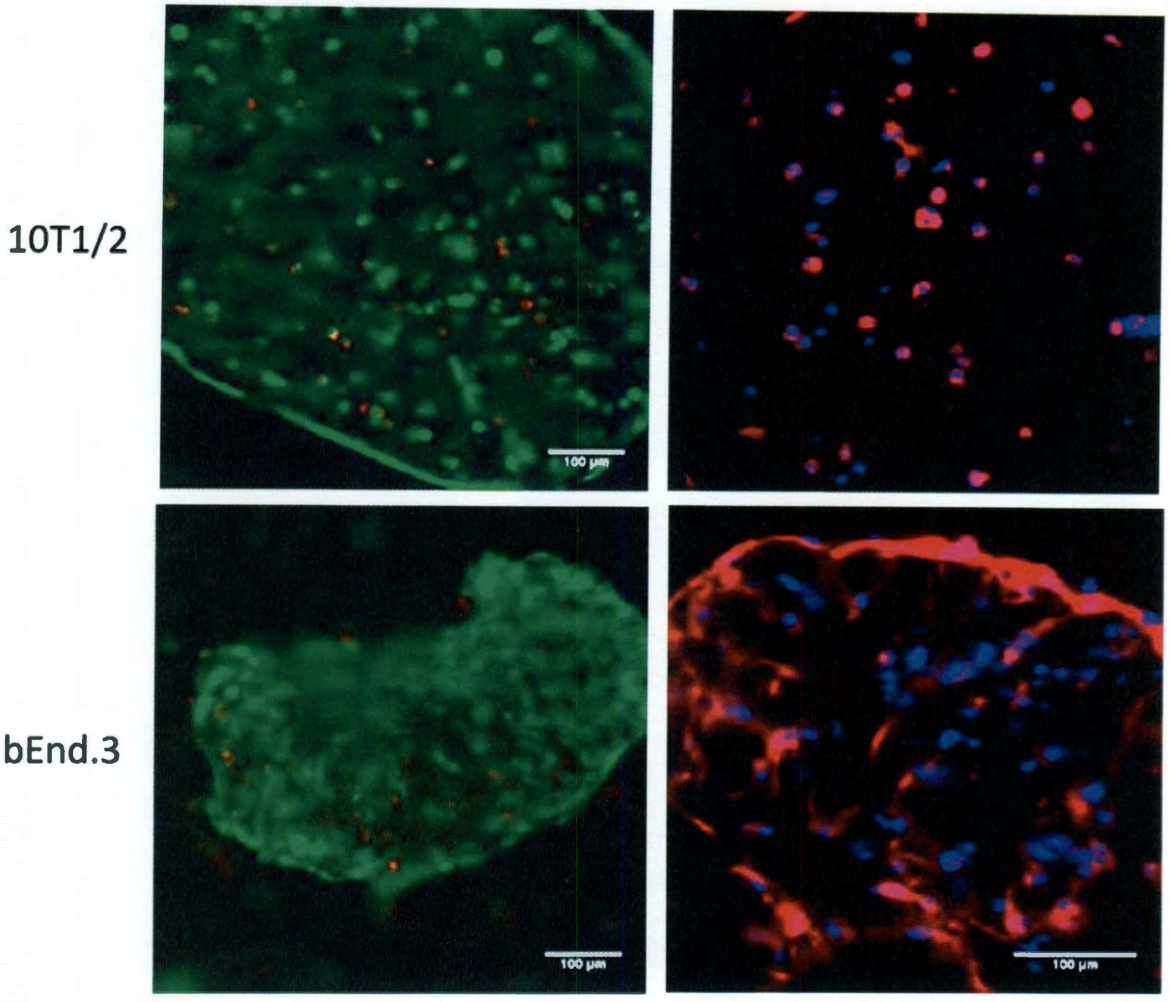

Figure 5-4: Individual cell types confirm cell viability and do not form tubule networks.

5.3.3 Anastomosis Between Cell-formed Tubules and Host Vasculature

mCherry-labeled capillaries sprouting from red blood cell-filled arterioles were seen connecting to tubules comprised of donor bEnd.3 cells (Figure 5-5 A-C). The presence of the originally seeded bEnd.3 cells in the tubules was confirmed using immunohistochemistry to stain for the middle T antigen, which was used to immortalize the bEnd.3 cells (Figure 5-5 D) (Rothermel et al., 2005). A cartoon rendering of cherry-

labeled vessels and cell-formed tubules highlights the site of anastomosis and presence of red blood cells in the cell-formed tubules (Figure 5-5 E-F).

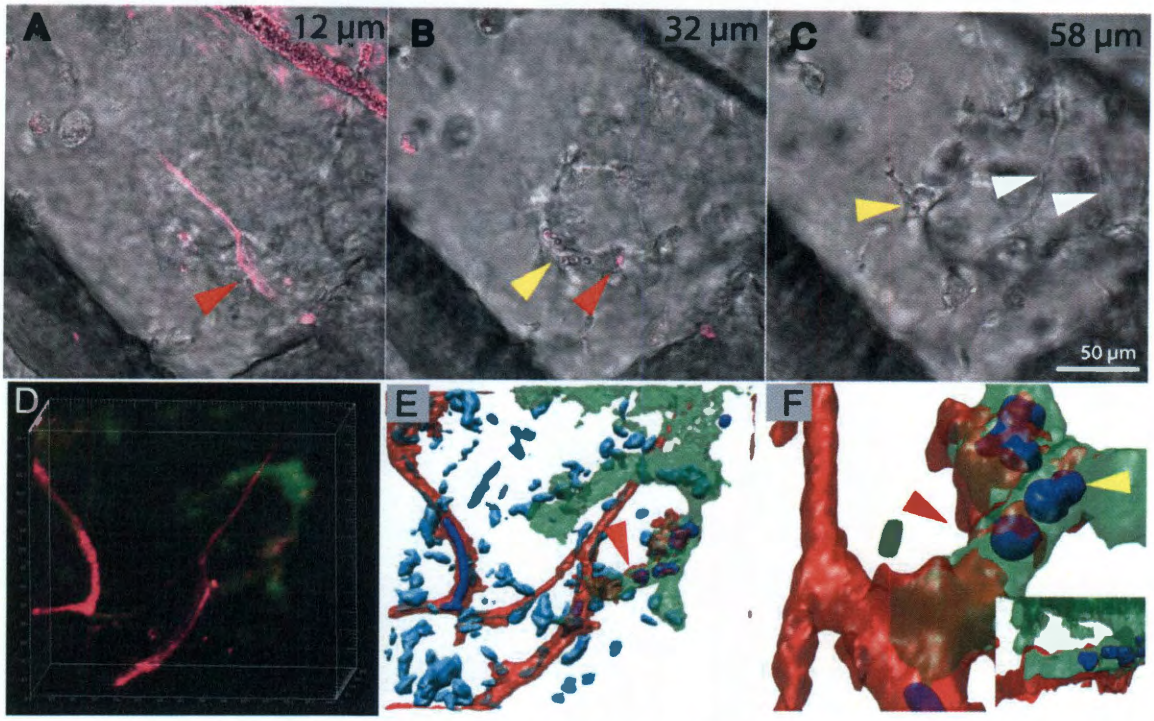

Figure 5-5: Anastomosis between cell-formed tubules and host vasculature. Transgenic mice with fluorescently-tagged endothelial cells (red) enable visualization of smaller vessels (A, red arrow) branching from red blood cell filled arterioles 12 μm into the hydrogel. B) cherry-labeled capillaries (red arrow) connect to unlabeled cell-formed tubules containing red blood cells (yellow arrow) 32 μm into the hydrogel. C) Cells are seen spreading (yellow arrow) and forming tubules as deep as 58 μm into the hydrogel. D-F) To confirm the connection between implanted cells and host vasculature, bEnd.3 cells were stained for expression of the middle T antigen (green). D) Cherry labeled vessels anastomose to middle t antigen-positive bEnd.3 cells in a 3D rendering. E) A three dimensional rendering of red labeled host vasculature connecting to green labeled bEnd.3 cells confirms the presence of red blood cells (dark blue) in the cell-formed tubule. F) Upon closer examination, the precise location of anastomosis (red arrow) and presence of red blood cells (yellow arrow) is visible.

These functional tubules had an average diameter of 8.2 μm $\pm$ 2.3 μm while nonfunctional tubules had an average diameter of 4.5 $\pm$ 0.9 μm μm (Figure 5-6). The diameter of cell-formed tubules enlargened from 6.9 μm $\pm$ 2.2 μm before implantation to 8.2 μm $\pm$ 2.3 μm upon perfusion. Furthermore, no statistical difference existed between

host vessels of diameter 9.5 $\pm$ 3.3 μm and cell-formed tubules (Figure 5-6).

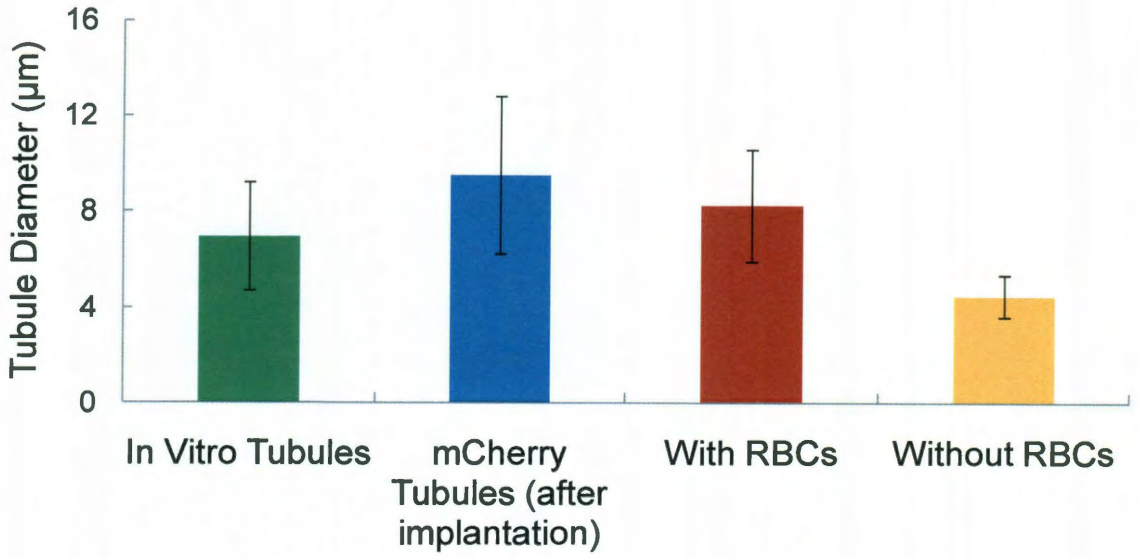

Figure 5-6: Tubule Diameter. The tubule diameter confirms that larger diameter tubules (8 μm) are similar in size to host vasculature and contain red blood cells while smaller diameter tubules (4 μm) remain nonfunctional. Furthermore, in vitro tubules enlarged upon red blood cell perfusion.

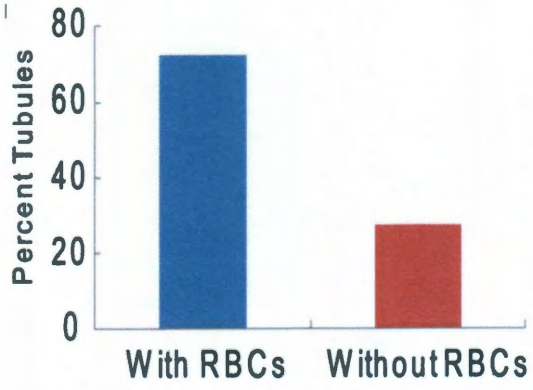

Figure 5-7: High perfusion of implanted tubules. 72% of cell-formed tubules contain red blood cells.

Notably, 72% of the cell-formed tubules contained red blood cells, confirming their functionality (Figure 5-7).

5.4 Discussion

This work presents the first precise visualization and confirmation of anastomosis between tubules formed by self-assembling cells *in vitro* and the host vasculature only 24 hours after implantation in a synthetic material. Additionally, the time of *in vitro* incubation was shortened to only 48 hours, and networks formed by encapsulated bEnd.3 and 10T1/2 cells were maintained once implanted *in vivo*. PDGF has previously been shown to induce an angiogenic response in the mouse cornea model (Saik et al., 2011). Previous studies had demonstrated the importance of *in vitro* incubation before implantation but required at least seven days incubation time and 5 days prior to anastomosis (Chen et al., 2008). For ultimate translation into clinical applications with cells derived from human patients, this work reduces the time of incubation before implantation and shortens the time to anastomosis to 24 hours and suggests that pre-vascularization may help facilitate anastomosis. Furthermore, while long term stable vessels were formed in natural matrices(Koike et al., 2004), a synthetic PEG-based polymer can be used as a more advanced platform for testing and identifying key processes in vessel development and anastomosis. This system is widely applicable to vessel development and disease, including ischemia and organ transplant, and will likely shed insight on mechanisms and therapies. Future studies of this *in vivo* assay will pinpoint the exact moment of anastomosis and the required factors. Furthermore, this technological feat will allow for greater development in complexity and scale, including expansion of incorporated cell types and implant locations.

5.5 Conclusion

The formation of stable and functional vessels remains a tremendous challenge for replacement of damaged or diseased tissues. 48 hours after encapsulation, tubule networks consisting of endothelial cells and pericytes in poly(ethylene glycol) based hydrogels were implanted into a prevascularized mouse cornea micropocket. Cell-formed tubules anastomosed to host vasculature within 24 hours, with 72% containing red blood cells, a major advance for design of perfused tissues.

Chapter 6: Conclusions and Future Directions

6.1 Thesis Summary

Currently, successfully engineered tissues are thin and avascular. In order to engineer more complex tissues for the hundreds of thousands of people awaiting an organ transplant in the US alone, engineering constructs need a microvasculature. The microvasculature is essential to provide oxygen for cell survival, as well as transport of nutrients and waste. This thesis presents rationally designed materials and cell culture techniques capable of supporting functional tubule formation and stabilization. Combining a synthetic scaffold material with cells and their cell-secreted signals instigated tubule formation throughout the scaffold. Poly(ethylene glycol) (PEG) based hydrogels were modified to induce desired cell characteristics. In order to mimic the body's natural process of new capillary formation, endothelial cells and pericytes were used in these constructs. Human umbilical vein endothelial cells were used as a reproducible and readily available cell type with mouse pericyte precursor 10T1/2 cells. First, this thesis research showed the importance of testing angiogenic hydrogels *in vivo* in a mouse cornea micropocket angiogenesis assay, a naturally avascular tissue for easy imaging in a reproducible and quantifiable assay. Second, platelet derived growth factor-BB (PDGF-BB), known for stabilizing newly formed tubule networks, was covalently immobilized via conjugation to PEG to enable prolonged bioactive signaling and controlled local delivery. Immobilized PDGF-BB led to tubule formation in two dimensions and three dimensions as well as angiogenesis *in vivo.* Similarly, immobilized ephrinA1, a receptor tyrosine kinase also known for tubule stabilization also induce

tubule formation and extracellular matrix production. Finally, a co-culture of endothelial and pericyte cells encapsulated into hydrogels formed tubules that anastomosed to the host vasculature and contained red blood cells. PEG-based hydrogels represent a promising technique to induce microvascular formation in engineered constructs, leading to stable and functional vessel formation using covalently immobilized growth factors and encapsulated cells. These materials can be used for replacement of damaged or diseased tissues as the current supply of cadaveric donations cannot meet the demand of tissues for the 110,000 people awaiting an organ in the US.

6.2 Conclusions

This thesis research presents the first *in vivo* application of angiogenic PEG-based hydrogels. In order to move this translational research ever closer to clinical applications, an *in vivo* assay was necessary. PEG-based hydrogels were shown to induce functional vessel formation, which could be adjusted based on hydrogel design. Using rational design of these materials, the resulting vascular response was adjusted.

This thesis presents the first work to covalently conjugate PEG to PDGF-BB, enabling precise control and local delivery to promote angiogenic activity *in vitro* and *in vivo*. Previous work showed that PDGF-BB signaled via endocytosis. However, the immobilized PDGF-BB confirms that PDGF-BB does not need to be internalized in order to signal. Additionally, PDGF-BB does not need to be cleaved from a matrix to promote angiogenic activity. One remaining hurdle is the stabilization of tubule formation. For example, tubules forming on 2D modified surfaces regressed. This phenomena was

visible for endothelial cells alone and for the co-culture of endothelial cells and pericyte precursor cells. In order for the tubule networks to be clinically relevant, tubules will need to remain functional until the material is replaced by host tissue. PDGF-BB does seem to prolong tubule formation but ultimate regression still occurred.

Similar to PEG-PDGF, ephrinA1 was immobilized to PEG and used to enhance angiogenic activity in 3D *in vitro* hydrogels and *in vivo*. PEG-ephrinA1 induced collagen IV and laminin production. Still, the precise mechanism of ephrinA1 angiogenesis activity still remains unknown. EphrinA1 has not been as widely studied in angiogenesis applications, and its effects on signaling pathways remains to be explored.

For ultimate clinical application, this thesis work implanted encapsulated cells into the mouse cornea and identified precise areas of anastomosis and tubule perfusion with red blood cells. Areas of anastomosis were identified by 24 hours, the earliest in all the literature. Furthermore, encapsulated cells were cultured *in vitro* for only 48 hours, which is the shortest incubation time for clinical applicability. In order to further verify this approach, the immune response to the implanted cells will need to be further investigated. For example, only mouse cells were used for implantation. Do suitable human cell lines exist or can the patient's own cells be used?

6.3 Future Directions

In order to advance this translational research, additional *in vivo* models will need to be developed. Several common *in vivo* angiogenic assays were discussed in chapter 2, including the mouse backpack chamber and CAM assay. Larger animal models will also

be necessary before clinical applications. Different *in vivo* models enable precise tuning of growth factor doses necessary for different species as well as different locations throughout the body. While the cornea provides an ideal place to determine the capabilities to induce angiogenesis, the cornea is mostly collagen I with low levels of oxygen, unlike the rest of the body. The presence of immune suppressant molecules and soluble VEGF receptors is unlike any other tissue.

Since the cornea has a reduced immune response, the role of immune cells on angiogenesis will need to be examined. The role of macrophages on vessel development has recently been investigated using transgenic mouse models. For example, in chapter 2 PDGF-BB and FGF-2 induced more organized branching networks than PDGF-BB, FGF-2, or VEGF alone. Interestingly, it was found that hydrogels releasing a combination of PDGF-BB and FGF-2 induced a synergistic macrophage response (Figure 6-1). While many bioengineers attempt to reduce the immune response to implanted hydrogels, this finding may suggest that a macrophage response is necessary and actually enhances the angiogenic response. These macrophages may be capable of acting as pericytes to support the newly formed capillaries (Figure 6-2).

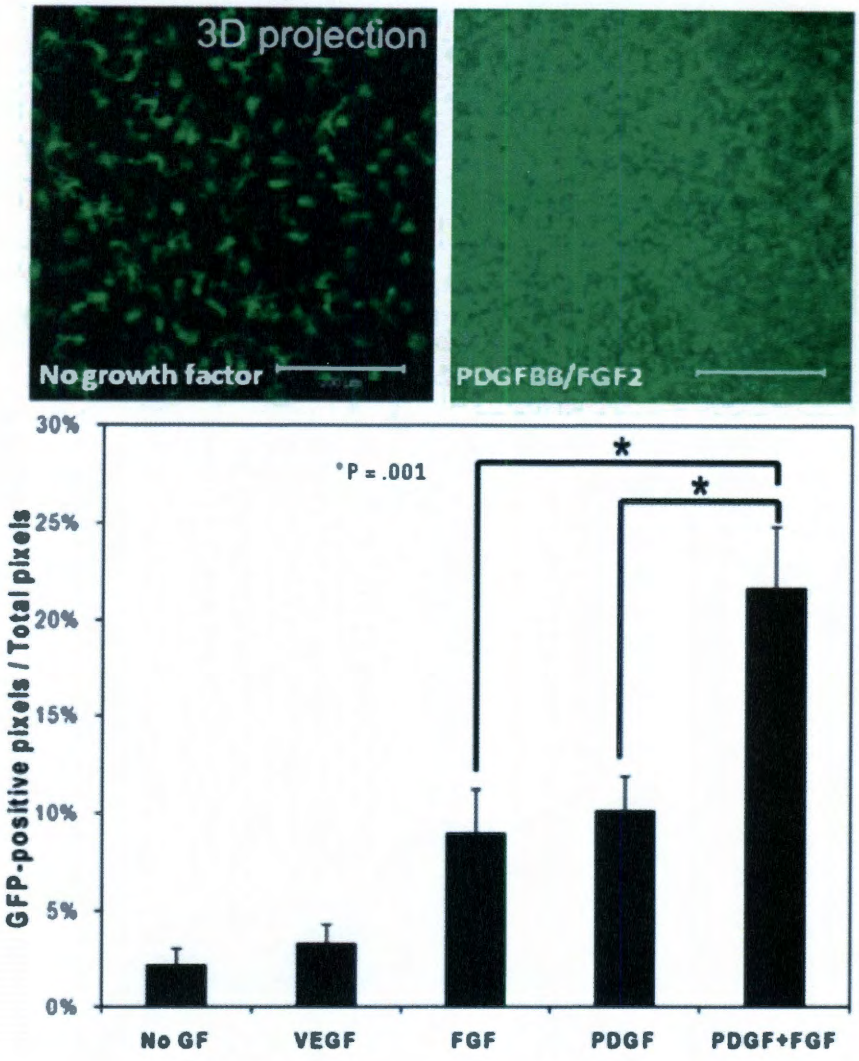

Figure 6-1: Macrophage response to growth factor releasing hydrogels. Using a transgenic mouse line where macrophages fluoresce green, the macrophage response was quantified at 3 days post implantation. Normal corneas and hydrogels with no growth factor do not stimulate and angiogenic response. Hydrogels with VEGF, FGF-2, or PDGF-BB alone induce a mild macrophage response. However, hydrogels with both PDGF-BB and FGF-2 induce a synergistic macrophage response.

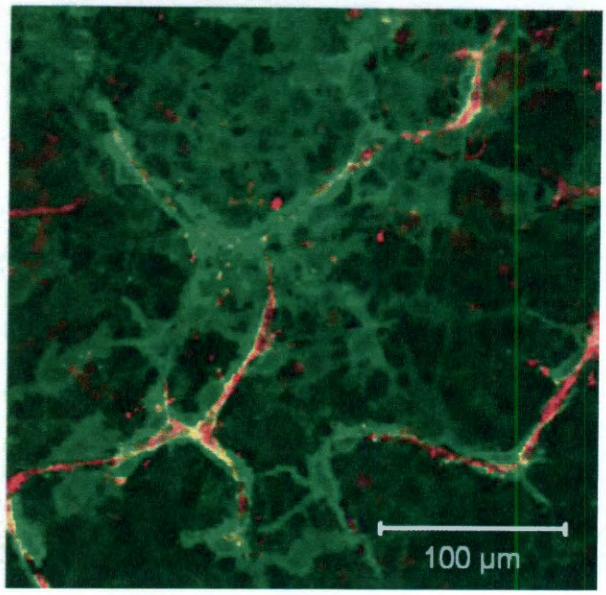

Figure 6-2: Macrophages acting as pericytes. A high magnification image of the PDGF-BB and FGF-2 releasing gels shows vessels (red) are tightly surrounded by macrophages (green). Macrophages have a typical pericyte morphology in wrapping around the capillary over multiple endothelial cells.

As the formation of new capillaries is better understood, the knowledge can be applied to therapies for cancer. As tumors growth larger than 1 mm in diameter, the tumor must form its own blood supply. Tumors are rapidly growing and often induce leaky vessel formation. The knowledge gained through inducing angiogenesis in biomaterials can be applied to better understanding tumor vessel formation in order to develop more targeted therapies. For example, previous work has shown that endothelial cells form tubule networks on soft matrices, but the tubule formation decreases with increasing stiffness (Ingber et al., 1989; Deroanne et al., 2001). Using this information, tumor stiffness could be examined in order to identify soft tumors with rapidly growing vessels. Furthermore, PEG hydrogels represent an optimal system to study individual components of the extracellular environment that induce cancer activity, including

metastasis. Some hypothesize that the location of a cancer's metastasis is due to the extracellular matrix cues. PEG-based hydrogels can incorporate specific signal or mechanical properties to induce a metastatic phenotype.

Summary

PEG-based hydrogels represent a promising technique to induce microvascular formation in engineered constructs for the replacement of damaged or diseased tissues. Using immobilized growth factors and encapsulated cells, stable and functional vessel were formed throughout the hydrogel material. Furthermore, all materials were tested in an *in vivo* mouse cornea micropocket angiogenesis assay to illustrate the achievability of implanting angiogenic materials. This novel hydrogel-based system can be used to support angiogenesis for the development of clinically applicable vascularized tissues.

References

Adams, R. H., and A. Eichmann. 2010. Axon guidance molecules in vascular patterning. *Cold Spring Harb Perspect Biol* 2 (5):a001875.

Aizawa, Y., N. Leipzig, T. Zahir, and M. Shoichet. 2008. The effect of immobilized platelet derived growth factor AA on neural stem/progenitor cell differentiation on cell-adhesive hydrogels. *Biomaterials* 29 (35):4676-83.

Ambati, B. K., E. Patterson, P. Jani, C. Jenkins, E. Higgins, N. Singh, T. Suthar, N. Vira, K. Smith, and R. Caldwell. 2007. Soluble vascular endothelial growth factor receptor-1 contributes to the corneal antiangiogenic barrier. *Br J Ophthalmol* 91 (4):505-8.

Atala, A., S. B. Bauer, S. Soker, J. J. Yoo, and A. B. Retik. 2006. Tissue-engineered autologous bladders for patients needing cystoplasty. *Lancet* 367 (9518):1241-6.

Au, P., J. Tam, D. Fukumura, and R. K. Jain. 2007. Small blood vessel engineering. *Methods Mol Med* 140:183-95.

Auerbach, R., R. Lewis, B. Shinners, L. Kubai, and N. Akhtar. 2003. Angiogenesis assays: A critical overview. *Clinical Chemistry* 49 (1):32.

Bar, R. S., M. Boes, B. A. Booth, B. L. Dake, S. Henley, and M. N. Hart. 1989. The effects of platelet-derived growth factor in cultured microvessel endothelial cells. *Endocrinology* 124 (4):1841-8.

Baumgartner, I., G. Rauh, A. Pieczek, D. Wuensch, M. Magner, M. Kearney, R. Schainfeld, and J. M. Isner. 2000. Lower-extremity edema associated with gene transfer of naked DNA encoding vascular endothelial growth factor. *Ann Intern Med* 132 (11):880-4.

Beebe, D. C. 2008. Maintaining transparency: a review of the developmental physiology and pathophysiology of two avascular tissues. *Semin Cell Dev Biol* 19 (2):125-33.

Bendeck, M. P., C. Irvin, M. Reidy, L. Smith, D. Mulholland, M. Horton, and C. M. Giachelli. 2000. Smooth muscle cell matrix metalloproteinase production is stimulated via alpha(v)beta(3) integrin. *Arterioscler Thromb Vasc Biol* 20 (6):1467-72.

Bentz, H., J. A. Schroeder, and T. D. Estridge. 1998. Improved local delivery of TGF-beta2 by binding to injectable fibrillar collagen via difunctional polyethylene glycol. *J Biomed Mater Res* 39 (4):539-48.

Berk, B. C., R. W. Alexander, T. A. Brock, M. A. Gimbrone, Jr., and R. C. Webb. 1986. Vasoconstriction: a new activity for platelet-derived growth factor. *Science* 232 (4746):87-90.

Betsholtz, C. 2003. Biology of platelet-derived growth factors in development. *Birth Defects Res C Embryo Today* 69 (4):272-85.

Betsholtz, C., P. Lindblom, and H. Gerhardt. 2005. Role of pericytes in vascular morphogenesis. *EXS* (94):115-25.

Bikfalvi, A., S. Klein, G. Pintucci, and D. B. Rifkin. 1997. Biological roles of fibroblast growth factor-2. *Endocr Rev* 18 (1):26-45.

Bjornsson, C. S., G. Lin, Y. Al-Kofahi, A. Narayanaswamy, K. L. Smith, W. Shain, and B. Roysam. 2008. Associative image analysis: a method for automated quantification of 3D multi-parameter images of brain tissue. *J Neurosci Methods* 170 (1):165-78.

Brantley-Sieders, D. M., J. Caughron, D. Hicks, A. Pozzi, J. C. Ruiz, and J. Chen. 2004. EphA2 receptor tyrosine kinase regulates endothelial cell migration and vascular assembly through phosphoinositide 3-kinase-mediated Rac1 GTPase activation. *J Cell Sci* 117 (Pt 10):2037-49.

Brantley, D. M., N. Cheng, E. J. Thompson, Q. Lin, R. A. Brekken, P. E. Thorpe, R. S. Muraoka, D. P. Cerretti, A. Pozzi, D. Jackson, C. Lin, and J. Chen. 2002. Soluble Eph A receptors inhibit tumor angiogenesis and progression in vivo. *Oncogene* 21 (46):7011-26.

Cao, R., E. Brakenhielm, R. Pawliuk, D. Wariaro, M. J. Post, E. Wahlberg, P. Leboulch, and Y. Cao. 2003. Angiogenic synergism, vascular stability and improvement of hind-limb ischemia by a combination of PDGF-BB and FGF-2. *Nat Med* 9(5):604-13.

Cao, R., Brakenhielm, E., Pawliuk, R., Wariaro, D., Post, M. J., Wahlberg, E., Leboulch, P. and Cao, Y. 2003. Angiogenic synergism, vascular stability and improvement of hind-limb ischemia by a combination of PDGF-BB and FGF-2. *Nat Medicine* 9:604-13.

Cao, Y., R. Cao, and E. M. Hedlund. 2008. R Regulation of tumor angiogenesis and metastasis by FGF and PDGF signaling pathways. *J Mol Med* 86 (7):785-9.

Caplan, Arnold I. 1985. The vasculature and limb development. *Cell Differentiation* 16 (1):1.

Carlson, Bruce M. 1973. The regeneration of skeletal muscle — a review. *American Journal of Anatomy* 137 (2):119.

Carmeliet, P., V. Ferreira, G. Breier, S. Pollefeyt, L. Kieckens, M. Gertsenstein, M. Fahrig, A. Vandenhoeck, K. Harpal, C. Eberhardt, C. Declercq, J. Pawling, L. Moons, D. Collen, W. Risau, and A. Nagy. 1996. Abnormal blood vessel development and lethality in embryos lacking a single VEGF allele. *Nature* 380 (6573):435-9.

Chen, L., Z. He, B. Chen, Y. Zhao, W. Sun, Z. Xiao, J. Zhang, M. Yang, Z. Gao, and J. Dai. 2009. Direct chemical cross-linking of platelet-derived growth factor-BB to the demineralized bone matrix improves cellularization and vascularization. *Biomacromolecules* 10 (12):3193-8.

Chen, R. R., E. A. Silva, W. W. Yuen, and D. J. Mooney. 2007. Spatio-temporal VEGF and PDGF delivery patterns blood vessel formation and maturation. *Pharm Res* 24 (2):258-64.

Chen, X., A. S. Aledia, C. M. Ghajar, C. K. Griffith, A. J. Putnam, C. C. Hughes, and S. C. George. 2008. Prevascularization of a Fibrin-Based Tissue Construct Accelerates the Formation of Functional Anastomosis with Host Vasculature. *Tissue Eng Part A* 15 (6):1363-71.

Cheng, N., D. Brantley, W. B. Fang, H. Liu, W. Fanslow, D. P. Cerretti, K. N. Bussell, A. Reith, D. Jackson, and J. Chen. 2003. Inhibition of VEGF-dependent multistage carcinogenesis by soluble EphA receptors. *Neoplasia* 5 (5):445-56.

Cheng, N., D. M. Brantley, and J. Chen. 2002. The ephrins and Eph receptors in angiogenesis. *Cytokine Growth Factor Rev* 13 (1):75-85. 166

Cheng, N., D. M. Brantley, H. Liu, Q. Lin, M. Enriquez, N. Gale, G. Yancopoulos, D. P. Cerretti, T. O. Daniel, and J. Chen. 2002. Blockade of EphA receptor tyrosine kinase activation inhibits endothelial cell growth factor-induced angiogenesis. *Mol Cancer Res* 1 (1):2-11.

Chinen, N., M. Tanihara, M. Nakagawa, K. Shinozaki, E. Yamamoto, Y. Mizushima, and Y. Suzuki. 2003. Action of microparticles of heparin and alginate crosslinked gel when used as injectable artificial matrices to stabilize basic fibroblast growth factor and induce angiogenesis by controlling its release. *J Biomed Mater Res A* 67 (1):61-8.

Cho, S. W., S. H. Moon, S. H. Lee, S. W. Kang, J. Kim, J. M. Lim, H. S. Kim, B. S. Kim, and H. M. Chung. 2007. Improvement of postnatal neovascularization by human embryonic stem cell derived endothelial-like cell transplantation in a mouse model of hindlimb ischemia. *Circulation* 116 (21):2409-19.

Cursiefen, C. 2007. Immune privilege and angiogenic privilege of the cornea. *Chem Immunol Allergy* 92:50-7.

Cursiefen, C., S. Masli, T. F. Ng, M. R. Dana, P. Bornstein, J. Lawler, and J. W. Streilein. 2004. Roles of thrombospondin-1 and -2 in regulating corneal and iris angiogenesis. *Invest Ophthalmol Vis Sci* 45 (4):1117-24.

Daniel, T. O., E. Stein, D. P. Cerretti, P. L. St John, B. Robert, and D. R. Abrahamson. 1996. ELK and LERK-2 in developing kidney and microvascular endothelial assembly. *Kidney Int Suppl* 57:S73-81.

Davies, N., S. Dobner, D. Bezuidenhout, C. Schmidt, M. Beck, A. H. Zisch, and P. Zilla. 2008. The dosage dependence of VEGF stimulation on scaffold neovascularisation. *Biomaterials* 29 (26):3531-8.

De Coppi, P., D. Delo, L. Farrugia, K. Udompanyanan, J. J. Yoo, M. Nomi, A. Atala, and S. Soker. 2005. Angiogenic gene-modified muscle cells for enhancement of tissue formation. *Tissue Eng* 11 (7-8):1034-44.

De la Riva, B., E. Sanchez, A. Hernandez, R. Reyes, F. Tamimi, E. Lopez-Cabarcos, A. Delgado, and C. Evora. 2009. Local controlled release of VEGF and PDGF from a combined brushite-chitosan system enhances bone regeneration. *J Control Release*.

DeLong, S. A., J. J. Moon, and J. L. West. 2005. Covalently immobilized gradients of bFGF on hydrogel scaffolds for directed cell migration. *Biomaterials* 26 (16):3227-34.

Deroanne, C. F., C. M. Lapiere, and B. V. Nusgens. 2001. In vitro tubulogenesis of endothelial cells by relaxation of the coupling extracellular matrix-cytoskeleton. *Cardiovasc Res* 49 (3):647-58.

Diaz-Flores, L., R. Gutierrez, J. F. Madrid, H. Varela, F. Valladares, E. Acosta, P. Martin-Vasallo, and L. Diaz-Flores, Jr. 2009. Pericytes. Morphofunction, interactions and pathology in a quiescent and activated mesenchymal cell niche. *Histol Histopathol* 24 (7):909-69.

Dobrzanski, P., K. Hunter, S. Jones-Bolin, H. Chang, C. Robinson, S. Pritchard, H. Zhao, and B. Ruggeri. 2004. Antiangiogenic and antitumor efficacy of EphA2 receptor antagonist. *Cancer Res* 64 (3):910-9. 167

Drury, J. L., and D. J. Mooney. 2003. Hydrogels for tissue engineering: scaffold design variables and applications. *Biomaterials* 24 (24):4337-51.

Durbeej, M. 2010. Laminins. *Cell Tissue Research* 339:259-268.

Edelman, D. A., Y. Jiang, J. Tyburski, R. F. Wilson, and C. Steffes. 2006. Pericytes and their role in microvasculature homeostasis. *J Surg Res* 135 (2):305-11.

Ehrbar, M., S. M. Zeisberger, G. P. Raeber, J. A. Hubbell, C. Schnell, and A. H. Zisch. 2008. The role of actively released fibrin-conjugated VEGF for VEGF receptor 2 gene activation and the enhancement of angiogenesis. *Biomaterials* 29 (11):1720-9.

Ennett, A. B., D. Kaigler, and D. J. Mooney. 2006. Temporally regulated delivery of VEGF in vitro and in vivo. *J Biomed Mater Res A* 79 (1):176-84.

Epstein, S. E., R. Kornowski, S. Fuchs, and H. F. Dvorak. 2001. Angiogenesis therapy: amidst the hype, the neglected potential for serious side effects. *Circulation* 104 (1):115-9.

Falanga, V., and M. Sabolinski. 1999. A bilayered living skin construct (APLIGRAF) accelerates complete closure of hard-to-heal venous ulcers. *Wound Repair Regen* 7 (4):201-7.

Francis, M. E., S. Uriel, and E. M. Brey. 2008. Endothelial cell-matrix interactions in neovascularization. *Tissue Eng Part B Rev* 14 (1):19-32.

Frerich, B., N. Lindemann, J. Kurtz-Hoffmann, and K. Oertel. 2001. In vitro model of a vascular stroma for the engineering of vascularized tissues. *Int J Oral Maxillofac Surg* 30 (5):414-20.

Fujita, M., M. Ishihara, M. Shimizu, K. Obara, S. Nakamura, Y. Kanatani, Y. Morimoto, B. Takase, T. Matsui, M. Kikuchi, and T. Maehara. 2007. Therapeutic angiogenesis induced by controlled release of fibroblast growth factor-2 from injectable chitosan/non-anticoagulant heparin hydrogel in a rat hindlimb ischemia model. *Wound Repair Regen* 15 (1):58-65.

Gale, N. W., and G. D. Yancopoulos. 1999. Growth factors acting via endothelial cell-specific receptor tyrosine kinases: VEGFs, angiopoietins, and ephrins in vascular development. *Genes Dev* 13 (9):1055-66.

Gaudric, A., T. N'Guyen, M. Moenner, A. Glacet-Bernard, and D. Barritault. 1992. Quantification of angiogenesis due to basic fibroblast growth factor in a modified rabbit corneal model. *Ophthalmic Research* 24 (3):181.

Gimbrone, M. A., Jr., S. B. Leapman, R. S. Cotran, and J. Folkman. 1973. Tumor angiogenesis: iris neovascularization at a distance from experimental intraocular tumors. *J Natl Cancer Inst* 50 (1):219-28.

Gou, M., M. Dai, Y. Gu, X. Li, Y. Wen, L. Yang, K. Wang, Y. Wei, and Z. Qian. 2008. Basic fibroblast growth factor loaded biodegradable PCL-PEG-PCL copolymeric nanoparticles: preparation, in vitro release and immunogenicity study. *J Nanosci Nanotechnol* 8 (5):2357-61.

Gould, D. J., T. J. Vadakkan, R. A. Poche, and M. E. Dickinson. 2011. Multifractal and lacunarity analysis of microvascular morphology and remodeling. *Microcirculation* 18 (2):136-51.

Greenberg, J. I., D. J. Shields, S. G. Barillas, L. M. Acevedo, E. Murphy, J. Huang, L. Scheppke, C. Stockmann, R. S. Johnson, N. Angle, and D. A. Cheresh. 2008. A role for VEGF as a negative regulator of pericyte function and vessel maturation. *Nature* 456 (7223):809-13.

Guan, J., J. J. Stankus, and W. R. Wagner. 2007. Biodegradable elastomeric scaffolds with basic fibroblast growth factor release. *J Control Release* 120 (1-2):70-8.

Gunn, J. W., S. D. Turner, and B. K. Mann. 2005. Adhesive and mechanical properties of hydrogels influence neurite extension. *J Biomed Mater Res A* 72 (1):91-7.

Hahn, M. S., M. K. McHale, E. Wang, R. H. Schmedlen, and J. L. West. 2007. Physiologic pulsatile flow bioreactor conditioning of poly(ethylene glycol)-based tissue engineered vascular grafts. *Ann Biomed Eng* 35 (2):190-200.

Hamill, K. J., K. Kligys, S. B. Hopkinson, and J. C. Jones. 2009. Laminin deposition in the extracellular matrix: a complex picture emerges. *J Cell Sci* 122 (Pt 24):4409-17.

Hart, C. E., M. Bailey, D. A. Curtis, S. Osborn, E. Raines, R. Ross, and J. W. Forstrom. 1990. Purification of PDGF-AB and PDGF-BB from human platelet extracts and identification of all three PDGF dimers in human platelets. *Biochemistry* 29 (1):166-72.

Hegen, A., A. Blois, C. E. Tiron, M. Hellesoy, D. R. Micklem, J. E. Nor, L. A. Akslen, and J. B. Lorens. 2010. Efficient in vivo vascularization of tissue-engineering scaffolds. *J Tissue Eng Regen Med* 5 (4):e52-62.

Helbig, H., J. P. Hinz, U. Kellner, and M. H. Foerster. 1993. Oxygen in the anterior chamber of the human eye. *Ger J Ophthalmol* 2 (3):161-4.

Heldin, C. H., U. Eriksson, and A. Ostman. 2002. New members of the platelet-derived growth factor family of mitogens. *Arch Biochem Biophys* 398 (2):284-90.

Heldin, C. H., and B. Westermark. 1999. Mechanism of action and in vivo role of platelet-derived growth factor. *Physiol Rev* 79 (4):1283-316.

Hendrix, M. J., E. A. Seftor, A. R. Hess, and R. E. Seftor. 2003. Molecular plasticity of human melanoma cells. *Oncogene* 22 (20):3070-5.

Hern, DL, and J. A. Hubbell. 1997. Incorporation of adhesion peptides into nonadhesive hydrogels useful for tissue resurfacing. *Journal of Biomedical Materials Research* 39 (2):266-276.

Heroult, M., F. Schaffner, and H. G. Augustin. 2006. Eph receptor and ephrin ligand-mediated interactions during angiogenesis and tumor progression. *Exp Cell Res* 312 (5):642-50.

Himanen, J. P., N. Saha, and D. B. Nikolov. 2007. Cell-cell signaling via Eph receptors and ephrins. *Curr Opin Cell Biol* 19 (5):534-42.

Hirschi, K. K., S. A. Rohovsky, and P. A. D'Amore. 1998. PDGF, TGF-beta, and heterotypic cell-cell interactions mediate endothelial cell-induced recruitment of 10T1/2 cells and their differentiation to a smooth muscle fate. *J Cell Biol* 141 (3):805-14.

Hoffmann, JC, and J. L. West. 2010. Three-dimensional photolithographic patterning of multiple bioactive ligands in poly(ethylene glycol) hydrogels. *Soft Matter* 6:5056-63.

Hollinger, J. O., C. E. Hart, S. N. Hirsch, S. Lynch, and G. E. Friedlaender. 2008. Recombinant human platelet-derived growth factor: biology and clinical applications. *J Bone Joint Surg Am* 90 Suppl 1:48-54.

Hoppe, J., H. A. Weich, W. Eichner, and D. Tatje. 1990. Preparation of biologically active platelet-derived growth factor isoforms AA and AB. Preferential formation of AB heterodimers. *Eur J Biochem* 187 (1):207-14.

Hudon, V., F. Berthod, A. F. Black, O. Damour, L. Germain, and F. A. Auger. 2003. A tissue-engineered endothelialized dermis to study the modulation of angiogenic and angiostatic molecules on capillary-like tube formation in vitro. *Br J Dermatol* 148 (6):1094-104.

Humphrey, J. D., K. H. Jürgen Buschow, W. Cahn Robert, C. Flemings Merton, Ilschner Bernard, J. Kramer Edward, Mahajan Subhash, and Veyssière Patrick. 2001. Blood Vessels, Mechanical and Physical Properties of. In *Encyclopedia of Materials: Science and Technology*. Oxford: Elsevier.

Iida, H., M. Honda, H. F. Kawai, T. Yamashita, Y. Shirota, B. C. Wang, H. Miao, and S. Kaneko. 2005. Ephrin-A1 expression contributes to the malignant characteristics of {alpha}-fetoprotein producing hepatocellular carcinoma. *Gut* 54 (6):843-51.

Ikeda, Y., N. Fukuda, M. Wada, T. Matsumoto, A. Satomi, S. Yokoyama, S. Saito, K. Matsumoto, K. Kanmatsuse, and H. Mugishima. 2004. Development of angiogenic cell and gene therapy by transplantation of umbilical cord blood with vascular endothelial growth factor gene. *Hypertens Res* 27 (2):119-28.

Ingber, D. E., and J. Folkman. 1989. How does extracellular matrix control capillary morphogenesis? *Cell* 58 (5):803-5.

Iruela-Arispe, M. L., and G. E. Davis. 2009. Cellular and molecular mechanisms of vascular lumen formation. *Dev Cell* 16 (2):222-31.

Jackson, C. L., and M. A. Reidy. 1993. Basic fibroblast growth factor: its role in the control of smooth muscle cell migration. *Am J Pathol* 143 (4):1024-31.

Jain, R. K. 2005. Normalization of tumor vasculature: an emerging concept in antiangiogenic therapy. *Science* 307:58 - 62.

Jain, R. K., P. Au, J. Tam, D. G. Duda, and D. Fukumura. 2005. Engineering vascularized tissue. *Nat Biotechnol* 23 (7):821-3.

Jain, R.K. 2003. Molecular regulation of vessel maturation. *Nat Med* 9 (6):685. .

Jakobsson, L., A. Domogatskaya, K. Tryggvason, D. Edgar, and L. Claesson-Welsh. 2008. Laminin deposition is dispensable for vasculogenesis but regulates blood vessel diameter independent of flow. *FASEB J* 22 (5):1530-9.

Jin, Q., G. Wei, Z. Lin, J. V. Sugai, S. E. Lynch, P. X. Ma, and W. V. Giannobile. 2008. Nanofibrous scaffolds incorporating PDGF-BB microspheres induce chemokine expression and tissue neogenesis in vivo. *PLoS ONE* 3 (3):e1729.

Kamei, M., W. B. Saunders, K. J. Bayless, L. Dye, G. E. Davis, and B. M. Weinstein. 2006. Endothelial tubes assemble from intracellular vacuoles in vivo. *Nature* 442 (7101):453-6.

Kano, M. R., Y. Morishita, C. Iwata, S. Iwasaka, T. Watabe, Y. Ouchi, K. Miyazono, and K. Miyazawa. 2005. VEGF-A and FGF-2 synergistically promote neoangiogenesis through enhancement of endogenous PDGF-B-PDGFRbeta signaling. *J Cell Sci* 118 (Pt 16):3759-68.

Kawai-Kowase, K., H. Sato, Y. Oyama, H. Kanai, M. Sato, H. Doi, and M. Kurabayashi. 2004. Basic fibroblast growth factor antagonizes transforming growth factor-beta1-induced smooth muscle gene expression through extracellular signal-regulated kinase 1/2 signaling pathway activation. *Arterioscler Thromb Vasc Biol* 24 (8):1384-90.

Kenyon, B. M., E. E. Voest, C. C. Chen, E. Flynn, J. Folkman, and R. J. D'Amato. 1996. A model of angiogenesis in the mouse cornea. *Invest Ophthalmol Vis Sci* 37 (8):1625-32.

Khachigian, L. M., N. Resnick, M. A. Gimbrone, Jr., and T. Collins. 1995. Nuclear factor-kappa B interacts functionally with the platelet-derived growth factor B-chain shear-stress response element in vascular endothelial cells exposed to fluid shear stress. *J Clin Invest* 96 (2):1169-75.

Khoshnoodi, J., V. Pedchenko, and B. G. Hudson. 2008. Mammalian collagen IV. *Microsc Res Tech* 71 (5):357-70.

King, T. W., and C. W. Patrick, Jr. 2000. Development and in vitro characterization of vascular endothelial growth factor (VEGF)-loaded poly(DL-lactic-co-glycolic acid)/poly(ethylene glycol) microspheres using a solid encapsulation/single emulsion/solvent extraction technique. *J Biomed Mater Res* 51 (3):383-90.

Koch, S., Ch Yao, G. Grieb, P. Prevel, E. M. Noah, and G. C. Steffens. 2006. Enhancing angiogenesis in collagen matrices by covalent incorporation of VEGF. *J Mater Sci Mater Med* 17 (8):735-41.

Koike, N., D. Fukumura, O. Gralla, P. Au, J. S. Schechner, and R. K. Jain. 2004. Tissue engineering: creation of long-lasting blood vessels. *Nature* 428 (6979):138-9.

Kruegel, J., and N. Miosge. 2010. Basement membrane components are key players in specialized extracellular matrices. *Cell Mol Life Sci* 67 (17):2879-95.

Kuhl, P. R., and L. G. Griffith-Cima. 1996. Tethered epidermal growth factor as a paradigm for growth factor-induced stimulation from the solid phase. *Nat Med* 2 (9):1022-7.

Kuijper, S., C. J. Turner, and R. H. Adams. 2007. Regulation of angiogenesis by Eph-ephrin interactions. *Trends Cardiovasc Med* 17 (5):145-51.

Lange, S., J. Heger, G. Euler, M. Wartenberg, H. M. Piper, and H. Sauer. 2009. Platelet-derived growth factor BB stimulates vasculogenesis of embryonic stem cell-derived endothelial cells by calcium-mediated generation of reactive oxygen species. *Cardiovasc Res* 81 (1):159-68.

Langham, M. 1953. Observations on the growth of blood vessels into the cornea; application of a new experimental technique. *Br J Ophthalmol* 37 (4):210-22.

Larina, I. V., W. Shen, O. G. Kelly, A. K. Hadjantonakis, M. H. Baron, and M. E. Dickinson. 2009. A membrane associated mCherry fluorescent reporter line for studying vascular remodeling and cardiac function during murine embryonic development. *Anat Rec (Hoboken)* 292 (3):333-41.

Laschke, M. W., Y. Harder, M. Amon, I. Martin, J. Farhadi, A. Ring, N. Torio-Padron, R. Schramm, M. Rucker, D. Junker, J. M. Haufel, C. Carvalho, M. Heberer, G. Germann, B. Vollmar, and M. D. Menger. 2006. Angiogenesis in tissue engineering: breathing life into constructed tissue substitutes. *Tissue Eng* 12 (8):2093-104.

Lee, J. G., and E. P. Kay. 2006. FGF-2-induced wound healing in corneal endothelial cells requires Cdc42 activation and Rho inactivation through the phosphatidylinositol 3-kinase pathway. *Invest Ophthalmol Vis Sci* 47 (4):1376-86.

Lee, K. Y., M. C. Peters, K. W. Anderson, and D. J. Mooney. 2000. Controlled growth factor release from synthetic extracellular matrices. *Nature* 408 (6815):998-1000.

Lee, K. Y., M. C. Peters, and D. J. Mooney. 2003. Comparison of vascular endothelial growth factor and basic fibroblast growth factor on angiogenesis in SCID mice. *J Control Release* 87 (1-3):49-56.

Lee, S., S. M. Jilani, G. V. Nikolova, D. Carpizo, and M. L. Iruela-Arispe. 2005. Processing of VEGF-A by matrix metalloproteinases regulates bioavailability and vascular patterning in tumors. *J Cell Biol* 169 (4):681-91.

Leslie-Barbick, J. E., J. J. Moon, and J. L. West. 2009. Covalently-immobilized vascular endothelial growth factor promotes endothelial cell tubulogenesis in poly(ethylene glycol) diacrylate hydrogels. *J Biomater Sci Polym Ed* 20 (12):1763-79.

Leunig, M., F. Yuan, M. D. Menger, Y. Boucher, A. E. Goetz, K. Messmer, and R. K. Jain. 1992. Angiogenesis, microvascular architecture, microhemodynamics, and interstitial fluid pressure during early growth of human adenocarcinoma LS174T in SCID mice. *Cancer Res* 52 (23):6553-60.

Levenberg, S., J. S. Golub, M. Amit, J. Itskovitz-Eldor, and R. Langer. 2002. Endothelial cells derived from human embryonic stem cells. *Proc Natl Acad Sci U S A* 99 (7):4391-6.

Lindahl, P., B. R. Johansson, P. Leveen, and C. Betsholtz. 1997. Pericyte loss and microaneurysm formation in PDGF-B-deficient mice. *Science* 277 (5323):242-5.

Liu, H. W., C. H. Chen, C. L. Tsai, I. H. Lin, and G. H. Hsiue. 2007. Heterobifunctional poly(ethylene glycol)-tethered bone morphogenetic protein-2-stimulated bone marrow mesenchymal stromal cell differentiation and osteogenesis. *Tissue Eng* 13 (5):1113-24.

Lopes, R., and N. Betrouni. 2009. Fractal and multifractal analysis: A review. *Medical Image Analysis* 13 (4):634.

Lutolf, M. P., J. L. Lauer-Fields, H. G. Schmoekel, A. T. Metters, F. E. Weber, G. B. Fields, and J. A. Hubbell. 2003. Synthetic matrix metalloproteinase-sensitive hydrogels for the conduction of tissue regeneration: engineering cell-invasion characteristics. *Proc Natl Acad Sci U S A* 100 (9):5413-8.

Madeddu, P. 2005. Therapeutic angiogenesis and vasculogenesis for tissue regeneration. *Exp Physiol* 90 (3):315-26.

Mandelbrot, Benoit B. 1982. *The Fractal Geometry of Nature*. 20th ed. New York: Freeman.

Mann, B. K., R. H. Schmedlen, and J. L. West. 2001. Tethered-TGF-beta increases extracellular matrix production of vascular smooth muscle cells. *Biomaterials* 22 (5):439-44.

Marti, H. H. 2005. Angiogenesis--a self-adapting principle in hypoxia. *EXS* (94):163-80.

Martinez-Lemus, L. A., M. A. Hill, and G. A. Meininger. 2009. The plastic nature of the vascular wall: a continuum of remodeling events contributing to control of arteriolar diameter and structure. *Physiology (Bethesda)* 24:45-57.

Maynard, H. D., and J. A. Hubbell. 2005. Discovery of a sulfated tetrapeptide that binds to vascular endothelial growth factor. *Acta Biomater* 1 (4):451-9.

Mittermayr, R., T. Morton, M. Hofmann, S. Helgerson, M. van Griensven, and H. Redl. 2008. Sustained (rh)VEGF(165) release from a sprayed fibrin biomatrix induces angiogenesis, up-regulation of endogenous VEGF-R2, and reduces ischemic flap necrosis. *Wound Repair Regen* 16 (4):542-50.

Miyoshi, M., T. Kawazoe, H. H. Igawa, Y. Tabata, Y. Ikada, and S. Suzuki. 2005. Effects of bFGF incorporated into a gelatin sheet on wound healing. *J Biomater Sci Polym Ed* 16 (7):893-907.

Moioli, E. K., P. A. Clark, M. Chen, J. E. Dennis, H. P. Erickson, S. L. Gerson, and J. J. Mao. 2008. Synergistic actions of hematopoietic and mesenchymal stem/progenitor cells in vascularizing bioengineered tissues. *PLoS ONE* 3 (12):e3922.

Moon, J. J. 2008. James Moon Thesis.

Moon, J. J., S. H. Lee, and J. L. West. 2007. Synthetic biomimetic hydrogels incorporated with ephrin-A1 for therapeutic angiogenesis. *Biomacromolecules* 8 (1):42-9.

Moon, J. J., J. E. Saik, R. A. Poche, J. E. Leslie-Barbick, S. H. Lee, A. A. Smith, M. E. Dickinson, and J. L. West. 2010. Biomimetic hydrogels with pro-angiogenic properties. *Biomaterials* 31 (14):3840-7.

Moon, J. J., and J. L. West. 2008. Vascularization of engineered tissues: approaches to promote angio-genesis in biomaterials. *Curr Top Med Chem* 8 (4):300-10.

Moon, J.J., M.S. Hahn, I.Kim, B.A. Nsiah, and J.L. West. 2008. Micropatterning of Poly(Ethylene Glycol) Diacrylate Hydrogels with Biomolecules to Regulate and Guide Endothelial Morphogenesis. *Tissue Engineering: Part A* Volume 14:1-7.

Mukouyama, Y. S., D. Shin, S. Britsch, M. Taniguchi, and D. J. Anderson. 2002. Sensory nerves determine the pattern of arterial differentiation and blood vessel branching in the skin. *Cell* 109 (6):693-705.

Muthukkaruppan, V., and R. Auerbach. 1979. Angiogenesis in the mouse cornea. *Science* 205 (4413):1416-8.

Nillesen, S. T., P. J. Geutjes, R. Wismans, J. Schalkwijk, W. F. Daamen, and T. H. van Kuppevelt. 2006. Increased angiogenesis in acellular scaffolds by combined release of FGF2 and VEGF. *J Control Release* 116 (2):e88-90.

Nomi, M., H. Miyake, Y. Sugita, M. Fujisawa, and S. Soker. 2006. Role of growth factors and endothelial cells in therapeutic angiogenesis and tissue engineering. *Curr Stem Cell Res Ther* 1 (3):333-43.

Nor, J. E., M. C. Peters, J. B. Christensen, M. M. Sutorik, S. Linn, M. K. Khan, C. L. Addison, D. J. Mooney, and P. J. Polverini. 2001. Engineering and characterization of functional human microvessels in immunodeficient mice. *Lab Invest* 81 (4):453-63.

Ogawa, K., K. Asonuma, Y. Inomata, I. Kim, Y. Ikada, Y. Tabata, and K. Tanaka. 2001. The efficacy of prevascularization by basic FGF for hepatocyte transplantation using polymer devices in rats. *Cell Transplant* 10 (8):723-9.

Ogawa, K., R. Pasqualini, R. A. Lindberg, R. Kain, A. L. Freeman, and E. B. Pasquale. 2000. The ephrin-A1 ligand and its receptor, EphA2, are expressed during tumor neovascularization. *Oncogene* 19 (52):6043-52.

Ostman, A., M. Andersson, U. Hellman, and C. H. Heldin. 1991. Identification of three amino acids in the platelet-derived growth factor (PDGF) B-chain that are important for binding to the PDGF beta-receptor. *J Biol Chem* 266 (16):10073-7.

Ostman, A., L. Rall, A. Hammacher, M. A. Wormstead, D. Coit, P. Valenzuela, C. Betsholtz, B. Westermark, and C. H. Heldin. 1988. Synthesis and assembly of a functionally active recombinant platelet-derived growth factor AB heterodimer. *J Biol Chem* 263 (31):16202-8.

Pandey, A., H. Shao, R. M. Marks, P. J. Polverini, and V. M. Dixit. 1995. Role of B61, the ligand for the Eck receptor tyrosine kinase, in TNF-alpha-induced angiogenesis. *Science* 268 (5210):567-9.

Park, J. E., G. A. Keller, and N. Ferrara. 1993. The vascular endothelial growth factor (VEGF) isoforms: differential deposition into the subepithelial extracellular matrix and bioactivity of extracellular matrix-bound VEGF. *Mol Biol Cell* 4 (12):1317-26.

Pasquale, E. B. 2008. Eph-ephrin bidirectional signaling in physiology and disease. *Cell* 133 (1):38-52.

Patel, Z. S., and A. G. Mikos. 2004. Angiogenesis with biomaterial-based drug- and cell-delivery systems. *J Biomater Sci Polym Ed* 15 (6):701-26.

Penn, John S., and Creston A. Gay. 1992. Computerized digital image analysis of retinal vessel density: Application to normoxic and hyperoxic rearing of the newborn rat. *Experimental Eye Research* 54 (3):329.

Peters, M. C., P. J. Polverini, and D. J. Mooney. 2002. Engineering vascular networks in porous polymer matrices. *J Biomed Mater Res* 60 (4):668-78.

Phelps, E. A., and A. J. Garcia. 2009. Update on therapeutic vascularization strategies. *Regen Med* 4 (1):65-80.

Pieper, J. S., T. Hafmans, P. B. van Wachem, M. J. van Luyn, L. A. Brouwer, J. H. Veerkamp, and T. H. van Kuppevelt. 2002. Loading of collagen-heparan sulfate matrices with bFGF promotes angiogenesis and tissue generation in rats. *J Biomed Mater Res* 62 (2):185-94.

Pierce, G. F., T. A. Mustoe, B. W. Altrock, T. F. Deuel, and A. Thomason. 1991. Role of platelet-derived growth factor in wound healing. *J Cell Biochem* 45 (4):319-26.

Pierce, G. F., T. A. Mustoe, R. M. Senior, J. Reed, G. L. Griffin, A. Thomason, and T. F. Deuel. 1988. In vivo incisional wound healing augmented by platelet-derived growth factor and recombinant c-sis gene homodimeric proteins. *J Exp Med* 167 (3):974-87.

Poche, R. A., I. V. Larina, M. L. Scott, J. E. Saik, J. L. West, and M. E. Dickinson. 2009. The Flk1-myr::mCherry mouse as a useful reporter to characterize multiple aspects of ocular blood vessel development and disease. *Dev Dyn* 238 (9):2318-26.

Poche, R. A., J. E. Saik, J. L. West, and M. E. Dickinson. The mouse cornea as a transplantation site for live imaging of engineered tissue constructs. *Cold Spring Harb Protoc* 2010 (4):pdb prot5416.

Reinmuth, N., W. Liu, Y. D. Jung, S. A. Ahmad, R. M. Shaheen, F. Fan, C. D. Bucana, G. McMahon, G. E. Gallick, and L. M. Ellis. 2001. Induction of VEGF in perivascular cells defines a potential paracrine mechanism for endothelial cell survival. *FASEB J* 15 (7):1239-41.

Richardson, T. P., M. C. Peters, A. B. Ennett, and D. J. Mooney. 2001. Polymeric system for dual growth factor delivery. *Nat Biotechnol* 19 (11):1029-34.

Rinsch, C., P. Quinodoz, B. Pittet, N. Alizadeh, D. Baetens, D. Montandon, P. Aebischer, and M. S. Pepper. 2001. Delivery of FGF-2 but not VEGF by encapsulated genetically engineered myoblasts improves survival and vascularization in a model of acute skin flap ischemia. *Gene Ther* 8 (7):523-33.

Risau, W., and V. Lemmon. 1988. Changes in the vascular extracellular matrix during embryonic vasculogenesis and angiogenesis. *Dev Biol* 125 (2):441-50.

Roberts, M. J., M. D. Bentley, and J. M. Harris. 2002. Chemistry for peptide and protein PEGylation. *Adv Drug Deliv Rev* 54 (4):459-76.

Rodt, S. A., K. Ahlen, A. Berg, K. Rubin, and R. K. Reed. 1996. A novel physiological function for platelet-derived growth factor-BB in rat dermis. *J Physiol* 495 (Pt 1):193-200.

Rogers, M. S., A. E. Birsner, and R. J. D'Amato. 2007. The mouse cornea micropocket angiogenesis assay. *Nat Protoc* 2 (10):2545-50.

Rothermel, T. A., B. Engelhardt, and N. Sheibani. 2005. Polyoma virus middle-T-transformed PECAM-1 deficient mouse brain endothelial cells proliferate rapidly in culture and form hemangiomas in mice. *J Cell Physiol* 202 (1):230-9.

Roysam, B., W. Shain, E. Robey, Y. Chen, A. Narayanaswamy, C. L. Tsai, Y. Al-Kofahi, C. Bjornsson, E. Ladi, and P. Herzmark. 2008. The FARSIGHT Project: Associative 4D/5D Image Analysis Methods for Quantifying Complex and Dynamic Biological Microenvironments. *Microscopy and Microanalysis* 14 (SupplementS2):60-61.

Saik, J. E., D. J. Gould, E. M. Watkins, M. E. Dickinson, and J. L. West. 2011. Covalently immobilized platelet-derived growth factor-BB promotes angiogenesis in biomimetic poly(ethylene glycol) hydrogels. *Acta Biomater* 7 (1):133-43.

Sanders, J. E., Y. N. Wang, S. G. Malcolm, and S. E. Lamont. 2003. Biomaterial mesh seeded with vascular remnants from a quail embryo has a significant and fast vascular templating effect on host implant tissue. *Tissue Eng* 9 (6):1271-9.

Seifalian, A. M., A. Tiwari, G. Hamilton, and H. J. Salacinski. 2002. Improving the clinical patency of prosthetic vascular and coronary bypass grafts: the role of seeding and tissue engineering. *Artif Organs* 26 (4):307-20.

Semenza, G. L. 2006. Therapeutic angiogenesis: another passing phase? *Circ Res* 98 (9):1115-6.

Shapira-Schweitzer, K., and D. Seliktar. 2007. Matrix stiffness affects spontaneous contraction of cardiomyocytes cultured within a PEGylated fibrinogen biomaterial. *Acta Biomater* 3 (1):33-41.

Silva, E. A., and D. J. Mooney. Effects of VEGF temporal and spatial presentation on angiogenesis. *Biomaterials* 31 (6):1235-41.

Stamenkovic, I. 2003. Extracellular matrix remodelling: the role of matrix metalloproteinases. *J Pathol* 200 (4):448-64.

Steffens, G. C., C. Yao, P. Prevel, M. Markowicz, P. Schenck, E. M. Noah, and N. Pallua. 2004. Modulation of angiogenic potential of collagen matrices by covalent incorporation of heparin and loading with vascular endothelial growth factor. *Tissue Eng* 10 (9-10):1502-9.

Stosich, M. S., B. Bastian, N. W. Marion, P. A. Clark, G. Reilly, and J. J. Mao. 2007. Vascularized adipose tissue grafts from human mesenchymal stem cells with bioactive cues and microchannel conduits. *Tissue Eng* 13 (12):2881-90.

Stratman, A. N., A. E. Schwindt, K. M. Malotte, and G. E. Davis. 2010. Endothelial-derived PDGF-BB and HB-EGF coordinately regulate pericyte recruitment during vasculogenic tube assembly and stabilization. *Blood* 116 (22):4720-30.

Streilein, J. W. 2003. Ocular immune privilege: the eye takes a dim but practical view of immunity and inflammation. *J Leukoc Biol* 74 (2):179-85.

Tayalia, P., and D. J. Mooney. 2009. Controlled growth factor delivery for tissue engineering. *Adv Mater* 21 (32-33):3269-85.

Thomopoulos, S., R. Das, S. Sakiyama-Elbert, M. J. Silva, N. Charlton, and R. H. Gelberman. 2009. bFGF and PDGF-BB for Tendon Repair: Controlled Release and Biologic Activity by Tendon Fibroblasts In Vitro. *Ann Biomed Eng.*

Tolle, Charles R., Timothy R. McJunkin, and David J. Gorsich. 2008. An efficient implementation of the gliding box lacunarity algorithm. *Physica D: Nonlinear Phenomena* 237 (3):306.

Tong, Ricky T., Yves Boucher, Sergey V. Kozin, Frank Winkler, Daniel J. Hicklin, and Rakesh K. Jain. 2004. Vascular Normalization by Vascular Endothelial Growth Factor Receptor 2 Blockade Induces a Pressure Gradient Across the Vasculature and Improves Drug Penetration in Tumors. *Cancer Research* 64 (11):3731-3736.

Tremblay, P. L., V. Hudon, F. Berthod, L. Germain, and F. A. Auger. 2005. Inosculation of tissue-engineered capillaries with the host's vasculature in a reconstructed skin transplanted on mice. *Am J Transplant* 5 (5):1002-10.

Unger, R. E., A. Sartoris, K. Peters, A. Motta, C. Migliaresi, M. Kunkel, U. Bulnheim, J. Rychly, and C. J. Kirkpatrick. 2007. Tissue-like self-assembly in cocultures of endothelial cells and osteoblasts and the formation of microcapillary-like structures on three-dimensional porous biomaterials. *Biomaterials* 28 (27):3965-76.

UNOS. 2011. United Network for Organ Sharing.

Vadakkan, Tegy. 2009. Lacunarity of a binary image. *MATLAB Central.*
2009. Multifractal spectrum of a binary image. *MATLAB Central.*

Vargas, A., M. Zeisser-Labouebe, N. Lange, R. Gurny, and F. Delie. 2007. The chick embryo and its chorioallantoic membrane (CAM) for the in vivo evaluation of drug delivery systems. *Adv Drug Deliv Rev* 59 (11):1162-76.

Veronese, F. M. 2001. Peptide and protein PEGylation: a review of problems and solutions. *Biomaterials* 22 (5):405-17.

Veronese, F. M., and A. Mero. 2008. The impact of PEGylation on biological therapies. *BioDrugs* 22 (5):315-29.

Wang, Z. Z., P. Au, T. Chen, Y. Shao, L. M. Daheron, H. Bai, M. Arzigian, D. Fukumura, R. K. Jain, and D. T. Scadden. 2007. Endothelial cells derived from human embryonic stem cells form durable blood vessels in vivo. *Nat Biotechnol*25 (3):317-8.

West, J. L., and J. A. Hubbell. 1999. Polymeric biomaterials with degradation sites for proteases involved in cell migration. *Macromolecules* 32:241-244.

Wong, C., E. Inman, R. Spaethe, and S. Helgerson. 2003. Fibrin-based biomaterials to deliver human growth factors. *Thromb Haemost* 89 (3):573-82.

Wykosky, J., and W. Debinski. 2008. The EphA2 receptor and ephrinA1 ligand in solid tumors: function and therapeutic targeting. *Mol Cancer Res* 6 (12):1795-806.

Yuan, F., M. Leunig, S. K. Huang, D. A. Berk, D. Papahadjopoulos, and R. K. Jain. 1994. Microvascular permeability and interstitial penetration of sterically stabilized (stealth) liposomes in a human tumor xenograft. *Cancer Res* 54 (13):3352-6.

Zhang, D., J. Ouyang, N. Wang, Y. Zhang, and J. Bie. Promotion of PDGF-induced endothelial cell migration by phosphorylated VASP depends on PKA anchoring via AKAP. *Mol Cell Biochem* 335 (1-2):1-11.

Zhang, G., X. Wang, Z. Wang, J. Zhang, and L. Suggs. 2006. A PEGylated fibrin patch for mesenchymal stem cell delivery. *Tissue Eng* 12 (1):9-19.

Zhang, J., R. Cao, Y. Zhang, T. Jia, Y. Cao, and E. Wahlberg. 2009. Differential roles of PDGFR-alpha and PDGFR-beta in angiogenesis and vessel stability. *FASEB J* 23 (1):153-63. 177

Zieske, J. D. 2004. Corneal development associated with eyelid opening. *Int J Dev Biol* 48 (8-9):903-11.